Cloud condensation nuclei concentrations from spaceborne lidar measurements – Methodology and validation

Von der Fakultät für Physik und Geowissenschaften

der Universität Leipzig

genehmigte

D I S S E R T A T I O N

zur Erlangung des akademischen Grades

Doctor rerum naturalium

Dr. rer. nat.

vorgelegt

von **M.Sc. Goutam Choudhury**

geboren am 28. November 1995 in Kashipur, Indien

1. Gutachter: PD Dr. Matthias Tesche
2. Gutachter: Prof. Dr. Mira Pöhlker

Tag der Verleihung: 23. Januar 2023

The present study was prepared between July 2019 and September 2022 at the

Leipzig Institute for Meteorology
Leipzig University
Stephanstraße 3
04103 Leipzig
Germany

The work was supervised by
PD Dr. Matthias Tesche

Bibliographic Description

Goutam Choudhury

Cloud condensation nuclei concentrations from spaceborne lidar measurements – Methodology and validation

Leipzig University, Doctoral Thesis

September 2022

121 pages, 157 references, 25 figures, 12 tables

Abstract

Aerosol-cloud interactions are the most uncertain component of the anthropogenic radiative forcing. A substantial part of this uncertainty comes from the limitations of currently used spaceborne CCN proxies that (i) are column integrated and do not guarantee vertical co-location of aerosols and clouds, (ii) have retrieval issues over land, and (iii) do not account for aerosol hygroscopicity. A possible solution to overcome these limitations is to use height-resolved measurements of the spaceborne lidar aboard the CALIPSO (Cloud-Aerosol Lidar and Infrared Pathfinder Satellite Observation) satellite. This thesis presents a novel CCN retrieval algorithm based on Optical Modelling of CALIPSO Aerosol Microphysics (OMCAM) that is designed particularly for CALIPSO lidar measurements, along with its validation with airborne and surface in-situ measurements.

OMCAM uses a set of normalized size distributions from the CALIPSO aerosol model and modifies them to reproduce the CALIPSO measured aerosol extinction coefficient. It then uses the modified size distribution and aerosol type-specific CCN parameterizations to estimate the number concentration of CCN (n_{CCN}) at different supersaturations. The algorithm accounts for aerosol hygroscopicity by using the kappa parametrization. Sensitivity studies suggest that the uncertainty associated with the output n_{CCN} may range between a factor of 2 and 3. OMCAM-estimated aerosol number concentrations (ANCs) and n_{CCN} are validated using temporally and spatially co-located in-situ measurements. In the first part of validation, the airborne observations collected during the Atmospheric Tomography (ATom) mission are used. It is found that the OMCAM estimates of ANCs are in good agreement with the in-situ measurements with a correlation coefficient of 0.82, an RMSE of 247.2 cm^{-3}, and a bias of 44.4 cm^{-3}. The agreement holds for all aerosol types, except for marine aerosols, in which the OMCAM estimates are about an order of magnitude smaller than the in-situ measurements. An update of the marine model in OMCAM improve the agreement significantly. In the second part of validation, the OMCAM-estimated ANC and n_{CCN} are compared to measurements from seven surface in-situ stations covering a variety of aerosol environments. The OMCAM-estimated monthly n_{CCN} are found to be in reasonable agreement with the in-situ measurements with a 39 % normalized mean bias and 71 % normalized mean error. Combining the validation studies, the algorithm outputs are found to be consistent with the co-located in-situ measurements at different altitude ranges over both land and ocean. Such an agreement has not yet been achieved for spaceborne-derived CCN concentrations and demonstrates the potential of using CALIPSO lidar measurements for inferring global 3D climatologies of CCN concentrations related to different aerosol types.

Bibliografische Beschreibung

Goutam Choudhury

Konzentrationen von Wolkenkondensationskernen aus weltraumgestützten Lidar-Messungen – Methodik und Validierung

Universität Leipzig, Doktorarbeit
September 2022
121 Seiten, 157 Literaturverweise, 25 Abbildungen, 12 Tabellen

Kurzzusammenfassung

Die Wechselwirkungen zwischen Aerosolen und Wolken sind die unsicherste Komponente des anthropogenen Strahlungsantriebs. Ein wesentlicher Teil dieser Ungewissheit ergibt sich aus den Einschränkungen der derzeit verwendeten weltraumgestützten CCN-Proxies, die (i) säulenintegriert sind und keine vertikale Überlappung von Aerosolen und Wolken garantieren, (ii) Probleme bei der Bestimmung über Land haben, und (iii) die Hygroskopizität von Aerosolen nicht berücksichtigen. Eine mögliche Lösung zur Überwindung dieser Einschränkungen ist die Verwendung höhenaufgelöster Messungen des satellitengestützten Lidars an Bord des CALIPSO-Satelliten (Cloud-Aerosol Lidar and Infrared Pathfinder Satellite Observation). In dieser Arbeit wird ein neuartiger CCN-Retrieval-Algorithmus vorgestellt, der auf der Optischen Modellierung der CALIPSO-Aerosol-Mikrophysik (OMCAM) basiert und speziell für CALIPSO-Lidarmessungen entwickelt wurde, sowie seine Validierung mit in-situ-Messungen vom Flugzeug und am Boden.

OMCAM verwendet normalisierte Größenverteilungen aus dem CALIPSO-Aerosolmodell und skaliert sie, um den von CALIPSO gemessenen Aerosolextinktionskoeffizienten zu reproduzieren. Anschließend werden die modifizierte Größenverteilung und aerosoltypenspezifische CCN-Parametrisierungen verwendet, um die Anzahlkonzentration von CCN (n_{CCN}) bei verschiedenen Übersättigungen abzuschätzen. Der Algorithmus berücksichtigt die Aerosolhygroskopizität durch Verwendung der Kappa-Parametrisierung. Sensitivitätsstudien deuten darauf hin, dass die mit n_{CCN} verbundene Unsicherheit bei einem Faktor zwei bis drei liegt. Die von OMCAM geschätzten Aerosolzahlkonzentrationen (ANCs) und n_{CCN} werden anhand von zeitlich und räumlich gleichzeitig durchgeführten in-situ-Messungen validiert. Im ersten Teil der Validierung werden die während der Atmospheric Tomography (ATom)-Mission gesammelten Flugzeugbeobachtungen verwendet. Die OMCAM-Schätzungen der ANCs stimmen mit einem Korrelationskoeffizienten von 0,82, einem RMSE von 247,2 cm^{-3} und einer Abweichung von 44,4 cm^{-3} gut mit den in-situ-Messungen überein. Die Übereinstimmung gilt für alle Aerosolarten, mit Ausnahme der marinen Aerosole, bei denen die OMCAM-Schätzungen etwa eine Größenordnung unter den in-situ-Messungen liegen. Eine Aktualisierung des marinen Modells in OMCAM verbessert die Übereinstimmung erheblich. Im zweiten Teil der Validierung werden die von OMCAM geschätzten ANC- und n_{CCN}-Werte mit Messungen an sieben in-situ-Stationen am Boden verglichen, die eine Vielzahl von Aerosolumgebungen abdecken. Die von OMCAM geschätzten monatlichen Werte für n_{CCN} stimmen mit den in-situ-Messungen mit einer durchschnittlichen Abweichung von 39 % und einem durchschnittlichen Fehler von 71 % überein. Die Kombination der Validierungsstudien zeigt, dass die Ergebnisse des OMCAM-Algorithmus mit den in-situ-Messungen in verschiedenen Höhenbereichen sowohl über Land als auch dem Meer übereinstimmen. Eine solche Übereinstimmung wurde bisher für aus Satellitenbeobachtungen abgeleiteten CCN-Konzentrationen noch nicht erreicht und zeigt das Potenzial der Verwendung von CALIPSO-Lidarmessungen für die Bestimmung globaler 3D-Klimatologien von CCN-Konzentrationen bezüglich verschiedener Aerosolarten.

Contents

1 Introduction **1**

1.1 Background: Aerosols in the climate system . . . 1

1.1.1 Aerosol-induced effective radiative forcing . . . 3

1.1.2 Significance of aerosol-cloud interactions . . . 3

1.2 Observation-based ACI studies . . . 4

1.2.1 In-situ studies . . . 5

1.2.2 Spaceborne studies . . . 5

1.3 Spaceborne CCN proxies and their limitations . . . 8

1.4 CCN concentrations from lidars . . . 10

1.5 Objective: CCN from spaceborne lidar . . . 11

2 Paper 1: Estimating cloud condensation nuclei concentrations from CALIPSO lidar measurements **15**

2.1 Introduction . . . 16

2.2 Data and retrievals . . . 18

2.2.1 CALIPSO . . . 18

2.2.2 MOPSMAP . . . 19

2.2.3 POLIPHON . . . 19

2.3 Methodology . . . 20

2.3.1 Aerosol size distribution . . . 20

2.3.2 Aerosol hygroscopicity . . . 23

2.3.3 CCN parameterizations . . . 23

2.3.4 Application of OMCAM to CALIPSO retrieval . . . 23

2.4 Results . . . 24

2.4.1 Sensitivity analysis . . . 24

2.4.2 Comparison with POLIPHON . . . 30

2.4.3 Case study . . . 32

2.5 Summary and conclusions . . . 35

3 Paper 2: Evaluation of aerosol number concentrations from CALIPSO with ATom airborne in situ measurements **39**

3.1 Introduction . . . 40

3.2 Data, retrievals, and methods . . . 42

3.2.1 ATom . . . 42

3.2.2 CALIOP . . . 43
3.2.3 Aerosol number concentration from CALIOP . . . 44
3.2.4 Data matching and comparison . . . 48
3.3 Results . . . 52
3.3.1 Example cases . . . 52
3.3.2 General findings . . . 55
3.4 Discussion . . . 59
3.5 Summary . . . 61
3.6 Appendix . . . 63

4 Paper 3: Assessment of CALIOP-derived CCN concentrations by in situ surface measurements 65
4.1 Introduction . . . 66
4.2 Data and methods . . . 68
4.2.1 In situ observations . . . 68
4.2.2 CALIOP . . . 69
4.2.3 Comparison Methodology . . . 71
4.3 Comparison of CCN Concentrations . . . 73
4.4 Conclusions . . . 76

5 Summary and conclusions 79

6 Outlook 83

References 88

List of Abbreviations 107

List of Variables 109

List of Figures 111

List of Tables 113

A List of Publications 115

B Acknowledgements 117

Chapter 1

Introduction

1.1 Background: Aerosols in the climate system

Aerosols are microscopic suspensions of solid, liquid, or mixed particles that can be generated from anthropogenic activities such as the burning of fossil fuels and biomass, or from natural sources like volcanic eruptions, deserts, forests, and the ocean. While the immediate effects of airborne aerosols relevant to human beings are seen in terms of reduced air quality leading to respiratory illness and reduced atmospheric visibility, over the long term, they play a major role in modulating our climate by interacting with the Earth's radiation balance.

Aerosol interactions with Earth's radiation budget are complex and involve multiple pathways. A schematic of some major pathways is shown in Figure 1.1. In clear sky conditions, aerosols directly scatter the incoming solar radiation, thereby blocking a fraction of energy that would otherwise have reached the surface, resulting in a cooling effect. Anthropogenic aerosols such as black carbon can also absorb and trap the radiation, warming the atmosphere and the surface, thus offsetting the cooling effect. This warming can lead to a more stable atmosphere and, thus, lead to reduced surface moisture fluxes, limiting the formation of surface-forced clouds. This effect of absorbing aerosols on cloud cover and ultimately the interaction of clouds and radiation is also called the semi-direct effect. These direct and semi-direct effects of aerosols on radiation are collectively termed aerosol-radiation interactions (ARI). Aerosols are also needed in cloud formation. This is because a subset of them have the ability to act as cloud condensation nuclei (CCN) and ice nucleating particles (INP), which are necessary to initialize the formation and glaciation of clouds, respectively, under most atmospheric conditions. Thus, any change in the aerosol concentration may also change the cloud properties, thereby modifying how clouds interact with radiation. For a constant cloud liquid water content, an increase in the number of aerosols may increase the number of CCN, resulting in more, but smaller, cloud droplets. This may enhance the cloud reflectance, resulting in a cooling effect, also called the cloud-albedo effect or Twomey effect (Twomey, 1974). Moreover, such smaller droplets

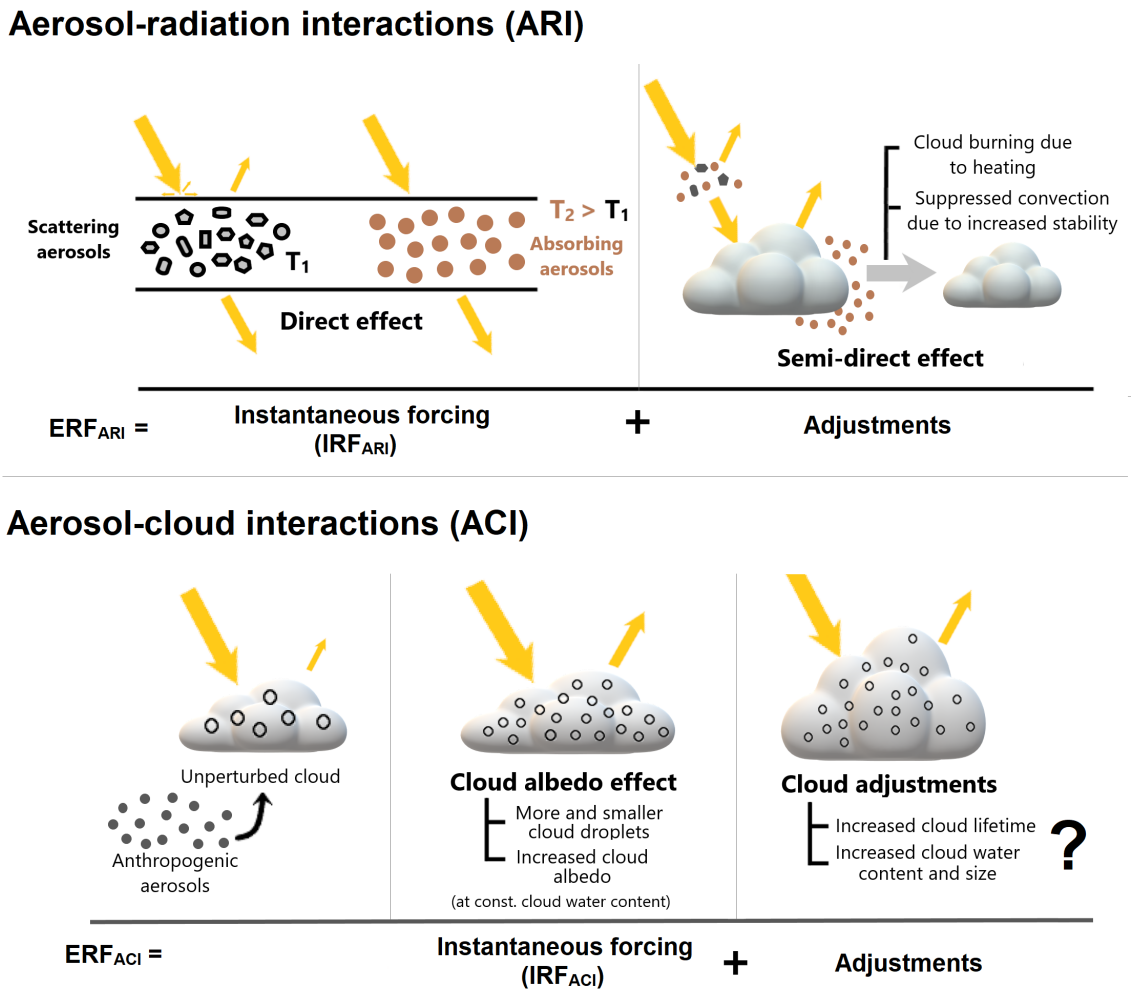

Figure 1.1: Schematic representation of various pathways associated with aerosol-cloud-radiation interactions. Yellow arrows represent the incident and reflected solar radiation. Arrow thickness indicates intensity and is exaggerated for better visualization. Circles within clouds indicate cloud droplets. ERF refers to the effective radiative forcing, IRF means the instantaneous radiative forcing, and T is the atmospheric temperature.

will require a longer time to grow large enough to fall as precipitation. This increases the cloud lifetime (Albrecht, 1989) and may also increase cloud cover, thereby imposing an additional cooling effect. Such indirect interactions of aerosols and radiation via clouds are called aerosol-cloud interaction (ACI).

The beginning of industrialization in the late 1700s marked the starting point of an increase in man-made emissions of greenhouse gasses and particulate pollutants into the atmosphere. Compare to the pre-industrial era, the concentration and composition of aerosols in our atmosphere have changed significantly and are still changing with the growth in urbanization and industrialization to sustain the increasing world population. Thus, it is of utmost importance to understand and quantify these aerosol impacts on the Earth's

radiation balance to accurately predict our future climate and devise appropriate mitigation policies.

1.1.1 Aerosol-induced effective radiative forcing

Radiative forcing is a measure of the change induced in the Earth's energy balance because of a change in an external climate driver or a forcing agent, for instance, aerosols or greenhouse gases. As there is an approximately linear relationship between the radiative forcing and the surface temperature, it has been used extensively in the field of climate research to quantify the contributions of different forcing agents to the global warming (Boucher et al., 2013; Forster et al., 2021). It is not only used as a standard tool by the Intergovernmental Panel on Climate Change (IPCC) to create plans for policymakers but also to constrain climate models and to quantify the uncertainty in future predictions. Starting from the fifth Assessment Report (AR5) of IPCC (Boucher et al., 2013), the traditional radiative forcing concept was replaced with a more accurate quantity called the effective radiative forcing (ERF). ERF due to a forcing agent is defined as the sum of the instantaneous radiative forcing (IRF; previously called radiative forcing) induced by the agent and the forcing due to rapid adjustments (or responses). Surface temperature response to such adjustments usually occur within a few weeks because of subsequent changes in cloud properties or other climate components that alter the radiation budget (Boucher et al., 2013). Likewise, the aerosol-induced ERF is defined as the sum of ERF due to aerosol-radiation interactions ($\mathrm{ERF_{ARI}}$) and aerosol-cloud interactions ($\mathrm{ERF_{ACI}}$), where each one has two components – the instantaneous forcing and the adjustments. Thus, $\mathrm{ERF_{ARI}}$ includes the instantaneous forcing due to direct aerosol interaction with radiation ($\mathrm{IRF_{ARI}}$) and the subsequent adjustments in the cloud cover because of modifications in the atmospheric profile or stability (semi-direct effect). Similarly, $\mathrm{ERF_{ACI}}$ includes the instantaneous effect of changing aerosols (that may serve as CCN or INP) on the cloud albedo ($\mathrm{IRF_{ACI}}$) as well as the subsequent adjustments in the cloud liquid water path (LWP) and lifetime.

1.1.2 Significance of aerosol-cloud interactions

As per the latest IPCC report (Forster et al., 2021, AR6), the $\mathrm{ERF_{ARI}}$ estimated from combined modelling and observational-based evidence is found to be $-0.3 \pm 0.3\,\mathrm{W/m^2}$ with a medium level of confidence. Similarly, the $\mathrm{ERF_{ACI}}$ is estimated to be $-1 \pm 0.7\,\mathrm{W/m^2}$, also with a medium level of scientific understanding, leading to a net aerosol-induced ERF of $-1.3\,[-2.0\text{ to }-0.6]\,\mathrm{W/m^2}$. The estimates of aerosol-induced ERF and its components along with their uncertainties are shown in Figure 1.2. Compared to the previous assessments (AR4 and AR5), the overall estimates of ERF is now more certain with the level of scientific understanding improved from low to medium level. It is now certain that aerosols have a net cooling effect on climate, with ACI being the dominant contributor. Even so, the net magnitude of aerosol-induced cooling is still uncertain because of inadequate understanding of the forcing pathways and of observational limitations. The uncertainty associated with

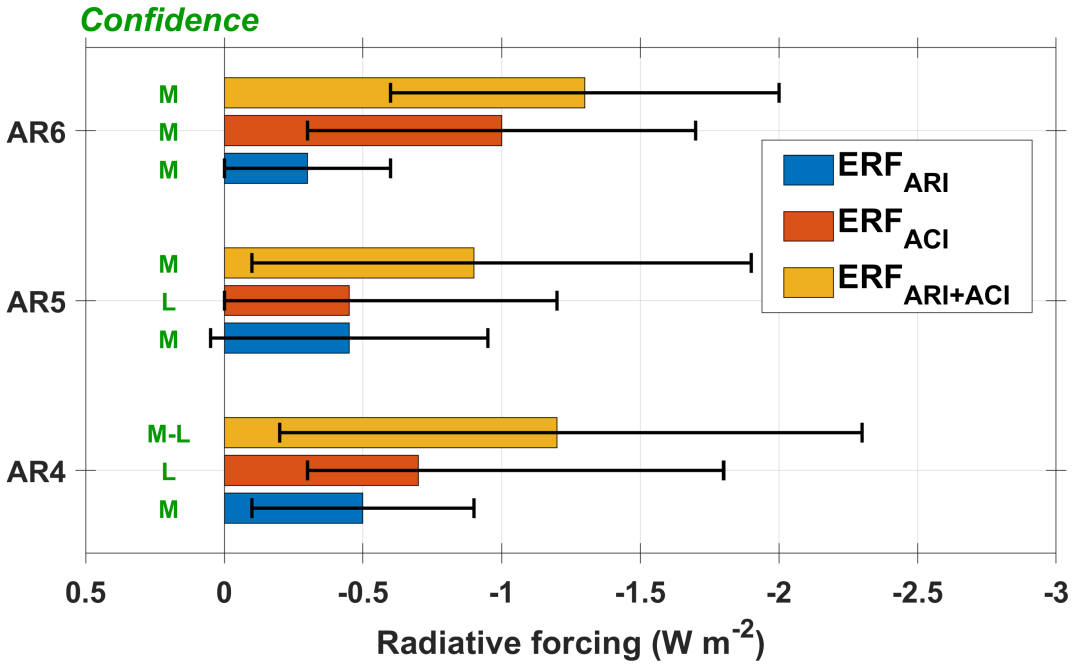

Figure 1.2: Net effective radiative forcing (ERF) and its components from aerosol-cloud interactions and aerosol-radiation interactions from the fourth, fifth and sixth IPCC Assessment Reports (AR). L and M stand for a low and medium level of confidence, respectively. Error bars represent the forcing uncertainty.

ACI has not improved much over the past two decades and is still the largest among all the forcing agents (Forster et al., 2021). This can be attributed to many factors. For instance, the forcing estimates for ACI only consider liquid clouds, as the role of (anthropogenic) aerosols on ice-containing clouds is still not clear. Moreover, the adjustments associated with ACI are highly uncertain, with only little observational-based evidence (Chen et al., 2014; Christensen et al., 2016, 2017). Thus, it is of utmost importance to improve our present understanding of the pathways involved in the interactions between aerosols and clouds, and their contributions to the ERF to better constrain climate models and reduce the uncertainties in future climate projections. A comprehensive overview of the existing observation-based aerosol-cloud interaction studies, their limitation, and possible alternatives for improved quantification of $\mathrm{ERF_{ACI}}$ are discussed in the following sections.

1.2 Observation-based ACI studies

The roots of aerosol and cloud studies can be traced back to the late 19^{th} century when laboratory experiments showed that the supersaturation of several hundred per cent needed for homogeneous condensation of water vapour to form droplets reduces to less than 2 % in the presence of aerosols (Coulier, 1875; Aitken, 1923). Such aerosols with the ability to initiate heterogeneous cloud nucleation in the atmosphere were termed cloud condensation

nuclei and were deemed necessary for cloud formation in the lower troposphere. Thereafter, several studies were performed involving controlled laboratory experiments, in-situ measurement campaigns, and remote-sensing observations to understand and quantify the impact of aerosols on cloud properties.

1.2.1 In-situ studies

In the late 20^{th} century, the impact of an increase in the number of aerosol particles that may serve as CCN on clouds was first hypothesized to lead to more number of small cloud droplets at a constant cloud water content, leading to an increase in the overall scattering surface area and therefore the cloud albedo (Twomey, 1974, 1977), also called the Twomey effect. The hypothesis was based on the results from local in-situ aircraft measurements that showed a decrease in droplet size when clouds were exposed to smoke from forest fires (Warner and Twomey, 1967; Eagan et al., 1974). Thereafter, several studies involving in-situ aircraft measurements provided ample evidence of the existence of such instantaneous aerosol-cloud microphysical interactions, for instance, the increase in cloud droplet number and decrease in their size for cumulus (Andreae et al., 2004; Lu et al., 2008) and stratocumulus clouds (Twohy et al., 2005; Lu et al., 2007; Hegg et al., 2012) with an increase in aerosol concentration.

The second hypothesis on the after-effects (rapid adjustments) of the instantaneous Twomey effect implies an increase in cloud extent and lifetime as a response to an increase in the number of cloud droplets and suppressed precipitation (Albrecht, 1989). Precipitation reduces the lifetime and the water content of a cloud. Thus, any suppression or delay of the onset of precipitation by aerosols would also increase the LWP and cloud cover. Compared to the Twomey effect, however, the relationship between aerosol concentration and cloud extent or water content is complex. Some studies have found a positive relationship between them (Nakajima et al., 2001; Kaufman and Koren, 2006), while some report a negative relation (Coakley and Walsh, 2002; Twohy et al., 2005). This is perhaps because the impact of aerosols on cloud cover and LWP is also perturbed by external meteorological factors like cloud entrainment, humidity, and updraft velocity (Lu et al., 2007; Chen et al., 2012). Such complexities and dependence of ACI on the type of cloud, aerosol, and ambient meteorology are responsible for the diverse relationships between aerosols and cloud microphysical properties.

1.2.2 Spaceborne studies

Instantaneous effect

Satellite measurements provide global and long-term measurements of aerosols and clouds that not only enable global quantification of ACI but also its regional and regime-wise changes (Jiang et al., 2018). Satellite-based studies have also found ample evidence of

the instantaneous Twomey effect. Initially, cloud images from the Advanced Very High Resolution Radiometer (AVHRR) aboard National Oceanic and Atmospheric Administration (NOAA) satellite were used to study the effects of ship emissions on cloud properties (Coakley et al., 1987; Durkee et al., 2000; Coakley and Walsh, 2002). These studies found an increase in cloud droplet number concentrations (CDNC) and a decrease in their size for the smoke-affected cloudy pixels. Few studies also identify similar changes in cloud properties over land (with expected higher concentrations of anthropogenic aerosols) compared to over ocean (Han et al., 1998a,b). Thereafter, studies incorporated aerosol parameters like aerosol optical depth (AOD), Angstrom exponent (AE), and aerosol index (AI; defined as the product of AOD and AE) as derived from spaceborne sensors like the Moderate Resolution Imaging Spectroradiometer (MODIS) and Polarization and Directionality of the Earth's Reflectances (POLDER) in satellite-based ACI studies. Evidence of the Twomey effect such as a positive correlation between AOD and cloud optical depth or CDNC and a negative correlation between AOD and cloud effective radius was identified (Wetzel and Stowe, 1999; Nakajima et al., 2001). A similar correlation of cloud properties with AI instead of AOD further support the importance of the Twomey effect (Bréon et al., 2002; Quaas et al., 2004).

Followed by such spaceborne evidence, several studies have used satellite-derived aerosol and cloud information to quantify the forcing due to the indirect aerosol effect. One of the main challenges in estimating the $\mathrm{IRF_{ACI}}$ is to properly quantify the anthropogenic component of present-day aerosol emissions. Some studies assume fine-mode aerosol properties represent the anthropogenic aerosols, while some use the difference between present-day and pre-industrial (from global model simulations) aerosol properties. Quaas et al. (2006) used the relationship between MODIS-derived fine-mode AOD and CDNC to quantify the sensitivity of cloud properties to changes in aerosol concentration. They further used this approach to constrain the global model simulations and found the $\mathrm{IRF_{ACI}}$ to be within -0.5 and $-0.3\,\mathrm{W/m^2}$ depending on the type of global model considered. Quaas et al. (2008) combined the AOD-CDNC regression derived from MODIS and the short-wave albedo measurements from the Clouds and the Earth's Radiant Energy System (CERES) sensor and found the overall forcing due to the Twomey effect to be similar to the findings of Quaas et al. (2006) with a value of $-0.2 \pm 0.1\,\mathrm{W/m^2}$. A similar methodology was also used by Bellouin et al. (2013), where they used fine-mode AOD from reanalysis data and found the $\mathrm{IRF_{ACI}}$ to be $-0.6 \pm 0.4\,\mathrm{W/m^2}$, more negative than previous estimates. However, these $\mathrm{IRF_{ACI}}$ estimates were still lower in magnitude compared to those from global models (Boucher et al., 2013). One of the main reasons behind this disagreement was attributed to the use of AOD, which was argued to be a poor representative of CCN close to cloud-base (Penner et al., 2011; Shinozuka et al., 2015; Stier, 2016). Gryspeerdt et al. (2017) show that using AOD–CDNC relationship leads to an underestimation of $\mathrm{IRF_{ACI}}$ by 30 % and suggest the use of AI instead of AOD. However, they found a similar net negative $\mathrm{IRF_{ACI}}$ value of $-0.4\,[-0.2$ to $-1.0]\,\mathrm{W/m^2}$. Christensen et al. (2016) using AI as a CCN proxy also report similar forcing estimates. Recent studies have, however, derived a more negative indirect forcing. Compare to the previous studies which use aerosol optical properties as CCN

proxies, Hasekamp et al. (2019) use POLDER-derived column-integrated aerosol number concentrations and estimate a more negative $\mathrm{IRF_{ACI}}$ of -1.14 $[-1.72$ to $-0.84]\,\mathrm{W/m^2}$. Similar negative values were also reported in McCoy et al. (2017) and McCoy et al. (2020). Summing up all the satellite-based evidences, it is now highly likely that human-generated aerosols result in an increase in CDNC and therefore have a cooling effect on the climate via the cloud-albedo effect with an average $\mathrm{IRF_{ACI}}$ value of -0.7 ± 0.5 $\mathrm{W/m^2}$ with a medium level of confidence (Forster et al., 2021).

Adjustments

Satellite-based studies have also analyzed the relationship between aerosol load and cloud water content and/or cloud fraction. Lebsock et al. (2008) studied the impact of aerosol load (using AI) on precipitating and non-precipitating liquid clouds over oceans. They report contrasting results for those two scenarios: a decrease in LWP with an increase in aerosols for non-raining clouds and an increase in LWP with aerosol load for transitional or precipitating clouds. Ship emissions have also been used to characterise anthropogenic aerosols and analyze their impact on LWP and cloud cover. Christensen and Stephens (2011) investigated the impact of ship emissions on open and closed marine stratocumulus cloud systems. They found a significant increase in LWP (39 %) for open cloud systems (broken clouds) and a frail decrease in LWP (-6 %) for overcast or closed cloud systems. In contrast, Goren and Rosenfeld (2014) reported an increase in LWP and cloud fraction of both open and closed marine-stratocumulus cloud systems influenced by ship emissions, with the latter being more significant. Aerosols originating from volcanic eruptions are also used to study cloud adjustments. For instance, Yuan et al. (2011) reported an increase in cloud height, cloud fraction, and albedo of cumulus clouds with an increase in AI from Kilauea volcanic eruptions. A similar increase in cloud albedo and LWP is also documented in Ebmeier et al. (2014), who used AOD to quantify the volcanic emissions. The increase in LWP is perhaps due to the suppressed coalescence process, which prevents the cloud droplets to grow large enough to precipitate, thereby promoting the buildup of cloud water content. While Toll et al. (2017, 2019) report a non-significant or negative change in LWP. The decrease in LWP may be explained as a result of enhanced dry air entrainment and evaporation caused by increased aerosol concentrations.

On a global scale, most studies on aerosol-induced adjustments in cloud cover and LWP have found a negative forcing associated with cloud fraction adjustments. Chen et al. (2014) analyzed the relationship between AI and cloud fraction and estimated a forcing of -0.5 ± 0.5 $\mathrm{W/m^2}$. Christensen et al. (2017) using AI and Gryspeerdt et al. (2016) using AOD as CCN proxy found a similar negative forcing. Results are, however, different for LWP adjustments. Gryspeerdt et al. (2019) and Toll et al. (2019) found a positive radiative forcing associated with LWP with values between $+0.15$ and $+0.3$ $\mathrm{W/m^2}$, thereby offsetting the cooling from aerosol indirect effect. Nevertheless, as only a limited number of studies are available, the radiative forcing due to aerosol-induced cloud adjustments is highly uncertain. Other than that, there are also many limitations associated with the

currently used spaceborne CCN proxies in ACI studies that limit a proper quantification of the cloud-mediated aerosol radiative forcing as discussed in the next section.

1.3 Spaceborne CCN proxies and their limitations

Only a fraction of aerosols that can act as CCN can interact directly with cloud properties. As CCN concentrations are not measured directly by spaceborne sensors, most satellite-based studies rely on aerosol optical properties. In some studies, ACI is explored indirectly by analysing the change in the properties of clouds that are influenced by emissions from volcanoes and ships (Christensen et al., 2022). However, such indirect studies can only be used to infer a qualitative or process-level understanding of ACI and a proper CCN proxy measurement is required to quantify the cloud-mediated aerosol effects on Earth's radiative budget.

Traditionally, satellite-derived AOD is used in ACI studies (Quaas et al., 2006, 2008; Bellouin et al., 2013). However, it is now well established that AOD is not an appropriate CCN proxy (Penner et al., 2011; Stier, 2016; Bellouin et al., 2020; Quaas et al., 2020). This is because it neither account for aerosol microphysical properties nor for the position of aerosols within the atmospheric column. For instance, an atmospheric column with a small number of coarse-mode particles may have the same optical depth as one with a large number of fine-mode aerosols. This is problematic as the latter is more probable to include more CCN-active particles than the former. Therefore, AOD was replaced by AI, which weighs more on smaller aerosol particles, in many spaceborne ACI studies (Christensen et al., 2016, 2017; Gryspeerdt et al., 2017). However, Sayer et al. (2013) found the AI retrieved over land to be non-reliable. This limits the consideration of aerosols originating over land, which accommodates most of the anthropogenic sources in ACI studies. Another major drawback of using these aerosol optical parameters measured from passive sensors is that they are column-integrated and do not guarantee the vertical co-location of the aerosols and clouds that are studied (Costantino and Bréon, 2013; Shinozuka et al., 2015). Figure 1.3 depicts four simple possible scenarios of different arrangements of aerosols and clouds as derived from Cloud-Aerosol Lidar and Infrared Pathfinder Satellite Observation (CALIPSO) version-4 Vertical Feature Mask product. In situations like Scenario 1, clouds and aerosols lie more or less in the same height range and there are no additional aerosol or cloud layers present at other height levels. The usage of column-integrated properties may be valid in such a situation as aerosols are likely to interact with the clouds. However, in other situations where aerosol and cloud layers are either not linked (Scenario 2) or present at multiple layers (Scenarios 3 and 4), the necessary assumption of vertical co-location for using column-integrated parameters is not fulfilled. Moreover, retrieval-related issues for passive sensors like aerosol swelling in humid conditions in the proximity of clouds (Várnai and Marshak, 2015; Quaas et al., 2020) and cloud contamination of aerosols resulting from 3D scattering effects on the edges of clouds (Várnai and Marshak, 2015; Christensen et al., 2017) have been identified to further complicate the use of AOD or AI for ACI studies.

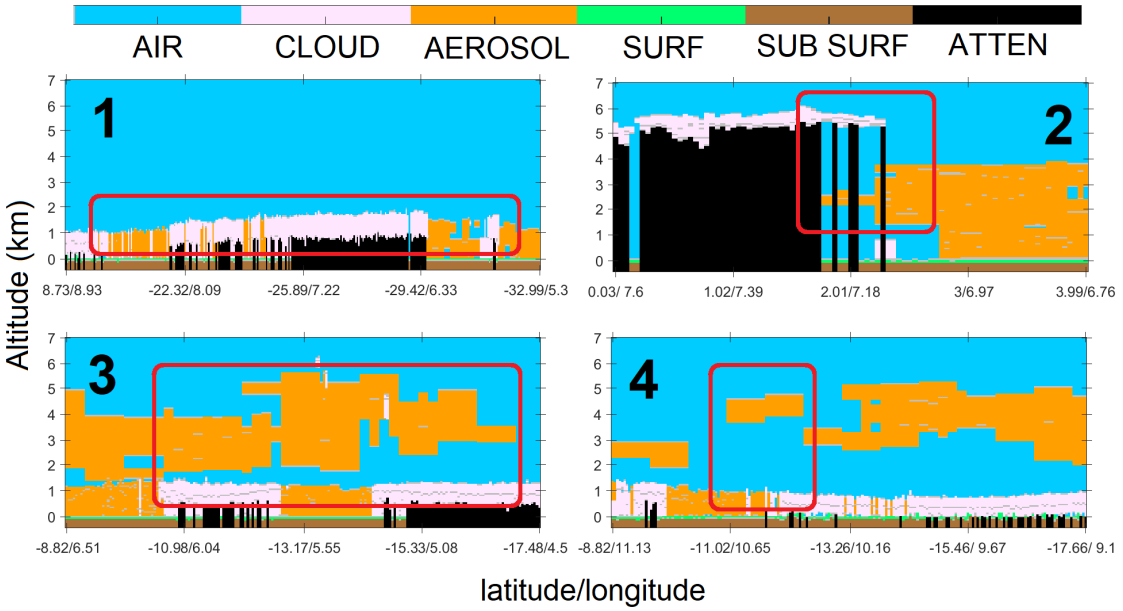

Figure 1.3: CALIPSO level 2 version 4.2 Vertical Feature Mask product for four selected overpasses over different regions of Africa in February 2007. The red rectangles highlight four scenarios with different arrangements of aerosols (orange) and clouds (pink) that illustrate the importance of information on the vertical distribution of those layers when column-integrated parameters are used for ACI studies.

Satellite-derived aerosol optical properties are also used to derive aerosol microphysical properties. The PSML003_Ocean data product retrieved from MODIS (Remer et al., 2005, Appendix B) provides the column-integrated number concentration of aerosols with a radius $> 30\,\text{nm}$. The retrieval algorithm first considers the MODIS measured spectral radiance as a reference. It then matches the observed radiance with that estimated from a combination of nine pre-set model aerosol types defined through a set size distribution and a refractive index. However, the data has not been validated yet and has not been used in spaceborne ACI studies. Column-integrated aerosol number concentrations are also available from multi-angle multi-wavelength polarimetric measurements from POLDER (Hasekamp et al., 2011; Stap et al., 2015). The data set was used in Lacagnina et al. (2017) and Hasekamp et al. (2019) to quantify the direct and indirect aerosol radiative forcing, respectively. While the derived microphysical properties may be a better CCN proxy compared to the optical ones, they are still column integrated and might not represent the aerosols present close to the cloud base that interact with clouds. Moreover, the POLDER retrievals face quality issues over land (Hasekamp et al., 2019; Quaas et al., 2020). One possible way to overcome the limitations associated with currently used column-integrated CCN proxies derived from passive sensors is to switch to active height-resolved measurements derived from spaceborne lidar that are not affected by changes in surface properties. Costantino and Bréon (2013) already showed that height-resolved measurements from spaceborne lidar are invaluable for assessing the co-location of aerosol and cloud layers in spaceborne ACI studies.

1.4 CCN concentrations from lidars

Lidar is an active sensor that provides range-resolved measurements. The derived aerosol optical properties include extinction coefficient, backscatter coefficient, and particle depolarization ratio. The retrieved backscatter and extinction coefficients can be further separated into contributions from dust and non-dust (continental and marine) using the particle depolarization ratio (Tesche et al., 2009). Shinozuka et al. (2015) use in-situ measurements to report a linear relationship between aerosol extinction coefficient and number concentration of CCN (n_{CCN}) on a log-log scale. This implies that the aerosol extinction coefficient profiles measured by lidar can be used to derive height-resolved n_{CCN}. However, the simple parametrization did not differentiate between aerosol types that can be measured by polarization lidars. Using the full potential of lidars in measuring type-specific aerosol properties and considering the different aerosol signatures that are most commonly found in the atmosphere, Mamouri and Ansmann (2015, 2016) formulated a CCN retrieval algorithm specifically designed for ground-based lidar, namely the Polarization Lidar Photometer Networking (POLIPHON) technique. POLIPHON uses the ability of polarization lidar to derive aerosol type-specific extinction coefficients and estimates the corresponding n_{CCN} using two steps. It first converts the extinction coefficient (α) to an aerosol number concentration within a predefined radius limit as

$$n_{j,\mathrm{dry}} = C \cdot \alpha^{x}, \tag{1.1}$$

where $n_{j,\mathrm{dry}}$ is the aerosol number concentration with a dry radius $> j$ nm, C and x are the regression constants called conversion factor (with unit $\mathrm{cm}^{-3}\mathrm{Mm}$) and extinction exponent (unit less), respectively. The values of j, C, and x depend on the aerosol type. For continental and marine aerosols, j is 50 nm and it is 100 nm for desert dust aerosols. Mamouri and Ansmann (2016) estimated the values of C and x from a regression analysis of long-term AERONET measurements for different aerosol environments that correspond to different aerosol types. The second step then involves estimating n_{CCN} using $n_{j,\mathrm{dry}}$ through simple size-based CCN parametrizations provided in the literature. These parameterizations conclude that continental and marine particles with a dry radius > 50 nm (Quinn et al., 2008; Rose et al., 2010; Deng et al., 2011) and dust aerosols with a dry radius > 100 nm (Koehler et al., 2009; Kumar et al., 2011) are most favourable to act as CCN at a supersaturation of 0.15–0.2 %. Thus, the $n_{j,\mathrm{dry}}$ in equation (1.1) represents n_{CCN} at a supersaturation of 0.15–0.2 %. Furthermore, Mamouri and Ansmann (2016) provide enhancement factors (f_{ss}) to compute n_{CCN} at higher supersaturation as

$$n_{\mathrm{CCN}} = f_{\mathrm{ss}} \cdot n_{j,\mathrm{dry}}, \tag{1.2}$$

where $f_{\mathrm{ss}} = 1.0$, 1.35, and 1.7 for supersaturation 0.15–0.2 %, 0.25 %, and 0.40 %, respectively. The enhancement factors for 0.25 % and 0.4 % supersaturation are estimated from the ratios $n_{40,\mathrm{dry}}/n_{50,\mathrm{dry}}$ and $n_{30,\mathrm{dry}}/n_{50,\mathrm{dry}}$, respectively, as $n_{40,\mathrm{dry}}$ and $n_{30,\mathrm{dry}}$ form the most favourable CCN reservoir at the respective supersaturation (Mamouri and Ansmann,

2016). The uncertainty in the POLIPHON algorithm comes from the extinction to number concentration conversion (equation 1.1) and the CCN parametrization (equation 1.2). Mamouri and Ansmann (2016) estimated the uncertainty to be between a factor of 2 and 3. Most of the uncertainty (factor of 1.5–2.0) comes from the conversion of extinction-to-number concentration. Factors like varying chemical (hygroscopicity) and microphysical (size distribution) properties of aerosol types with location and aerosol age are the main contributors to the errors. Additional uncertainties may arise from a pure size-based CCN parametrization scheme. Not all aerosols over a certain size ($> j$ nm) may be CCN active at a certain supersaturation. This results in an intrinsic overestimation of n_{CCN} at all supersaturations. This level of uncertainty (factor of 2–3) is also reported in Shinozuka et al. (2015) for remote sensing of n_{CCN}.

Haarig et al. (2019) applied the POLIPHON algorithm to ground-based lidar measurements and found the derived n_{CCN} to be in reasonable agreement with concurrent airborne in-situ measurements. Even though the algorithm is developed for ground-based lidars, it has also been applied to spaceborne Cloud-Aerosol Lidar with Orthogonal Polarization (CALIOP) aboard CALIPSO (Marinou et al., 2019; Georgoulias et al., 2020) and compared to airborne in-situ measurements. Georgoulias et al. (2020) found a very good agreement between the CALIOP-derived aerosol number concentrations and in-situ measurements over sea surface close to Thessaloniki, Greece. However, the algorithm resulted in an overestimation for retrievals over land. Moreover, the extinction to number concentration conversion in POLIPHON is not resolved with respect to ambient relative humidity (RH) and is only valid for situations with RH between 40 and 80 %. Assumption of uniform aerosol extinction coefficient over such a wide RH window may introduce additional errors in the presence of hygroscopic aerosols. Further, the conversion factors used in equation (1.1) vary with geographical location for dust and smoke aerosols (Ansmann et al., 2019, 2021b) which may result in additional errors when applied to satellite measurements that provide global aerosol measurements. However, such situations can be controlled and filtered for ground-based lidar retrievals and, thus, POLIPHON shows a great promise for measuring height-resolved cloud-relevant aerosol concentrations operationally at ground-based stations (Haarig et al., 2019). Having said that, there is still a need for a better CCN-retrieval algorithm for spaceborne lidar that is consistent globally and accounts for varying RH conditions.

1.5 Objective: CCN from spaceborne lidar

The primary objective of this dissertation is to formulate a CCN retrieval algorithm specifically designed for the spaceborne CALIPSO lidar that is (i) uniform with respect to geographical location, (ii) self-consistent with CALIPSO's retrieval algorithm, and (iii) accounts for aerosol hygroscopicity. Further goals include the validation of the output of the novel algorithm with co-located in-situ measurements (Schmale et al., 2017; Wofsy et al., 2018) at different height levels over both land and ocean surfaces and the comparison to

the outputs from the existing lidar-based POLIPHON algorithm. Such comparisons will determine the algorithm's efficacy in retrieving height-resolved long-term global CCN concentrations from CALIPSO measurements.

To construct an aerosol retrieval algorithm that is consistent across all regions, a global aerosol model is generally used, for instance, in the MODIS retrieval algorithm (Remer et al., 2005). The CALIPSO-retrieval features an aerosol model that provides size distributions and refractive indices of the considered aerosol types. The model was designed by combining multidecadal measurements from AERONET and in-situ campaigns (Omar et al., 2009). This aerosol model can be used to retrieve aerosol size distributions from CALIPSO measurements, which makes the subsequent CCN retrieval self-consistent within the CALIPSO analysis chain. This methodology is similar to the MODIS retrieval of aerosol number concentration (Remer et al., 2005, Appendix B) but is aimed to achieve a height-resolved retrieval of n_{CCN} much needed to study the interaction of vertically co-located aerosols and clouds. The final retrieved size distributions can then be used in the aerosol size- and type-based CCN parametrizations by Mamouri and Ansmann (2016) to estimate n_{CCN} at multiple supersaturations (equation 1.2). To consider the aerosol hygroscopicity, the kappa-parametrization (Petters and Kreidenweis, 2007) can be implemented with globally averaged kappa values for different aerosol types (Andreae and Rosenfeld, 2008). The correction can be applied either to the initial size distributions or to the CALIPSO-derived ambient aerosol extinction coefficients. A similar hygroscopicity correction methodology was also used in Altaratz et al. (2013) to correct MODIS-derived AOD to quantify the effect of humidity growth in enhancing AOD. Implementing such parametrization would make the CCN-retrieval reliable in high RH conditions like in the proximity of clouds, which is crucial for studying ACI.

To access the reliability of the retrieved CCN concentrations, it is necessary to compare them with spatially and temporally co-located in-situ measurements. Although the collection of in-situ data has its complications, they are often more controlled, manageable, and quantifiable relative to remote-sensing observations that may involve complicated inversion algorithms. Thus, remote-sensing products are generally compared with in-situ observations to check for consistency. For the proposed retrieval algorithm, both the inferred aerosol number concentrations or $n_{j,\mathrm{dry}}$ (that form the input to the CCN-parametrizations) and CCN concentrations or n_{CCN} (output of the CCN-parametrizations) need to be validated. For validating $n_{j,\mathrm{dry}}$, height-resolved in-situ aircraft measurements taken during the Atmospheric Tomography (ATom) mission over the Pacific and the Atlantic oceans between the years 2016 and 2018 (Wofsy et al., 2018) are used. As most of the in-situ data were collected over oceans, the comparison would evaluate the performance of the proposed algorithm in estimating $n_{j,\mathrm{dry}}$ over oceans. For validating the CALIPSO-derived n_{CCN}, the surface in-situ measurements from Schmale et al. (2017) are used, which include long-term n_{CCN} measurements at multiple in-situ stations covering a variety of aerosol environments over land. The comparison will also demonstrate the ability of the proposed algorithm in capturing the temporal variations of n_{CCN} at different locations over land. Combining

the results from both comparisons will yield useful insights into the applicability of the proposed algorithm for different aerosol environments and surface types.

In this dissertation, a novel CCN retrieval algorithm specifically designed for application to measurements from the spaceborne lidar CALIOP aboard the CALIPSO satellite is presented. The algorithm description and the validation of the retrieval results with independent in-situ measurements have been published in three papers. Choudhury and Tesche (2022a) (Paper 1) present a comprehensive description of the overall retrieval algorithm with an error estimate based on sensitivity studies. It also includes a theoretical comparison with the previously existing lidar-based POLIPHON technique for CCN retrieval. Furthermore, a preliminary validation study is shown where the CALIPSO retrievals are compared with the airborne in-situ measurements taken during the ACEMED campaign (Tsekeri et al., 2017). Choudhury et al. (2022) (Paper 2) compare the CALIPSO-derived aerosol number concentrations with the in-situ measurements taken during the airborne ATom campaign (Wofsy et al., 2018). A limitation of the algorithm in the case of fine-mode marine aerosols is identified and thus a modification to the marine model used in the algorithm is suggested. Choudhury and Tesche (2022b) (Paper 3) compare the monthly n_{CCN} time-series derived from Schmale et al. (2017) at seven selected ground-based in-situ stations with that estimated from CALIPSO. The ability of the algorithm in reproducing the monthly variations observed by in-situ measurements is assessed and the steps that should be considered when building a global 3D climatology of n_{CCN} from CALIPSO measurements are suggested. The findings are collectively summarized in Chapter 5 and future goals are discussed in the final chapter. The dissertation provides ample evidence to support the use of spaceborne lidar in constructing a global height-resolved CCN climatology, that will be extremely useful in studying ACI and validating as well as constraining the regional and global model simulations.

Chapter 2

Estimating cloud condensation nuclei concentrations from CALIPSO lidar measurements*

Short summary

A novel methodology to estimate CCN concentrations from CALIPSO lidar is presented. The algorithm utilises the normalised size distributions from the CALIPSO aerosol model and adjusts them to reproduce the CALIPSO measured extinction coefficient. The final adjusted size distributions are then used in the CCN parameterizations to estimate CCN concentrations at different supersaturations. Kappa parametrization is used to account for the hygroscopicity of continental and marine aerosols. The sensitivity of the derived CCN concentrations to variations in the initial size distributions is also examined. An initial application to a case with coincident airborne in-situ measurements for independent validation shows promising results and illustrates the potential of CALIPSO for constructing a global height-resolved CCN climatology.

*Published as: Choudhury, G. and Tesche, M.: Estimating cloud condensation nuclei concentrations from CALIPSO lidar measurements, Atmos. Meas. Tech., 15, 639–654, https://doi.org/10.5194/amt-15-639-2022, 2022.

2.1 Introduction

Aerosol particles act as cloud condensation nuclei (CCN) and ice-nucleating particles (INPs) and provide a surface for the condensation of atmospheric water vapour to form cloud droplets. The physical and chemical properties of such particles affect not only the cloud micro- and macro-physical properties, but also cloud development, lifetime, and the associated precipitation (Rosenfeld et al., 2014; Fan et al., 2016; Choudhury et al., 2019). The rapid adjustments in clouds resulting from aerosol–cloud interactions (ACIs) are not well understood and still remain the largest source of spread in global climate projections (Forster et al., 2021). This challenge has motivated the scientific community to study ACIs by using data from in situ and satellite measurements as well as by means of modelling and simulations.

Satellites provide long-term global coverage that enables ACI studies with constrained meteorology and cloud regimes (Oreopoulos et al., 2017; Douglas and L'Ecuyer, 2019; Jia et al., 2021). Satellite-based ACI studies relate cloud parameters (cloud reflectivity or albedo, cloud optical depth, cloud fraction, cloud drop effective radius, liquid water path), aerosol properties (aerosol optical depth (AOD), Ångström exponent (AE), aerosol index (AI)), and the precipitation pattern to understand the underlying mechanisms (Quaas et al., 2008, 2020; Gryspeerdt and Stier, 2012; McCoy et al., 2017; Kant et al., 2019; Liu et al., 2020; Choudhury et al., 2020). The use of AOD and (to a lesser extent) AI as CCN proxies results in a significant underestimation of the radiative forcing due to ACIs (Gryspeerdt et al., 2017; Hasekamp et al., 2019). Shinozuka et al. (2015) suggest that the satellite-derived AOD or AI, being a column-integrated product, may not be the appropriate proxies for cloud-relevant CCN particles that usually lie close to the cloud base. Moreover, Stier (2016) found a low correlation (< 0.5) between the ECHAM-HAM model-simulated AOD and CCN concentration near the cloud base and suggested the use of vertically resolved measurements from spaceborne lidar for ACI studies. The findings of Dusek et al. (2006) show that the ability of aerosols to act as CCN is predominantly dependent on their size rather than composition. This facilitates the use of satellite-derived aerosol number concentrations as accurate CCN proxies for ACI studies (Gryspeerdt et al., 2017; Hasekamp et al., 2019). The PSML003_Ocean data included in the MODIS (Moderate Resolution Imaging Spectroradiometer) ocean product give the aerosol number concentration with a radius greater than or equal to 30 nm or n_{30} (Remer et al., 2005, Appendix B). This product is formed by matching the spectral radiance measured by MODIS to the radiance estimated from a combination of the microphysical properties (size distributions and refractive indices) of nine aerosol types. However, the column-integrated n_{30} is proportional to the AOD and may not represent the atmospheric CCN particles located close to the cloud base altitudes (Shinozuka et al., 2015).

Lidar measurements provide height-resolved aerosol optical properties which are crucial to study vertically co-located aerosols and clouds (Costantino and Bréon, 2013). Mamouri and Ansmann (2015) for the first time presented the Polarization Lidar Photometer Net-

working (POLIPHON) technique to estimate INP concentrations from lidar-derived extinction coefficient for desert dust aerosols. The algorithm first converts the extinction coefficient to aerosol number concentration with radius $> 250\,\mathrm{nm}$ (n_{250}) by using conversion factors derived from the Aerosol Robotic Network (AERONET) correlation study. The INP concentration is then calculated from n_{250} using the parameterizations from DeMott et al. (2010, 2015). Mamouri and Ansmann (2016) further extend the methodology for estimating CCN concentrations at different supersaturation from lidar-derived extinction coefficient for dust, continental and marine aerosols, and more recently for aged and fresh smoke aerosols (Ansmann et al., 2021b). The POLIPHON technique to estimate CCN and INP concentrations is not only limited to ground-based lidars but can also be applied to the spaceborne lidar CALIOP (Cloud–Aerosol Lidar with Orthogonal Polarization) aboard the CALIPSO (Cloud–Aerosol Lidar and Infrared Pathfinder Satellite Observations) polar-orbiting satellite (Marinou et al., 2019; Georgoulias et al., 2020). Georgoulias et al. (2020) for the first time estimated CCN concentrations from CALIPSO measurements by using the POLIPHON technique and found good agreement with the coincident airborne in situ measurements taken during the ACEMED-EUFAR (evaluation of CALIPSO's aerosol classification scheme over the eastern Mediterranean) campaign (Tsekeri et al., 2017). This illustrates the potential of spaceborne lidar measurements to construct global 3D CCN and INP data sets.

The CALIPSO aerosol model includes a set of normalized volume size distributions (NVSDs) and refractive indices of six aerosol subtypes (Omar et al., 2009). Similar to the MODIS PSML003_Ocean algorithm, these microphysical properties along with the CALIPSO-measured aerosol optical properties can be used to derive the cloud-relevant aerosol number concentrations. In the present work, we utilize the CALIPSO aerosol model to calculate the extinction coefficient by using Mie scattering for spherical particles (continental and marine aerosols) and a combination of a T-matrix method and an improved geometric optics method for non-spherical particles (dust aerosols). We then modify the NVSD by preserving its shape (mode radii and standard deviation remain constant) until a closure is achieved between the extinction coefficient inferred from CALIPSO measurements and derived through light-scattering calculations. We finally use the modified size distribution to compute the aerosol number concentration favourable to act as CCN by using the CCN parameterizations that correspond to different aerosol types (Mamouri and Ansmann, 2016). Further, we carry out sensitivity tests by varying the initial NVSD to quantify the uncertainty associated with the retrieval algorithm. We compare our results with the existing CCN retrieval algorithm POLIPHON for different aerosol subtypes. Moreover, we present a case study where we apply our algorithm to a CALIPSO overpass over Thessaloniki and compare it with the in situ observations taken during the ACEMED-EUFAR campaign (Tsekeri et al., 2017). The approach for retrieving cloud-relevant aerosol microphysical properties has not yet been implemented for spaceborne lidar measurements. This study, therefore, presents a new methodology for obtaining height-resolved aerosol number concentrations from CALIPSO measurements within the CALIPSO framework, i.e. without relying on externally inferred conversion factors.

The paper is structured as follows. The data, optical modelling package used in this work, and a brief overview of the POLIPHON technique for retrieving CCN concentrations from lidars are described in Section 2.2.2. Section 2.2.3 describes our CCN retrieval algorithm for spaceborne lidar. The sensitivity analysis and comparison studies are presented in Section 2.2.4. We conclude the paper with a summary in Section 2.2.5.

2.2 Data and retrievals

2.2.1 CALIPSO

CALIPSO is a sun-synchronous polar-orbiting satellite launched on 28 April 2006, as a part of the afternoon or A-Train constellation (Winker et al., 2009). CALIOP is a polarization-sensitive lidar onboard CALIPSO that measures profiles of aerosol and cloud properties from an elevation of 30 km above mean sea level to the surface. The CALIPSO algorithm classifies the measured signal into aerosols, clouds, clear air, and surface and assigns a subtype to the detected aerosol signals (Omar et al., 2009). CALIPSO has a set of lidar ratios associated with each aerosol subtype. These lidar ratios are used in the CALIPSO retrieval algorithm to estimate the aerosol extinction and backscatter coefficient. In this work, we use the CALIPSO version 4.20 level 2 aerosol profile product with a uniform horizontal resolution of 5 km. Because of CALIPSO's data averaging scheme, the vertical resolution of aerosol profile data varies with altitude. It is 60 m for altitudes between 20 and -0.5 km and 180 m above 20 km. We use the profiles of aerosol extinction coefficient, backscatter coefficient, and particle depolarization ratio measured at 532 nm and the aerosol subtype information in the CCN retrieval algorithm. We also use the relative humidity profiles included in the CALIPSO data product, obtained by the Global Modelling and Assimilation Office Data Assimilation System (Molod et al., 2015).

The CALIPSO version 2 aerosol types include dust, smoke, clean continental, polluted continental, clean marine, and polluted dust. The microphysical properties of these six aerosol subtypes constitute the CALIPSO aerosol model (CAMel). The lidar ratios used in the retrieval of extinction coefficient for each aerosol type were modelled using these microphysical properties. Of the six aerosol subtypes, the properties of smoke, polluted continental, and polluted dust were obtained directly from a cluster analysis of long-term cloud-screened AERONET measurements (Omar et al., 2005). The dust model was derived from Kalashnikova and Sokolik (2002), and the clean marine model was derived from the dry measurements taken during the Shoreline Environment Aerosol Study (SEAS) campaign (Masonis et al., 2003; Clarke et al., 2003). The clean continental model was formed by adjusting the properties of the background continental aerosol cluster from Omar et al. (2005) to measurements of Anderson et al. (2000). The aerosol model has evolved with time. In version 4, a new aerosol subtype, namely the dusty marine (dust and marine), was introduced. Further, the polluted continental and smoke subtypes were renamed to polluted continental/smoke and elevated smoke, respectively (Kim et al., 2018). The lidar ratios were

also modified, leading to an increase in mean AOD by 52 % (40 %) for nighttime (daytime) retrievals, making it more comparable with MODIS-derived AOD. In our algorithm, we use the microphysical properties of five aerosol subtypes, namely marine, dust, polluted continental/smoke, clean continental, and elevated smoke. Note that the lidar ratios used in version 4 of the CALIPSO retrieval have been adjusted from earlier versions based on the findings from atmospheric measurements (Kim et al., 2018) and do not necessarily connect to the CALIPSO aerosol model. Since the changes in lidar ratio from version 2 to version 4 are minor ($\leq 1\,\%$) for all aerosol types except for clean continental (51 %), we believe the aerosol model can still be used in our algorithm. However, for the case of the clean continental aerosol subtype, further study is required to estimate the effect of change in lidar ratio on its microphysical properties. Having said that, we do not exclude it from our analysis for the completeness of our algorithm, leaving a scope of future validation study to examine its applicability in estimating the CCN concentrations from CALIPSO.

2.2.2 MOPSMAP

The modelled optical properties of ensembles of aerosol particles (MOPSMAP) package provides the aerosol optical properties of arbitrary, randomly oriented spherical or spheroidal particle ensembles for size parameters ranging up to 1000 and a refractive index range of [0.1, 3.0] and [0, 2.2] for real and imaginary parts, respectively (Gasteiger and Wiegner, 2018). It includes a data set of pre-calculated aerosol optical properties and a Fortran program, which estimates the properties of user-defined aerosol ensembles. The optical properties of spherical particles are modelled using Mie scattering. While for spheroids, based on the aerosol size parameter, MOPSMAP uses a combination of the T-matrix method and improved geometric optics method (IGOM). MOPSMAP has been used to simulate the optical properties of different aerosol types such as mineral (silica and alumina) and ash aerosols (Jiang et al., 2021) and Martian dust aerosols (Chen-Chen et al., 2021). We apply the MOPSMAP package to model the aerosol extinction coefficient of different aerosol subtypes with the bimodal log-normal volume size distributions and refractive indices from CAMel. The details of the MOPSMAP input parameters are discussed in the methodology section.

2.2.3 POLIPHON

The POLIPHON technique enables the retrieval of aerosol number concentration by combining the ability of polarization lidar to measure aerosol-type-specific optical properties with long-term AERONET measurements of aerosol microphysical properties and AOD (Shinozuka et al., 2015; Mamouri and Ansmann, 2015, 2016). It converts the lidar-derived extinction coefficient (α in km^{-1}) to number concentration of aerosols with a dry radius greater than 100 nm ($n_{100,\mathrm{dry}}$) for dust aerosols and greater than 50 nm ($n_{50,\mathrm{dry}}$) for marine and continental aerosols as

Table 2.1: POLIPHON conversion factors (C) and extinction exponents (x) for different aerosol subtypes.

Type	C	x	Source
Dust	8.855	0.7525	(Ansmann et al., 2019)
Continental	25.3	0.94	(Mamouri and Ansmann, 2016)
Marine	7.2	0.85	(Mamouri and Ansmann, 2016)
Smoke	17	0.79	(Ansmann et al., 2021b)

$$n_{j,\mathrm{dry}} = C \cdot \alpha^{x}(z), \tag{2.1}$$

where $n_{j,\mathrm{dry}}$ represents the total aerosol concentration with a dry radius greater than j nm, C is the conversion factor ($\mathrm{cm}^{-3}\mathrm{Mm}$), and x is the aerosol extinction exponent. The value of j is 50 nm for continental and marine aerosols and 100 nm for dust aerosols. The constants C and x are calculated from the regression analysis of AERONET measurements, and their values used in this work are listed in Table 2.1.

The CCN concentration at a certain supersaturation is estimated from the aerosol number concentration as

$$n_{\mathrm{CCN}} = f_{\mathrm{ss}} \cdot n_{j,\mathrm{dry}}, \tag{2.2}$$

where $f_{\mathrm{ss}} = 1.0$, 1.35, and 1.7 for supersaturations of 0.15 %, 0.25 %, and 0.40 %, respectively. In this study, we use the conversion factors and extinction exponents for continental and marine aerosols from Mamouri and Ansmann (2016). For dust aerosols, we use the globally averaged values as suggested by Ansmann et al. (2019) for application to satellite data. For smoke aerosols, we use the aged smoke conversion factor and extinction exponent values from Ansmann et al. (2021b).

2.3 Methodology

This section describes the algorithm used in the present work to derive CCN concentrations from the CALIPSO profiles of extinction coefficient, backscatter coefficient, depolarization ratio, and aerosol subtype information. We begin with the scaling procedure of the normalized size distributions from CAMel to obtain the actual aerosol size distribution. After that, we explain the hygroscopicity correction followed by the CCN parameterization adopted in our algorithm. Finally, we discuss the application of the CCN retrieval algorithm to CALIPSO level 2 aerosol profile data.

2.3.1 Aerosol size distribution

The remote sensing of aerosol number concentration requires an initial assumption of aerosol microphysical properties (size distribution and refractive index). For instance, the MODIS

algorithm over the ocean uses a combination of nine predefined aerosol size distributions and refractive indices and selects the one for which the difference in the measured and modelled radiance is minimum (Remer et al., 2005, Appendix B). In our study, we use the aerosol microphysical properties from CAMel and adopt a two-step algorithm to derive the aerosol size distribution: (i) select the appropriate initial normalized volume size distribution and refractive index, and (ii) scale the size distribution as per the CALIPSO-measured extinction coefficient. In contrast to MODIS, the aerosol type in CALIPSO is set prior to the computation of the extinction coefficient. This eases the selection of initial aerosol microphysics, which can now be done directly from CAMel as per the aerosol subtype information included in the CALIPSO retrieval.

The next step is to scale the NVSD as per the CALIPSO-measured extinction. The extinction coefficient (α) for a certain incident wavelength can be described as

$$\alpha = \int_{r_{\min}}^{r_{\max}} \frac{K_\alpha(m,r)}{V(r)} \cdot \frac{dV(r)}{d\ln r} \cdot d\ln r, \tag{2.3}$$

where r is the particle radius; $V(r)$ is the volume of the particle with radius r; K_α is the extinction cross-section which is a function of the complex refractive index (m) and r; and $dV(r)/d\ln r$ is the log-normal volume size distribution, which for a bimodal case can be given by

$$\frac{dV(r)}{d\ln r} = V_{\mathrm{t}} \cdot \sum_{i=1}^{2} \frac{\nu_i}{\sqrt{2\pi}\ln\sigma_i} \exp\left(\frac{-(\ln r - \ln\mu_i)^2}{2\ln{\sigma_i}^2}\right). \tag{2.4}$$

Here, ν_i, σ_i, and μ_i are the volume fractions, geometric standard deviations, and geometric mean radii of the i^{th} mode, respectively. V_{t} is the total volume of the size distribution. The above size distribution is normalized when $V_{\mathrm{t}} = 1$. Substituting Eq. (2.4) in Eq. (2.3), we get

$$\alpha = V_{\mathrm{t}} \cdot \int_{r_{\min}}^{r_{\max}} \frac{K_\alpha(m,r)}{V(r)} \cdot \sum_{i=1}^{2} \frac{\nu_i}{\sqrt{2\pi}\ln\sigma_i} \exp\left(\frac{-(\ln r - \ln\mu_i)^2}{2\ln{\sigma_i}^2}\right) \cdot d\ln r. \tag{2.5}$$

Thus, the extinction coefficient is a function of the size distribution parameters (V_{t}, ν_i, σ_i, and μ_i) and the extinction cross section (K_α). Out of these parameters, under ideal conditions, only V_{t} is an extensive property, while the rest are intensive and independent of aerosol amount or concentration (Omar et al., 2005). Eq. (2.5) can be simplified to

$$\alpha = V_{\mathrm{t}} \cdot \alpha_{\mathrm{n}}, \tag{2.6}$$

where α_{n} is the normalized extinction coefficient corresponding to the NVSD. If we consider α as the CALIPSO-measured extinction, V_{t} would be the scaling factor for the NVSD to compute the actual aerosol size distribution. From Eq. (2.6), we can compute V_{t} if the value of α_{n} is known.

We estimate α_{n} for each aerosol subtype by using the NVSDs and refractive indices from CAMel as input to the MOPSMAP optical modelling package. In the MOPSMAP input, we consider dust as spheroids and use the axis ratio distribution from Dubovik et al. (2006)

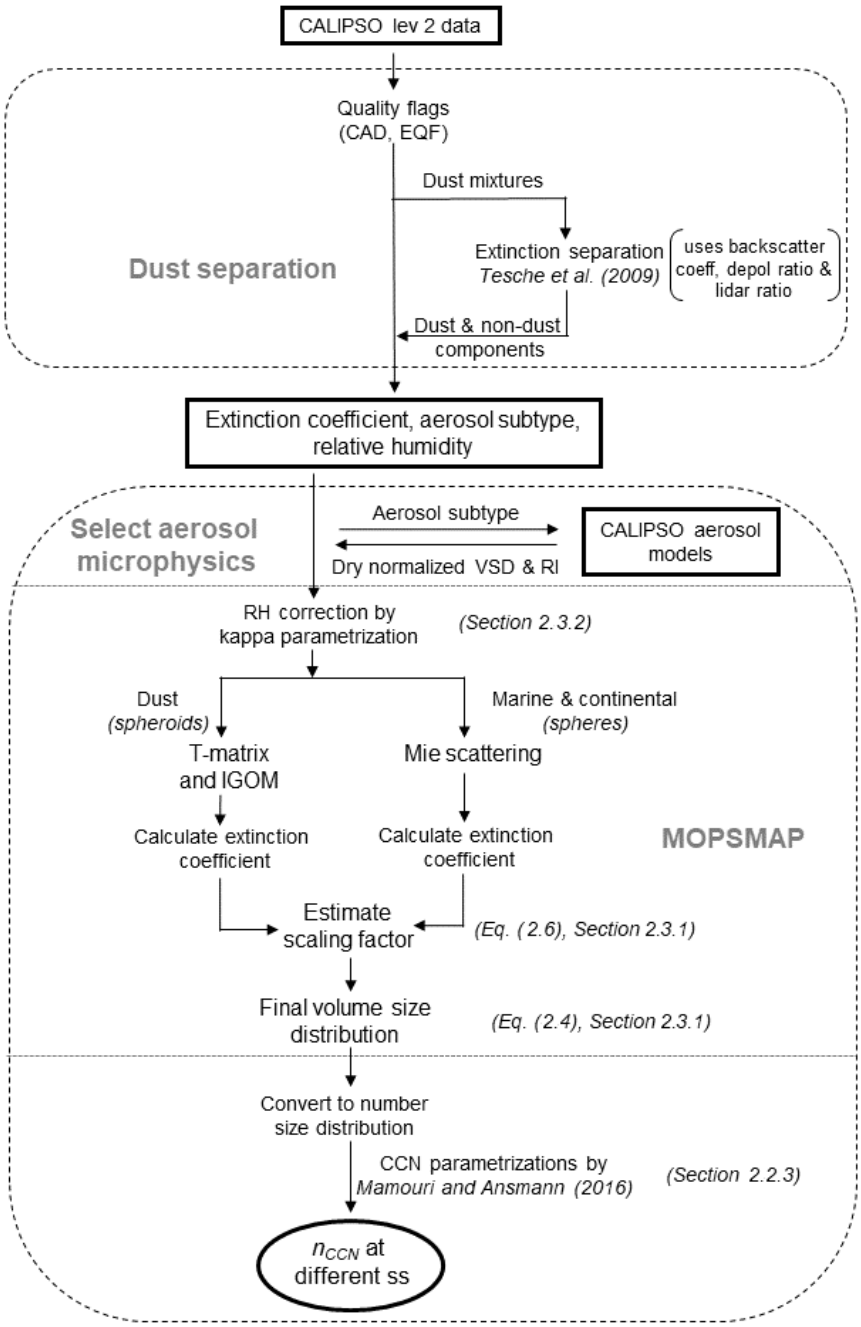

Figure 2.1: Flowchart of the OMCAM algorithm illustrating important steps involved in retrieving CCN concentrations from CALIPSO level 2 aerosol profile data. The upper part describes the pre-processing to infer information on the extinction coefficient, aerosol subtype, and the relative humidity. These parameters form the input to the CCN retrieval part which is outlined in the lower part. The chart also refers to the used equations and the sections in which specific parts are discussed.

(also used in the AERONET inversion). Other aerosol subtypes are considered spheres. We then compute V_t from the ratio of α and α_n (Eq. 2.6). On multiplying V_t with the

NVSD, we get the final scaled aerosol size distribution. Since the algorithm principally relies on the optical modelling of CALIPSO aerosol microphysics, we hereafter refer to it as OMCAM.

2.3.2 Aerosol hygroscopicity

The hygroscopic aerosol particles in the atmosphere can uptake water and grow in moist conditions. The hygroscopic growth needs to be accounted for before deriving the CCN concentrations. We consider continental (clean continental, polluted continental/smoke and elevated smoke) and marine aerosols as hygroscopic. We assume dust aerosols to be hydrophobic in accordance with previous studies (Mamouri and Ansmann, 2016; Ansmann et al., 2019). The hygroscopicity correction can be applied either to the ambient extinction coefficient measured by CALIPSO or to the initial NVSD in the retrieval algorithm. We consider the latter approach and modify the initial NVSD before modelling the extinction coefficient. There is an inbuilt functionality in the MOPSMAP package to account for the hygroscopicity using the kappa parameterization scheme (Petters and Kreidenweis, 2007; Zieger et al., 2013) as

$$\frac{r_{\mathrm{wet}}(\mathrm{RH})}{r_{\mathrm{dry}}} = \left(1 + \kappa \cdot \frac{\mathrm{RH}}{100 - \mathrm{RH}}\right)^{\frac{1}{3}}, \tag{2.7}$$

where RH is the relative humidity, and κ is the hygroscopic growth parameter. The r_{min}, r_{max}, and μ of the log-normal size distribution (Eq. 2.5) are multiplied with this ratio whereas the standard deviation (σ) remains unchanged. The refractive index of the hygroscopic aerosol is also modified following the volume-weighting rule (Gasteiger and Wiegner, 2018). The κ value is set to be 0.3 for continental and 0.7 for marine aerosols. The values are global averages and are suggested by Andreae and Rosenfeld (2008).

2.3.3 CCN parameterizations

We use the parameterizations listed in Mamouri and Ansmann (2016) to estimate CCN concentrations from the dry aerosol number concentration. The final scaled aerosol volume size distribution obtained from the scaling procedure is first converted to number size distribution. The number size distribution is integrated starting at 50 or 100 nm to compute $n_{50,\mathrm{dry}}$ or $n_{100,\mathrm{dry}}$ depending on the aerosol type. Finally, substituting the values in Eq. (2.2) results in the required CCN concentration at different supersaturations.

2.3.4 Application of OMCAM to CALIPSO retrieval

Figure 2.1 outlines the OMCAM retrieval algorithm for estimating CCN concentrations from CALIPSO measurements. In order to apply the OMCAM algorithm to CALIPSO level 2 version 4.20 data, we first start by pre-processing the data set. To begin with, we apply all the quality filters listed in Tackett et al. (2018, Table 1). The CALIPSO aerosol

typing algorithm consists of dust mixtures (dusty marine and polluted dust). In such a case, we separate the dust and non-dust extinction coefficients by using the methodology given in Tesche et al. (2009). This is a rather simple and accepted dust separation technique also used by Mamouri and Ansmann (2015, 2016) for lidar-based CCN retrieval. It uses the particle depolarization ratio (δ_{p}) to separate the particle backscatter coefficient (β_{p}) into dust (β_{d}) and non-dust (β_{nd}) contributions. β_{d} can be calculated as

$$\beta_{\mathrm{d}} = \beta_{\mathrm{p}} \frac{(\delta_{\mathrm{p}} - \delta_2)(1 + \delta_1)}{(\delta_1 - \delta_2)(1 + \delta_{\mathrm{p}})}, \tag{2.8}$$

where the values of δ_1 and δ_2 are 0.31 and 0.05, respectively. The aerosol mixture is assumed to be pure dust (non-dust) when $\delta_{\mathrm{p}} > 0.31$ (< 0.05). When $0.05 \leq \delta_{\mathrm{p}} \leq 0.31$, we first estimate β_{d} from Eq. (2.8) and then calculate β_{nd} by subtracting β_{d} from β_{p}. We compute the dust and non-dust extinction coefficient by multiplying the backscatter coefficient by the respective lidar ratio. The lidar ratios of dust, polluted continental and clean marine aerosol subtypes are taken from Kim et al. (2018) and are equal to 44, 70, and 23, respectively. The extinction coefficient of polluted dust is separated into polluted continental/smoke and dust, while that of dusty marine is separated into dust and marine contributions. Finally, the extinction coefficient, relative humidity, and aerosol subtype information is passed to the CCN retrieval algorithm.

In the CCN retrieval part, we first select the normalized size distribution and refractive index as per the aerosol subtype and modify them as per the RH value so as to account for the hygroscopicity of aerosols. In the next step, we model the extinction coefficient using the MOPSMAP package and calculate V_{t} from Eq. (2.6). Multiplying V_{t} by the initial dry normalized size distribution gives the final dry aerosol size distribution which is used in the CCN parameterizations (Eq. 2.2) to estimate the CCN concentrations at different supersaturation values. This methodology is applied to every bin of the CALIPSO profile. In the case of dust mixtures, the separated dust and non-dust extinction coefficients are passed through the CCN retrieval algorithm individually, and the results are finally added to compute the net CCN concentration for that bin. It is worthwhile to note that this algorithm can in principle be used to derive INP concentration from CALIPSO measurements. This can be done by first estimating n_{250} from the modified size distribution (Section 2.3.1) and then using the INP parameterizations (DeMott et al., 2010, 2015) to estimate INP concentrations. However, in the present study, we limit our focus to retrieving the CCN concentrations.

2.4 Results

2.4.1 Sensitivity analysis

The performance of OMCAM in retrieving CCN concentrations primarily relies on the initial NVSD given in CAMel. The aerosol size distributions may change depending on the

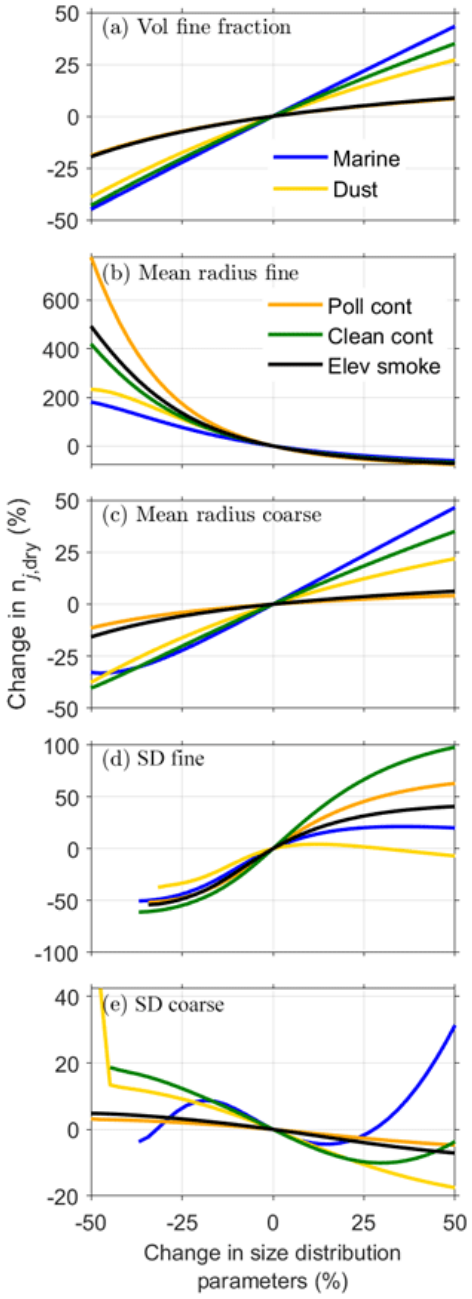

Figure 2.2: Sensitivity of $n_{j,\mathrm{dry}}$ ($j = 100$ for dust and 50 for other aerosol subtypes) to the size distribution parameters: volume fine fraction (a), mean radius fine (b), mean radius coarse (c), standard deviation fine (d), and standard deviation coarse (e). The x axis represents perturbations in the size distribution parameters in percentage of their original values taken from the CALIPSO aerosol model. The y axis represents the corresponding percentage change in $n_{j,\mathrm{dry}}$ relative to that estimated from the unperturbed size distribution.

age and composition of aerosols (region and type dependent) and the ambient meteorology. As most of the size distributions used in CAMel are derived from cluster analysis of the long-

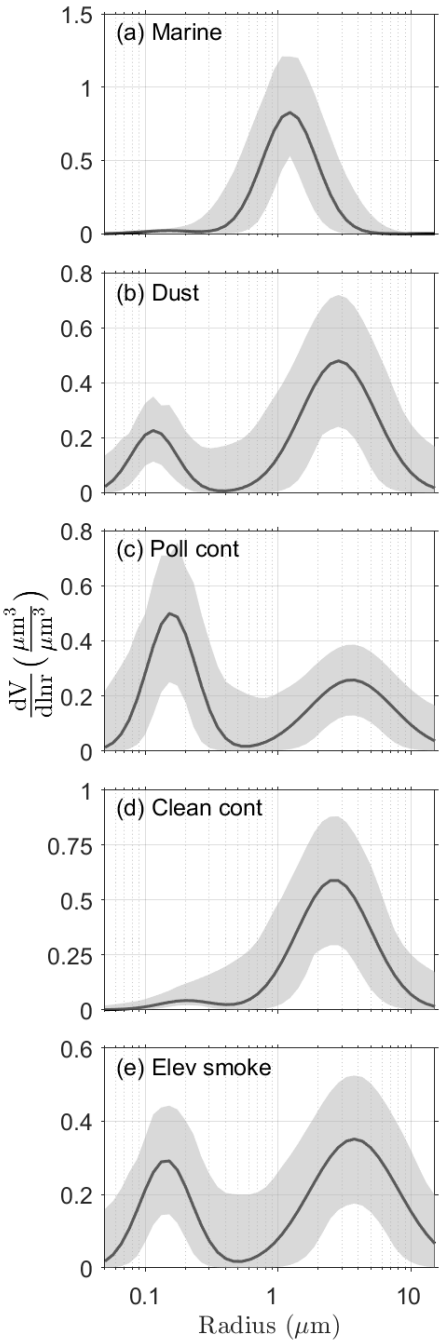

Figure 2.3: Normalized bimodal log-normal volume size distributions for marine (a), dust (b), polluted continental (c), clean continental (d), and elevated smoke (e) aerosol subtypes adopted from the CALIPSO aerosol model. The shaded region represents the input space along with the maximum and minimum limits of size distributions selected for the sensitivity analysis

term AERONET measurements (see Section 2.2.1), they incorporate the errors associated with the AERONET inversion algorithm. Dubovik et al. (2000) found that the relative error in the AERONET-retrieved volume size distribution for dust, biomass burning, and water-

soluble aerosols can go beyond 50 % for both small ($r < 0.1\,\mu m$) and large ($r > 7\,\mu m$) particles. In order to account for such errors and natural variability, we analysed the sensitivity of CCN concentrations to the initial normalized size distributions considered in our retrieval algorithm.

For each aerosol subtype, the initial NVSD can be perturbed by changing the size distribution parameters such as the volume fractions (ν_f & ν_c), geometric standard deviations (σ_f & σ_c), and mean radii (μ_f & μ_c) of fine and coarse modes. Since the sum of the volume fractions is unity, this leads to five independent size distribution parameters. We first study the individual effects of varying these parameters on the output $n_{j,\mathrm{dry}}$ ($j = 100$ for dust and 50 for other aerosol subtypes) as they are the main input to the CCN parameterizations. Figure 2.2 depicts the effect of varying these size distribution parameters by $\pm 50\,\%$ on the $n_{j,\mathrm{dry}}$ relative to that of unperturbed size distributions from CAMel for a preset $\alpha = 0.1\,\mathrm{km}^{-1}$ and $\mathrm{RH} = 0$ for different aerosol subtypes. The results show fine mode as the primary contributor to the output aerosol number concentration. A certain change in the volume size distribution in the fine mode will have a larger impact on the number concentration compared to the coarse mode as a much larger number of small particles is needed to produce the same change in volume. Out of the five parameters, μ_f has the maximum effect ($\approx 800\,\%$) on the output number concentration, followed by σ_f ($\approx 150\,\%$). This is because both μ_f and σ_f modify the distribution of volume across different radii in the fine-mode. Decreasing (increasing) μ_f shifts the fine mode towards a smaller (larger) radius thereby resulting in a comparatively larger (smaller) number of particles for a constant fine mode volume. However, for dust, the effect is opposite when μ_f is decreased. This is because the minimum cut-off radius for dust is set to be 100 nm and the fine mode moves out of this limit when μ_f is reduced leading to a decrease in the output number concentration. Increasing (decreasing) σ_f leads to an increase (decrease) in the fraction of smaller particles within the fine mode. This results in an increase (decrease) in the output number concentration for all aerosol subtypes except dust. The output number concentration is comparatively less sensitive to coarse-mode parameters (μ_c & σ_c), as they contribute primarily to the optical properties of the aerosol volume rather than the number concentration. When we change the value of α, the aerosol number concentration scales as per the ratio between α and α_n, resulting in no change in the relative $n_{100,\mathrm{dry}}$ and $n_{50,\mathrm{dry}}$.

The size distributions formed by varying the size distribution parameters separately may not be sufficient enough to capture the natural variability. Thus to imitate the natural variability in a better way, we further consider combinations of the variations in all the parameters. We do not expect extreme shifts in the size distribution parameters as well. For instance, reducing μ_f by 50 % results in abnormal size distributions with 30 %-50 % of the fine mode moving out of the AERONET size limits ($0.05 \leq r \leq 15\,\mu m$). Therefore, in order to exclude the non-physical size distributions, we limit the variations in the parameters in terms of the actual volume size distributions. To implement these constraints, we first vary the size distribution parameters linearly with a uniform spacing of 0.01 and then consider all possible combinations of the variations. The NVSDs generated from all the combinations

form the input NVSD set for the sensitivity analysis. We further fix the maximum limits of bimodal NVSD to $\pm 50\,\%$ of the amplitude of each of its modes and do not consider the NVSDs that fall outside this domain in the sensitivity studies. The resulting input NVSD space for each aerosol type is shown by the shaded region of Figure 2.3. The maximum and minimum values of all the size distribution parameters considered in the sensitivity analysis are given in Table 2.2.

Table 2.2: Bimodal log-normal volume size distribution parameters along with their limits considered in the sensitivity analysis. Abbreviations: VF - volume fraction, MR - mean radius, GSD - geometric standard deviation, CAM - CALIPSO aerosol microphysics.

Aerosol subtype	**Size distribution parameters**														
	VF fine			**MR fine**			**MR coarse**			**GSD fine**			**GSD coarse**		
	CAM	min	max	CAM	min	max	CAM	min	max	CAM	min	max	CAM	min	max
Clean marine	0.025	0.001	0.035	0.150	0.101	0.227	1.216	0.815	1.824	1.600	1.376	2.56	1.60	1.376	1.76
Dust	0.223	0.114	0.332	0.116	0.083	0.164	2.833	1.615	4.249	1.481	1.304	2.192	1.908	1.545	3.625
Polluted cont.	0.531	0.235	0.703	0.158	0.109	0.227	3.547	1.88	5.321	1.526	1.327	2.319	2.065	1.631	4.13
Clean cont.	0.050	0.001	0.069	0.206	0.136	0.310	2.633	1.501	3.950	1.61	1.385	2.592	1.899	1.538	3.589
Elevated smoke	0.329	0.168	0.49	0.144	0.098	0.211	3.726	1.938	5.589	1.562	1.359	2.437	2.143	1.671	4.285

As we have kept a constant spacing for varying the size distribution parameters, the number of NVSDs in the input space directly depends on the volume of particles present in each mode. While it is minimum for the clean marine subtype because of its almost non-existent fine mode (which reduces the range of variation), it is maximum for polluted continental and elevated smoke subtypes. The output ensembles of number concentrations for an extinction coefficient of $0.1\,\mathrm{km}^{-1}$ and relative humidity of $0\,\%$ are shown in the violin plots of Figure 2.4. The percentiles of the output $n_{j,\mathrm{dry}}$ set are given in Table 2.3. The number concentration of the output ensemble is primarily dependent on the fine mode of the input size distributions. The variations in the output ensemble relative to the output from unperturbed NVSD from CAMel is minimum (about a factor of 1) for dust mainly because we only consider particles with a radius $> 0.1\,\mu\mathrm{m}$. For clean marine, the spread is about a factor of 2 (95^{th} percentile; $200\,\%$). However, for polluted continental and elevated smoke, the output ensemble is bimodal. For the first mode, the values can go up to a factor of 1.5 for polluted continental and around 1 for elevated smoke. The second mode is relatively small and is related to the size distributions whose fine-mode mean radii are shifted to low values (extreme left in Figure 2.2). For this mode, the values can go up to a factor of 3 for polluted continental and 2.5 for elevated smoke. The largest spread in the output ensemble is found for clean continental (95^{th} percentile; factor of 2.7). This might be because the bimodality of the NVSD is not well defined for the clean continental aerosol subtype, thereby increasing the input space of variation. Neglecting the long tail of the distribution, we can assume the uncertainty due to the initial NVSD to be about a factor

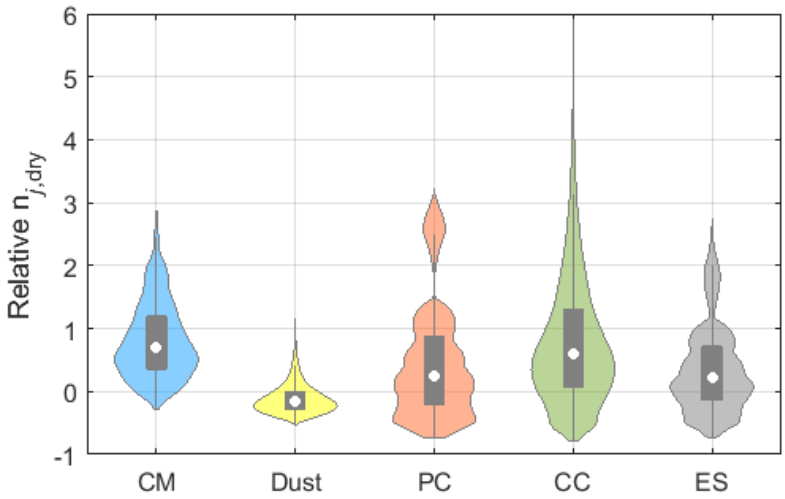

Figure 2.4: Violin plots for the output ensemble of $n_{j,\mathrm{dry}}$ ($j = 100$ for dust and 50 for other aerosol subtypes) relative to that of unperturbed NVSD from the CALIPSO aerosol model. The filled shape shows the probability density of the data (smoothed by non-parametric kernel density estimator) along the y axis, symmetric on either side, representing a violin-like shape. The box limits represent the first and third quartiles, the white circle inside the box is the median, and the ends of the grey line passing through the centre of the box represent the adjacent values (data excluding outliers). Abbreviations: CM - clean marine, PC - polluted continental, CC - clean continental, and ES - elevated smoke.

Table 2.3: Percentiles of output $n_{j,\mathrm{dry}}$ ensembles estimated from the sensitivity analysis relative to that of the unperturbed case.

Aerosol subtype	Percentiles of output $n_{j,\mathrm{dry}}$ ensembles relative to unperturbed (%)			
	5^{th}	25^{th}	75^{th}	95^{th}
Clean marine	0.044	35.8	119.25	194.05
Dust	-41.30	-28.54	-0.68	34
Polluted continental	-56.26	-20.77	88.15	259.38
Clean continental	-49.02	7.56	130.04	275
Elevated smoke	-52.23	-14.16	71.68	183.55

of 2.

We have also estimated the effect of change in RH on the output ensemble of $n_{100,\mathrm{dry}}$ and $n_{50,\mathrm{dry}}$ (not shown). Increasing RH decreases the spread of the output ensemble slightly, with a significant decrease for RH $> 90\,\%$ except for dust which is assumed to be hydrophobic. At RH $= 99\,\%$, the bi-modality of polluted continental and elevated smoke subtypes disappears. The variations in the relative number concentrations decrease to less than a factor of 2 for all subtypes. This might be a result of the decrease in the absolute number

concentration, as the particle size increases with RH, and fewer particles are needed to produce the same extinction. At a constant RH value, when α is modified, the output ensemble of aerosol number concentrations scales as per the ratio between α and α_{n} resulting in no change in the relative $n_{100,\mathrm{dry}}$ and $n_{50,\mathrm{dry}}$ (not shown). To summarize, if we neglect the contributions of extreme shifts in the size distribution (i.e., the long tails in the violin plots) and consider the effect of RH, we can assume that the overall uncertainty in the retrieval algorithm due to the initial NVSD is likely to range between a factor of 1.5 and 2.5.

Uncertainties in the OMCAM algorithm can also arise from the uncertainty in the CALIPSO measurements, the CCN parameterization, and the hygroscopicity parameterization. The CALIPSO-retrieved extinction coefficient can have an uncertainty of up to 30 % (Omar et al., 2009; Kim et al., 2018). The ability of aerosol to act as CCN depends on the composition, size, and atmospheric supersaturation value. In situations with complex aerosol mixtures and variable updraught velocity, the simple CCN parameterization developed by Mamouri and Ansmann (2016) may fail. The κ values used to account for the hygroscopicity are global averages and may vary regionally depending on the aerosol source, composition and age. Moreover, the hydrophobic approximation for dust may not work for cases in which dust is coated or mixed with soluble aerosols (Mamouri and Ansmann, 2016). In such a case, dust aerosols with a dry radius > 50 nm can also act as CCN (Mamouri and Ansmann, 2016). Furthermore, aerosol misclassification in the CALIPSO aerosol-typing scheme (Ansmann et al., 2021a) may introduce errors in the OMCAM algorithm. Accounting for the mentioned possibilities, we assume that the overall uncertainty in our retrieval algorithm is likely to range between a factor of 2 and 3. It is comparable to the uncertainty in POLIPHON retrieval. However, OMCAM incorporates additional uncertainties due to the hygroscopicity correction. Studies have found that the conversion factors used in the POLIPHON technique for dust and smoke aerosols vary with the source region and the age of aerosols (Ansmann et al., 2019, 2021b). Such factors further increase the uncertainties associated with the retrieval algorithm when applied to satellite or global data sets.

2.4.2 Comparison with POLIPHON

In this section, we present a theoretical comparison of the CCN concentrations estimated using the OMCAM and POLIPHON methods (Mamouri and Ansmann, 2016). Both algorithms' primary input is the aerosol-type-specific extinction coefficient. Hence, we consider a range of extinction coefficients and compute the corresponding theoretical CCN concentrations with both algorithms. To estimate CCN concentrations with POLIPHON, we use the extinction-to-CCN conversions given in Eq. (2.1). The ratio between the CCN concentrations estimated using POLIPHON ($\mathrm{CCN_{POLI}}$) and OMCAM ($\mathrm{CCN_{OMCAM}}$) algorithms for varying extinction coefficients at a supersaturation of 0.15 % and zero relative humidity is shown in Figure 2.5. The continental aerosols in POLIPHON represent a mixture of urban haze, biomass burning, road dust, and biological particles (Mamouri and Ansmann,

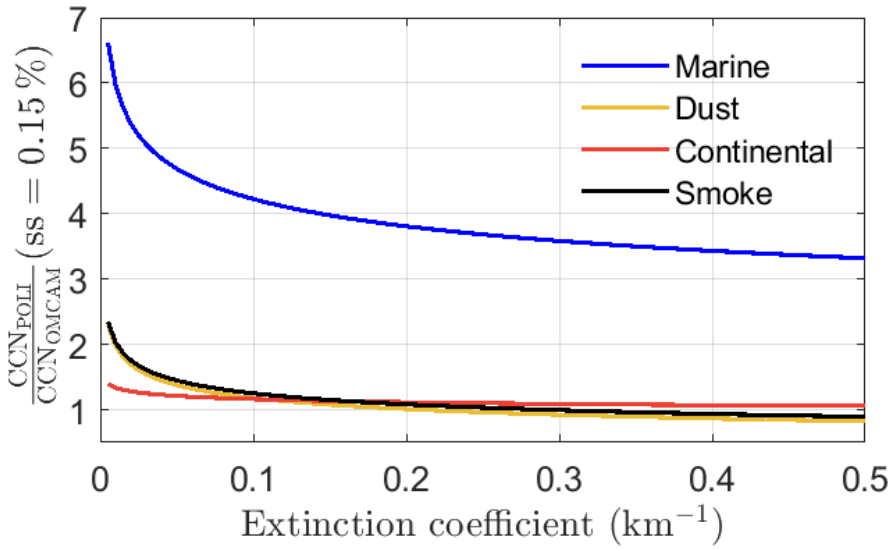

Figure 2.5: Ratio of $CCN_{ss=0.15}$ estimated from POLIPHON and OMCAM algorithms for varying extinction coefficient for marine, dust, continental, and smoke aerosol subtypes.

2016). Thus we compare it with the polluted continental aerosol subtype of CALIPSO. For continental aerosols, CCN_{POLI} and CCN_{OMCAM} are comparable, with the former always being larger than the latter. For smoke aerosols, both the algorithms yield similar values for $\alpha > 0.05\,km^{-1}$. For $\alpha < 0.05\,km^{-1}$, the POLIPHON values can be up to 2 times larger than those of OMCAM. The CCN concentrations estimated from both the algorithms yield similar results for dust as well, with comparable values for $\alpha > 0.1\,km^{-1}$ and increasing disparity for decreasing α below $0.05\,km^{-1}$. In the derivation of the conversion factors and extinction exponents in the POLIPHON method by regression analysis, the sample size for $AOD < 0.05$ is either zero for dust (Ansmann et al., 2019) or limited for smoke aerosols (Ansmann et al., 2021b). It might be a reason behind the difference between the CCN_{POLI} and CCN_{OMCAM} for smoke and dust aerosols for $\alpha < 0.05\,km^{-1}$. However, for the case of marine aerosols, the values estimated using POLIPHON are significantly larger than those of OMCAM (up to 6 times). This may be due to the different approaches followed and sample sizes considered to derive the size distributions used in the two algorithms. The POLIPHON conversion factor for marine aerosol is estimated from 7.5 years of measurements between 2007 and 2015 at the Barbados AERONET site (Mamouri and Ansmann, 2016). In contrast, the marine model used in OMCAM is derived from in-situ measurements of sea-salt size distributions produced from breaking waves, taken during the SEAS experiment at Bellows Air Force Station, Oahu, Hawaii between 21 and 30 April 2000 (Masonis et al., 2003; Clarke et al., 2003). Studies found that the AERONET size distributions can be significantly different from the in-situ measurements – especially under high-relative-humidity conditions (Chauvigné et al., 2016; Schafer et al., 2019). Further studies involving type-specific comparisons of both the aerosol number concentrations and the CCN concentrations with in-situ measurements are required to test the reliability of both algorithms

(Mamali et al., 2018). When it comes to ease of application, the POLIPHON method with its simple extinction-to-CCN conversion is more straightforward while the OMCAM algorithm – at the present stage – is more complex and computationally expensive. Despite the complexities, OMCAM incorporates a hygroscopicity correction methodology which is essential for a CALIPSO-based CCN retrieval (Georgoulias et al., 2020). Furthermore, the computation time in the OMCAM algorithm can be drastically reduced by either (i) parameterizing the output CCN concentrations in terms of the type-specific extinction coefficient and RH values or (ii) creating a look-up table of CCN concentrations at different extinction coefficients and RH values for different aerosol subtypes. However, such developments are not within the scope of the present work which focuses on the theoretical description of the OMCAM algorithm.

2.4.3 Case study

In this section, we compare the profiles of aerosol number concentrations derived using the OMCAM and POLIPHON algorithms with the in-situ observations taken during the ACEMED-EUFAR campaign (evaluation of CALIPSO's aerosol classification scheme over the eastern Mediterranean). Specifically, we use the $n_{50,\mathrm{dry}}$ concentrations estimated from the in-situ measurements taken on 9 September 2011 at 00:05-01:50 UTC over land and sea surface around Thessaloniki given in Tsekeri et al. (2017, Table 3, 5) (hereafter referred to as T17). The airborne in-situ measurements coincide in space and time with the CALIPSO nighttime overpass at 00:40 UTC over Thessaloniki. Georgoulias et al. (2020) (hereafter written as G20) applied the POLIPHON method to the overlapping CALIPSO measurements and estimated the CCN concentrations at a supersaturation of 0.15 % ($n_{100,\mathrm{dry}}$ for dust and $n_{50,\mathrm{dry}}$ for continental and marine aerosols) for comparison with the in-situ measurements from T17. We apply the OMCAM algorithm to the same CALIPSO overpass and compute the $n_{50,\mathrm{dry}}$ concentrations. The results are discussed in the following.

The profiles of CALIPSO-measured extinction coefficient, aerosol subtype, and the $n_{50,\mathrm{dry}}$ concentration calculated from the OMCAM algorithm for the CALIPSO overpass over Thessaloniki on 9 September 2011, are shown in Figure 2.6. Over the land areas (latitude from 40.6°–41.2°N), the CALIPSO aerosol typing algorithm identifies the presence of elevated smoke and polluted continental aerosols (Figure 2.6b). However, for retrieving the extinction coefficient for polluted continental aerosol layer, the lidar ratio was modified and, thus, is not considered in our present comparison (not shown). The presence of smoke over the land region was also identified by T17. The CALIPSO-measured extinction coefficient over land is highly variable in space, ranging from $0.07\,\mathrm{km}^{-1}$ to as high as $\approx 3\,\mathrm{km}^{-1}$ in the proximity of cloud. The OMCAM-estimated $n_{50,\mathrm{dry}}$ correspondingly varies from $617\,\mathrm{cm}^{-3}$ to $40000\,\mathrm{cm}^{-3}$. Over the sea region (latitude from 40°–40.6°N), T17 detected the presence of elevated smoke plumes. This was not detected by the aerosol typing algorithm of earlier version 3 CALIPSO data used in T17. However, with the modifications of version 4 used in this work, CALIPSO successfully detects elevated smoke, marine, and dust aerosols with elevated smoke being the dominant one. The overall extinction coefficient along with

its variability over the sea area is lower compared to land, with the values ranging from $0.026\,\mathrm{km}^{-1}$ to $0.36\,\mathrm{km}^{-1}$. The corresponding OMCAM-estimated $n_{50,\mathrm{dry}}$ concentrations vary from $33\,\mathrm{cm}^{-3}$ to $5000\,\mathrm{cm}^{-3}$.

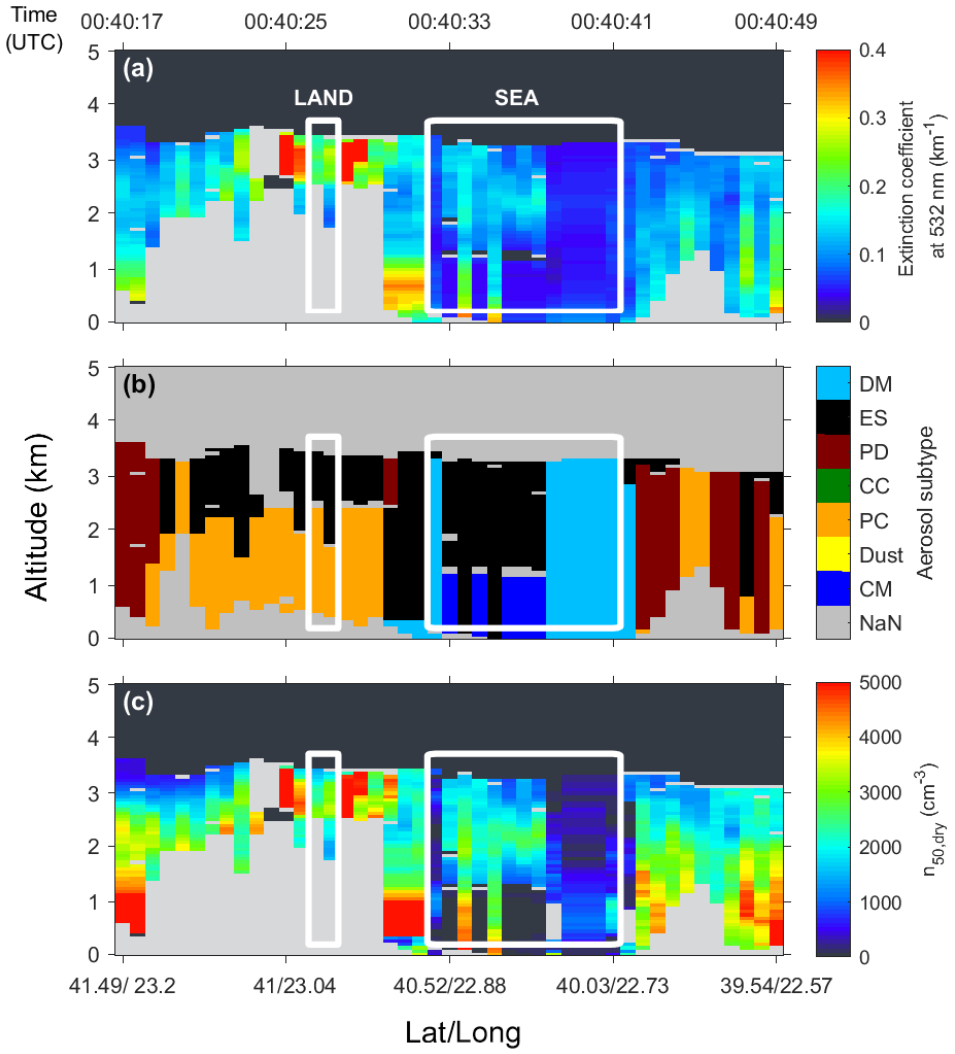

Figure 2.6: Plot of extinction coefficient (a), aerosol subtype mask (b), and the OMCAM estimated $n_{50,\mathrm{dry}}$ concentrations (c) for a CALIPSO overpass over the Thessaloniki region of northern Greece on 9 September 2011. The white lines mark the land ($40.85° - 40.95°N$) and sea ($40° - 40.6°N$) regions for which the in-situ observations at different altitudes are provided by Tsekeri et al. (2017). The grey color represents invalid values (NAN). Abbreviations: CM - clean marine, PC - polluted continental, CC - clean continental, PD - polluted dust, ES - elevated smoke, and DM - dusty marine.

T17 estimated the $n_{50,\mathrm{dry}}$ at different altitudes over the land region corresponding to two 5 km cloud-free segments of CALIPSO retrieval with latitudes between 40.85°N and 40.95°N. The average $n_{50,\mathrm{dry}}$ concentration estimated for the selected CALIPSO segments over land using OMCAM and POLIPHON (taken from G20) is plotted along with the in-situ

measurements from T17 in Figure 2.7a, and the values are listed in Table 2.4. On average, when no hygroscopicity correction is applied, the OMCAM and POLIPHON overestimate the $n_{50,\mathrm{dry}}$ concentration by 355 % and 370 %, respectively. A similar result from OMCAM and POLIPHON is expected given that elevated smoke was the dominant aerosol type over the land with extinction coefficient $> 0.1\,\mathrm{km}^{-1}$, for which both the algorithms yield a similar result (Figure 2.5). Upon accounting for the hygroscopic growth, the overestimation decreases to 167 % (130 % for POLIPHON). Note that the RH-corrected POLIPHON values in G20 are produced by using the in-situ dry to ambient extinction coefficient ratios (DARs) measured at different RH values during the aircraft measurements (Tsekeri et al., 2017). In contrast to the overestimation over the land, both the algorithms underestimate the $n_{50,\mathrm{dry}}$ concentrations over the sea (Figure 2.7b). When we do not account for the hygroscopic growth, both the OMCAM and POLIPHON algorithms underestimate the $n_{50,\mathrm{dry}}$ concentration by 22 % and 38 %, respectively. When the RH growth is corrected, the underestimation further increases to 40 % and 52 %, respectively. Similar to land regions, both the algorithms yield comparable results over the sea as the dominant aerosol type is elevated smoke in both scenarios.

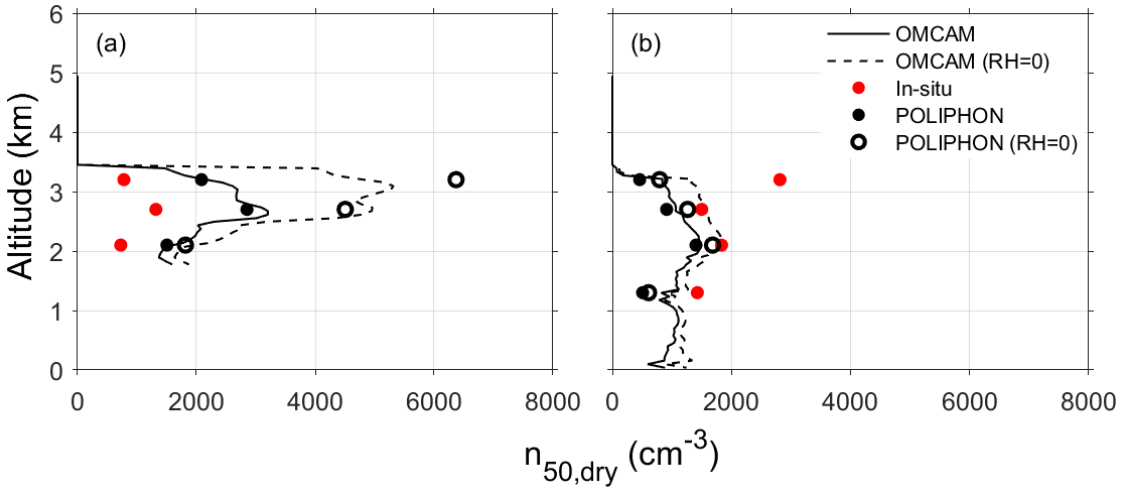

Figure 2.7: The $n_{50,\mathrm{dry}}$ concentrations estimated from CALIPSO satellite data using OMCAM (solid line), POLIPHON (black dots) incorporated from Georgoulias et al. (2020) and in-situ aircraft observations (red dots) adopted from Tsekeri et al. (2017) over the land (a) and sea (b) surface close to the Thessaloniki region. The dotted line and unfilled black circles represent the $n_{50,\mathrm{dry}}$ estimated from OMCAM and POLIPHON, respectively, when hygroscopicity correction is not considered.

The $n_{50,\mathrm{dry}}$ values estimated over the land and sea region from the OMCAM and POLIPHON algorithms are comparable to each other. The RH-corrected POLIPHON values (using in-situ DAR measurements) are in good agreement with those of OMCAM which uses kappa parameterization with globally averaged kappa values. Both the OMCAM and POLIPHON algorithms were able to capture the pattern of altitudinal variations in $n_{50,\mathrm{dry}}$ as observed by the in-situ measurements. However, the magnitudes of $n_{50,\mathrm{dry}}$ are

Table 2.4: The $n_{50,\mathrm{dry}}$ concentrations (in cm^{-3}) from in-situ measurements (Tsekeri et al., 2017) and CALIPSO measurements by using OMCAM and POLIPHON (Georgoulias et al., 2020) algorithms at different altitudes over land and sea regions around Thessaloniki, Greece. The values inside the brackets refers to zero-humidity case (no hygroscopicity correction applied).

Region	Altitude	In-situ	OMCAM (RH = 0)	POLIPHON (RH = 0)	CALIPSO - in-situ (%)	
					OMCAM (RH = 0)	POLIPHON (RH = 0)
Land	2.1	727	1590 (1957)	1504 (1816)	119 (169)	107 (150)
	2.7	1318	3171 (5296)	2851 (4505)	141 (302)	116 (242)
	3.2	779	2160 (5401)	2086 (6370)	177 (593)	168 (718)
Sea	1.3	1427	826 (926)	508 (609)	-42 (-35)	-64 (-57)
	2.1	1834	1476 (1796)	1405 (1683)	-20 (-2)	-23 (-8)
	2.7	1601	1065 (1504)	912 (1264)	-29 (0)	-39 (-16)
	3.2	2814	841 (1357)	459 (794)	-70 (-52)	-84 (-72)

overestimated by both the algorithms over the land by a factor of 1.5, whereas over the sea region, the underestimation by both the algorithms is about a factor of 0.5. One of the intrinsic limitations of this comparison results from the vast difference in measuring timescales of CALIPSO and the research aircraft. While for CALIPSO it is as small as 15 seconds, it is around 2 hours for the aircraft. From Figure 2.6c, we can clearly see that the extinction coefficient along with the $n_{50,\mathrm{dry}}$ concentrations is highly variable over the land region (ranging from $617\,\mathrm{cm}^{-3}$ to $40000\,\mathrm{cm}^{-3}$) compared to rather homogeneous concentrations over the sea. This might be the reason for the large discrepancy between in-situ and CALIPSO retrievals over the land region. Moreover, only two cloud-free CALIPSO 5 km profiles are considered for the comparison over land, which further increases the chances of disparity. Given the limited sample space, this comparison should not be considered to be validation but rather a demonstration of the capability for retrieving CCN concentrations from spaceborne lidar measurements. A detailed study comparing the CALIPSO-retrieved aerosol number and CCN concentrations with ground-based and aircraft in-situ measurements is required to evaluate the reliability of OMCAM and POLIPHON algorithms in estimating the CCN concentrations.

2.5 Summary and conclusions

We present the OMCAM algorithm to derive the height-resolved cloud-relevant CCN concentrations from CALIPSO measurements. The algorithm uses the normalized size distributions and refractive indices from CALIPSO aerosol models (Omar et al., 2009) as an input to MOPSMAP to calculate the extinction coefficient. The size distributions are then scaled to reproduce the CALIPSO-measured extinction coefficient. To account for the hygroscopicity, we use κ parameterization (Petters and Kreidenweis, 2007) and modify the size distribution and the refractive index before the scaling step. We then estimate the required aerosol number concentration by integrating the final scaled size distributions over

the size ranges relevant for different aerosol types. Utilizing the aerosol-type-specific CCN parameterizations from Mamouri and Ansmann (2016), we convert the aerosol number concentrations to cloud-relevant CCN concentrations for different supersaturation.

The OMCAM algorithm relies on the potentiality of the CALIPSO aerosol models to accurately describe the microphysical properties of the aerosol subtypes defined within the CALIPSO retrieval algorithm. We performed sensitivity tests by varying the normalized size distributions by up to $\pm 50\,\%$ of the amplitude of each mode and found that the uncertainty in the final aerosol number concentration ranges between a factor of 2 and 3.

We compared the CCN concentrations obtained from OMCAM with those of the POLIPHON method – the existing method for lidar-based CCN retrieval. For extinction coefficient $> 0.05\,\mathrm{km}^{-1}$, we found a good agreement for continental, dust, and smoke aerosols. However, as the extinction coefficients becomes smaller than $0.05\,\mathrm{km}^{-1}$, the difference increases, with the POLIPHON values going as high as twice the OMCAM values. For marine aerosols, the CCN concentration derived using the POLIPHON method is always higher (4-6 times) than that of OMCAM.

For an initial evaluation of the OMCAM algorithm, we compared the thus obtained $n_{50,\mathrm{dry}}$ with in-situ measurements taken over the land and sea region around Thessaloniki during the ACEMED campaign (Tsekeri et al., 2017). For the retrievals over sea, we found that CALIPSO underestimating the $n_{50,\mathrm{dry}}$ by about $40\,\%$. Over the land areas; however, CALIPSO overestimates $n_{50,\mathrm{dry}}$ by about $167\,\%$. The large discrepancies may be a result of the combination of highly variable $n_{50,\mathrm{dry}}$ over the land region and the instantaneous measurement by CALIPSO in contrast to the in-situ measurement, which was performed in a time period of 2 hours. All values remained within a factor of 2 which is in agreement with the estimated uncertainty. Moreover, the $n_{50,\mathrm{dry}}$ retrieved from CALIPSO using the OMCAM algorithm was comparable to that of POLIPHON (Georgoulias et al., 2020).

Our future goals include a comprehensive evaluation of the CALIPSO-derived aerosol number and CCN concentrations with ground-based and airborne in-situ measurements. We use the airborne Atmospheric Tomography Mission measurements of aerosol number concentration profiles from altitudes of 0.2 km to 12 km between the years 2016 and 2018 (Williamson et al., 2019) to access the quality of the respective parameter derived from CALIPSO. Furthermore, we also compare the CALIPSO products with the long-term surface measurements of CCN and aerosol size distributions from 11 atmospheric observatories around the globe between 2006 and 2016 (Schmale et al., 2017). The comparison study will enable us to test the applicability of OMCAM and POLIPHON algorithms in the context of estimating the aerosol number and CCN concentrations from spaceborne lidar measurements. Ultimately, we plan to apply the best-performing algorithm to more than 15 years of CALIPSO data to construct a global height-resolved CCN climatology. The data set when coupled with other satellite-based global cloud-related data or state-of-the-art numerical models will help in improving our current understanding of the aerosol-cloud interactions. Also, it will be interesting to compare the CALIPSO-derived CCN concentrations with emerging aerosol remote sensing techniques available for other satellites. For instance,

Rosenfeld et al. (2016) formulated an algorithm for estimating CCN concentrations from the measurements of the Visible/Infrared Imager Radiometer Suite (VIIRS) instrument aboard the Suomi National Polar-orbiting Partnership (NPP) satellite by treating clouds as CCN chambers for convective clouds and later on extended the algorithm for marine stratocumulus clouds (Efraim et al., 2020).

The ability of CALIPSO not only to measure vertically resolved aerosol optical properties but also to detect the responsible aerosol type has facilitated the retrieval of global 3D type-specific aerosol properties. We have described a novel methodology to retrieve cloud-relevant CCN concentrations from CALIPSO measurements illustrating the potential of CALIPSO to produce 3D global CCN climatology for ACI studies and climate model evaluations, opening new gates for further validation of the algorithm against ground-based and airborne in-situ measurements.

Chapter 3

Evaluation of aerosol number concentrations from CALIPSO with ATom airborne in situ measurements*

Short summary

The aerosol number concentrations derived from CALIPSO using the OMCAM algorithm are compared with the airborne in-situ measurements collected during the ATom campaigns between 2016 and 2018 over the Atlantic and Pacific oceans. HYSPLIT trajectories are used to match both the measurements in space and time. Based on the comparison results, a modification to the marine model used in OMCAM is suggested. With the revised treatment of marine aerosols, the aerosol number concentrations estimated using OMCAM over different size ranges are found to be in reasonable agreement with the in-situ measurements irrespective of the height levels considered. Such concurrence between the satellite-derived aerosol number concentrations and independent in-situ measurements emboldens the use of CALIPSO in studying aerosol-cloud interactions.

*Published as: Choudhury, G., Ansmann, A., and Tesche, M.: Evaluation of aerosol number concentrations from CALIPSO with ATom airborne in situ measurements, Atmos. Chem. Phys., 22, 7143–7161, https://doi.org/10.5194/acp-22-7143-2022, 2022.

3.1 Introduction

Aerosol particles are needed to form clouds under the majority of atmospheric conditions. They can act as cloud condensation nuclei (CCN) initiating liquid droplet nucleation in warm clouds, and as ice-nucleating particles (INPs), initiating heterogeneous ice nucleation in mixed-phase and cold clouds. Changes in the concentration of such particles influence the cloud extent, development, lifetime, and microphysical and radiative properties (Fan et al., 2016; Choudhury et al., 2019). Inadequate understanding of such complex aerosol-cloud interactions (ACIs) and the corresponding rapid adjustments in radiative forcing are the key reasons behind the uncertainty in our future climate projections (Forster et al., 2021).

The CCN and INP concentrations are the fundamental aerosol parameters needed to study the ACIs. A comprehensive representation of the same in the weather and climate models is necessary to obtain a realistic simulation of the impact of aerosols on cloud microphysics and the corresponding adjustments. By comparing the simulations from a total of 16 general circulation models and global chemistry transport models with the in situ measurements from nine ground-based stations, Fanourgakis et al. (2019) found that the models underestimate the aerosol number and CCN concentrations. Similar underestimation is also reported by Genz et al. (2020). Compared to CCN which may vary from anywhere between 10^2 and 10^5 cm^{-3}, INPs are sparse in nature, with about one in a million particles capable of forming ice crystals in the atmosphere (Nenes et al., 2014). By combining the GLOMAP (Global Model of Aerosol Processes)-mode global aerosol microphysics model (Mann et al., 2010) and field experiments of K-feldspar and marine organic aerosols, Vergara-Temprado et al. (2017) compared the INP concentrations with in situ measurements at marine locations and found the annual mean modelled INP values to be 1.5 orders of magnitude larger than the observations. Also, depending on the INP parametrization and temperature of measurement, the modelled INP concentrations can be as much as 4-6 orders of magnitude larger than the observations (Vergara-Temprado et al., 2017). Thus, a better global measurement of cloud-relevant aerosol microphysical properties is needed for constraining our weather and climate models. While the surface in situ measurements of such parameters are carried out continuously with a high temporal resolution, they are limited to certain point locations. One way to overcome this limitation is to switch to satellite observations, which provide global, continuous, and long-term monitoring of the atmosphere.

Satellite retrievals used in ACI studies include aerosol optical parameters like the aerosol backscatter coefficient, aerosol extinction coefficient, and aerosol optical depth (column integrated aerosol extinction coefficient). Compare to the column integrated products obtained from passive sensors, active sensors like lidars provide height resolved optical parameters which are necessary for studying vertically collocated aerosols and clouds (Costantino and Bréon, 2013). Cloud-Aerosol Lidar with Orthogonal Polarization (CALIOP) is a spaceborne lidar aboard the Cloud-Aerosol Lidar and Infra-Red Pathfinder Satellite Observation (CALIPSO) satellite, which provides profiles of aerosol optical parameters like the backscat-

ter coefficient, extinction coefficient, and particle depolarization ratio. Recent studies have shown that these optical parameters can be used to derive cloud-relevant aerosol microphysical parameters. Mamouri and Ansmann (2016) present the first CCN and INP retrieval algorithm for measurements with ground-based lidars. The algorithm includes the following two main steps: (1) the conversion of the lidar-derived extinction coefficient to aerosol number concentration (ANC) with dry radii $> 50\,\mathrm{nm}$ ($n_{50,\mathrm{dry}}$) and $> 250\,\mathrm{nm}$ ($n_{250,\mathrm{dry}}$) and (2) the subsequent use of the ANC estimates to compute CCN (at different supersaturations) and INP (at different temperatures) concentrations based on aerosol-type-specific parameterizations. The parameterizations for estimating CCN concentrations for different aerosol types are given in Mamouri and Ansmann (2016) and those for INP are available, for example, in DeMott et al. (2010, 2015) and Ullrich et al. (2017). Though the methodology for retrieving CCN and INP concentrations was developed for ground-based lidars, it has also been applied to measurements with the spaceborne lidar CALIOP (Marinou et al., 2019; Georgoulias et al., 2020). This highlights the potential of CALIOP for estimating global 3D CCN and INP concentrations for climatological datasets. More recently, Choudhury and Tesche (2022a) presented a CCN/INP retrieval algorithm developed specifically for CALIOP measurements. It uses the aerosol-type-specific normalized size distributions from the CALIPSO aerosol model (Omar et al., 2009) and scales them as per the extinction coefficient measured by CALIOP. The final size distribution is integrated to obtain the ANC required in the CCN and INP parameterizations. Of key importance is the accurate retrieval of ANC from satellites – the primary component of CCN and INP parameterizations. However, a thorough validation of the same is missing except for selected case studies (Marinou et al., 2019; Georgoulias et al., 2020).

The Atmospheric Tomography Mission (ATom; Wofsy et al., 2018) comprises a series of continuous flight measurements over different parts of the Pacific and Atlantic oceans from 2016 to 2018 measuring aerosol properties including the ANC. This dataset provides a unique opportunity to validate the available ANC retrieval algorithms for the spaceborne lidar CALIOP. In this study, we validate the ANC retrieval algorithms presently available for CALIOP measurements with the airborne in situ measurements from the ATom campaigns. Moreover, we suggest a revision to the ANC retrieval algorithm given by Choudhury et al. (2022). This paper is organized as follows. The description of the datasets, ANC retrieval algorithms for CALIOP, and the comparison methodology are given in Sect. 3.2. The results are presented in Sect. 3.3 and discussed in Sect. 3.4. The main findings are summarized in Sect. 3.5.

Table 3.1: Details of the ATom parameters used in the comparison study. Note: STP is standard temperature and pressure.

Instrument	Parameter name	Description
Laser aerosol spectrometer (LAS)	Nacc_LAS	Number concentration of dry aerosols for ammonium sulfate optical equivalent radius (R) = 0.05 to 0.44 µm at STP
	Ncoarse_LAS	Number concentration of dry aerosols for $0.44 \leq R \leq 2$ µm at STP
Nucleation-mode aerosol size spectrometer (NMASS), ultra-high sensitivity aerosol size spectrometer (UHSAS), LAS	calc_ext_532_AMP	Total calculated particle extinction at 532 nm wavelength assuming dry ammonium sulfate for $0.00135 \leq R \leq 2.4$ µm at STP

3.2 Data, retrievals, and methods

3.2.1 ATom

The ATom comprised four series of flights by the NASA DC-8 research aircraft over the Pacific and Atlantic oceans covering latitudes between 82°N and 86°S. The flight patterns included regular descents and ascents between altitudes of 200 m and 12 km. A total of four ATom campaigns were conducted between August and September 2016 (ATom1), January and February 2017 (ATom2), September and October 2017 (ATom3), and April and May 2018 (ATom4). The instruments employed for measuring the dry aerosol particle size distribution between a radius of 1.35 nm and 2.4 µm are a Laser Aerosol Spectrometer (LAS), a Nucleation-mode Aerosol Size Spectrometer (NMASS), and an Ultra-high Sensitivity Aerosol Size Spectrometer (UHSAS). The operating principles of these instruments and their inferred data products are described comprehensively in Brock et al. (2019). In the present study, we use version 1.5 of the "ATom: Merged Atmospheric Chemistry, Trace Gases, and Aerosols dataset" (Wofsy et al., 2018), with a very high temporal resolution of 10 s. The parameters used in our comparison study are given in Table 3.1. To compute $n_{50,\mathrm{dry}}$, we add the LAS measured number concentration in the accumulation mode ($0.05<R<0.4425$ µm) and coarse mode ($0.4425 \leq R <$ approx. 2 µm). During ATom2, a leak was found in the sheath flow of the LAS, leading to lower detection efficiency. Simultaneous measurements from other instruments were used to correct the LAS measurements (Brock et al., 2019). The extinction coefficient is calculated from the dry size distributions by using Mie theory (Bohren and Huffman, 2008) assuming that particles are composed of homogenous non-absorbing spheres of ammonium sulfate with a refractive index of 1.52. Note that this extinction coefficient is reported for particles with a dry radius $R \leq 2.4$ µm.

Coarse particles with a dry radius $R > 2.4\,\mu m$ may contribute significantly to the extinction coefficient within the marine boundary layer and dust-dominated air masses (Brock et al., 2019). The extinction coefficient in such scenarios is likely to be underestimated. All ATom parameters are given at standard temperature and pressure.

Table 3.2: POLIPHON conversion factors and extinction exponents for different aerosol types to be used in Eq. (3.1) for estimating the aerosol number concentrations from the extinction coefficient. The value of the extinction exponent (x) for $n_{250,dry}$ is 1 for all the aerosol types.

Type	$n_{50,dry}$ ($n_{100,dry}$ for dust)		$n_{250,dry}$	Source
	Conversion factor (Mm cm^{-3})	Extinction exponent (x)	Conversion factor (Mm cm^{-3})	
Dust	8.855	0.7525	0.1475	Ansmann et al. (2019)
Continental	25.3	0.94	0.1	Mamouri and Ansmann (2016)
Marine	7.2	0.85	0.06	Mamouri and Ansmann (2016)
Smoke	17	0.79	0.35	Ansmann et al. (2021b)

3.2.2 CALIOP

CALIOP is a dual-wavelength, three-channel polarization-sensitive lidar aboard the polar-orbiting CALIPSO (Winker et al., 2009) satellite that was launched on April 28, 2006, as a part of the A-Train constellation. CALIOP provides global height-resolved coverage of the occurrence and properties of aerosol and cloud layers. For inferring aerosol backscatter and extinction coefficients, the CALIPSO retrieval requires a priori information on the prevailing aerosol type. The aerosol types defined in the CALIPSO v4 retrieval algorithm include marine, desert dust, polluted continental/smoke, clean continental, elevated smoke, polluted dust, and dusty marine. A respective aerosol type is selected by considering the estimated 532 nm particle depolarization ratio, the 532 nm integrated attenuated backscatter coefficient, the aerosol layer height (top and bottom), and the underlying surface type (Kim et al., 2018). For each detected aerosol type, the retrieval uses a pre-set type-specific lidar ratio that has been estimated from a combination of long-term Aerosol Robotic Network (AERONET; Holben et al., 1998) measurements and field campaigns with a subsequent adjustment based on independent measurements with ground-based lidars (Omar et al., 2005, 2009; Kim et al., 2018). The thus obtained profiles of the backscatter and extinction coefficient of aerosols and clouds are provided in the corresponding level 2 profile products. In the present study, we use the CALIPSO level 2 v4.20 aerosol profile product (NASA/LARC/SD/ASDC, 2018). The parameters used to derive aerosol number concentrations from CALIPSO measurements are the 532 nm aerosol extinction coefficient, the 532 nm aerosol backscatter coefficient, the 532 nm aerosol depolarization ratio, and the aerosol subtype mask. Quality control flags are used to select the most reliable data. To account for the hygroscopicity of aerosols, we use relative humidity (RH) profiles attained

from the Global Modelling and Assimilation Office (GMAO) Data Assimilation System (Molod et al., 2015) included in the CALIPSO profile product. All parameters have a uniform horizontal resolution of 5 km and a vertical resolution of 60 m for tropospheric aerosols.

3.2.3 Aerosol number concentration from CALIOP

In this section, we discuss the two algorithms for estimating ANC from CALIOP measurements used in this study. In the analysis, we select only high-quality CALIOP data that fulfil the criteria given in Tackett et al. (2018) by utilizing the (i) cloud aerosol discrimination score (≤ -20), the (ii) extinction quality check flag ($= 0$, 1, 16, and 18), and the (iii) extinction uncertainty value ($\neq 99.9$). Also, for retrievals corresponding to the mixed aerosol types of polluted dust and dusty marine, we first separate the dust and non-dust contributions by using the particle depolarization ratio to separate the contributions of dust and non-dust aerosols to the particle backscatter coefficient (Tesche et al., 2009). The backscatter coefficient is then multiplied by the lidar ratio to yield the dust and non-dust extinction coefficients. We use the updated lidar ratios from Kim et al. (2018). The dust separation technique is also incorporated in many studies concerning the lidar-based retrieval of aerosol microphysical properties (Mamouri and Ansmann, 2015, 2016; Georgoulias et al., 2020; Choudhury et al., 2022). However, it does not consider the RH dependency of depolarization ratio which may result in additional errors especially in marine environments. The information on aerosol-type-specific extinction coefficient, aerosol type, and relative humidity are used to compute the ANC.

POLIPHON

The Polarization Lidar Photometer Networking (POLIPHON; Mamouri and Ansmann, 2015, 2016) method combines lidar-derived, type-specific aerosol optical properties with concurrent long-term AERONET measurements of aerosol optical depth (AOD) and retrieved column size distributions (Dubovik et al., 2000, 2006) to estimate the ANC. A regression analysis of the AERONET-derived column extinction coefficients and number concentrations (integral of the aerosol size distribution) yields the conversion equation to derive ANC from lidar-derived extinction coefficients. The regression analysis was based on AERONET observations at sites with pure marine or pure mineral dust conditions and observations in environments dominated by urban haze or wildfire smoke. The complex analysis resulted in aerosol-type-specific conversion equations of the form

$$n_{j,\mathrm{dry}} = C \cdot \alpha^{x}, \tag{3.1}$$

where $n_{j,\mathrm{dry}}$ is the aerosol number concentration with the dry radius $> j$ nm, α is the extinction coefficient, C is the conversion factor, and x is the extinction exponent. In this study, we use the regression parameters for marine and continental aerosols given in

Mamouri and Ansmann (2016). The one for desert dust is taken from Ansmann et al. (2019) and represents a global average. For smoke aerosols, we use the averaged value for aged smoke given in Ansmann et al. (2021b) as most of the ATom measurements were performed over oceans away from smoke sources. The values of the regression constants along with their sources are listed in Table 3.2. Typical RH of 80 % and 60 % were assumed while calculating the conversion factors for marine and continental (including smoke) aerosol types. Note that for dust aerosols, POLIPHON provides the ANC for the dry radius $\mathrm{R} > 100\,\mathrm{nm}$ ($n_{100,\mathrm{dry}}$), and we obtain $n_{50,\mathrm{dry}}$ from the ATom measurements.

Table 3.3: Bimodal lognormal size distribution parameters and refractive indices (real part (m_r) and imaginary part (m_i)) of the aerosol subtypes at a wavelength of 532 nm used in OMCAM conversion factors to calculate ANC algorithm. The AERONET-based marine model is adopted from Sayer et al. (2012)

Aerosol subtype	Dust	Polluted continental	Clean continental	Elevated smoke	Marine	Marine (AERONET)
μ_i fine	0.116	0.158	0.206	0.144	0.150	0.1137
μ_i coarse	2.833	3.547	2.633	3.726	1.216	1.8756
σ_i fine	1.481	1.526	1.61	1.562	1.6	1.6487
σ_i coarse	1.908	2.065	1.899	2.143	1.60	2.0544
ν_i fine	0.223	0.531	0.050	0.329	0.025	0.14
ν_i coarse	0.777	0.469	0.950	0.671	0.975	0.86
m_r fine	1.414	1.404	1.380	1.517	1.400	1.5478
m_i fine	0.0036	0.0063	0.0001	0.0234	0.0050	0.0053
m_r coarse	1.414	1.404	1.455	1.517	1.400	1.4108
m_i coarse	0.0036	0.0063	0.0034	0.0234	0.0005	0

OMCAM

The Optical Modelling of CALIPSO Aerosol Microphysics (OMCAM; Choudhury et al., 2022)) algorithm utilizes the normalized size distributions and refractive indices from the CALIPSO aerosol model (Omar et al., 2009) to derive those aerosol size distributions that lead to the best reproduction of the inferred aerosol extinction coefficient when used as input for light-scattering calculations with the MOPSMAP (Modelled Optical Properties of Ensembles Of Aerosol Particles) optical modelling package (Gasteiger and Wiegner, 2018). In the modelling of the extinction coefficient, we consider marine, continental, and smoke aerosols as spheres and apply the Mie scattering theory. Mineral dust is considered to be spheroidal and is treated with a combination of the T matrix method and the improved geometric optics method. The normalized size distribution from the CALIPSO aerosol model is scaled to reproduce the CALIOP-derived extinction coefficient (Choudhury et al., 2022) as follows:

$$\frac{\mathrm{d}V(r)}{\mathrm{d}\ln r} = \frac{\alpha}{\alpha_\mathrm{n}} \cdot \sum_{i=1}^{2} \frac{\nu_i}{\sqrt{2\pi}\ln\sigma_i} \exp\left(\frac{-(\ln r - \ln\mu_i)^2}{2\ln {\sigma_i}^2}\right). \tag{3.2}$$

where α_n is the extinction coefficient estimated from the normalized size distribution and refractive index using MOPSMAP and α is the CALIOP-derived extinction coefficient. σ_i, ν_i, and μ_i are the standard deviation, volume fraction, and mean radius of the i^{th} mode of the normalized size distribution, respectively, and their values for different aerosol subtypes are given in Table 3.3. Since the refractive index, σ_i, ν_i, and μ_i of the aerosol size distributions are intensive parameters, i.e. independent of the extinction coefficient or aerosol concentration, the volume size distribution and hence the ANC can be expressed linearly in terms of the extinction coefficient as follows:

$$n_{j,\mathrm{dry}} = C_\mathrm{o} \cdot \alpha \tag{3.3}$$

where $C_\mathrm{o} = \frac{1}{\alpha_\mathrm{n}} \int_j^{r_\mathrm{max}} \mathrm{d}N$ is a conversion factor whose value depends on the aerosol type and the lower limit j of integrating the particle size distribution. The values of C_o for different aerosol types are given in Table 3.4. Since the algorithm primarily relies on the assumption of fixed initial normalized size distributions for every aerosol subtype, Choudhury et al. (2022) analysed the sensitivity of the output $n_{j,\mathrm{dry}}$ to variations in these size distributions. By varying the magnitude of the fine and coarse modes of the size distributions by $\pm\,50\,\%$, they found the resulting $n_{j,\mathrm{dry}}$ to remain within a factor of 2. Such an uncertainty is expected for a spaceborne retrieval of aerosol microphysical properties and is also similar to that of POLIPHON (Mamouri and Ansmann, 2016).

Table 3.4: OMCAM conversion factors to calculate ANC from Eq. (3.3).

Type	Conversion factors (Mm cm^{-3})	
	$n_{50,\mathrm{dry}}$ ($n_{100,\mathrm{dry}}$)	$n_{250,\mathrm{dry}}$
Dust	42.9728 (11.0847)	0.0865
Clean continental	3.598	0.1995
Polluted continental	24.931	0.2601
Smoke	21.9948	0.1446
Marine	2.3988	0.2084
Modified marine	21.2077	0.1688

Choudhury et al. (2022) show a large discrepancy in their comparison of theoretically possible ANC for marine aerosols, as estimated by POLIPHON and OMCAM. This can be attributed to the difference in the temporal extent and geographical location of the measurements and different instruments employed in measuring of the marine size distributions used in the two algorithms. The regression constants for marine aerosols used in POLIPHON are estimated from 7.5 years of AERONET measurements from 2007 to 2015 at Barbados (Mamouri and Ansmann, 2016). However, the marine model used in OMCAM (Omar et al., 2009; Choudhury et al., 2022) was obtained from in situ measurements of sea-salt size distributions during the SEAS experiment from 21 to 30 April 2000 (Masonis et al., 2003; Clarke et al., 2003). AERONET provides long-term continuous measurements

of aerosol optical and microphysical properties at different locations around the globe. Sayer et al. (2012) presented a maritime aerosol model for use in satellite retrievals based on the aerosol microphysical properties at 11 AERONET island stations. In this work, we also utilize the microphysical properties recommended by Sayer et al. (2012) in the OMCAM algorithm to examine its potential for deriving the ANC from CALIOP measurements (presented in Section 3.2.1). The size distribution parameters along with the complex refractive indices are listed in Table 3.3. Please note that the parameters in Sayer et al. (2012) are given for ambient conditions and were converted to dry conditions assuming a uniform RH of 70 % before using them in the OMCAM algorithm. The size distribution was modified to dry conditions by using kappa parametrization (Petters and Kreidenweis, 2007) and the refractive index was modified as per the volume-weighting rule.

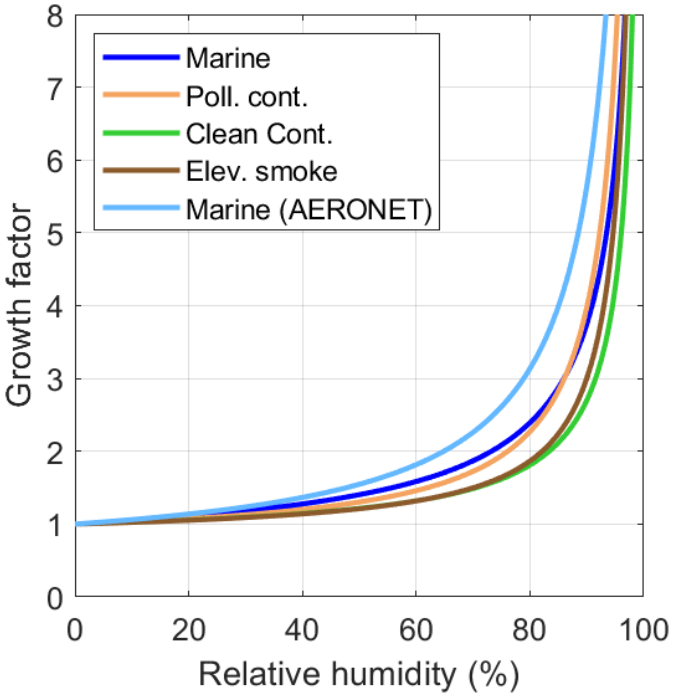

Figure 3.1: Hygroscopic growth factor for different values of relative humidity for different aerosol types estimated from the microphysical properties of CALIPSO aerosol models, with marine (blue), polluted continental (orange), clean continental (green), and elevated smoke (brown). The growth factor estimated using a new AERONET-based marine model (sky blue) from Sayer et al. (2012) is also shown. The hygroscopic growth factor at a certain relative humidity is defined as the ambient-to-dry extinction coefficient ratio.

Hygroscopicity correction

To compare the CALIOP-derived ambient extinction coefficients with the results of the dry measurements conducted during ATom, we need to correct the former for the effect of hygroscopic growth. Furthermore, the extinction coefficient to ANC conversion discussed in

Section 3.2.3 holds only for dry conditions. The POLIPHON method assumes a constant RH of 80 % for marine and 60 % for continental aerosols and may result in errors for higher RH conditions. MOPSMAP includes an in-built functionality to address hygroscopic growth based on the kappa parametrization (Petters and Kreidenweis, 2007) in the RH range from 0 % to 99 %. We use the normalized aerosol size distributions and refractive indices of different aerosol types from CALIPSO aerosol model to calculate the extinction coefficient for different values of relative humidity. Figure 3.1 shows the variation in the hygroscopic growth factor, i.e. the ratio between the ambient and dry extinction coefficient, with relative humidity for continental (polluted continental, clean continental, and elevated smoke) and marine CALIPSO aerosol types with kappa values of 0.3 and 0.7, respectively. The kappa values are global averages and are suggested by Andreae and Rosenfeld (2008) for use in satellite retrievals. Nevertheless, studies have found that the kappa values may vary with the aerosol composition and age (Pringle et al., 2010; Cheung et al., 2020). Thus, considering a fixed kappa value for a particular aerosol type defined in CALIPSO may incur additional uncertainties in the ANC retrieval. Moreover, the RH values included in the CALIPSO level 2 data product are estimated from global model simulations which may incorporate additional uncertainties. Having said that, we still use the parametrization with globally averaged kappa values, which were found to provide reasonable results in the case study presented in Choudhury and Tesche (2022a) and the example cases presented later in Section 3.3.1. Mineral dust is considered to be hydrophobic in our analysis. For every CALIOP data bin, the extinction coefficient is corrected based on the aerosol type and relative humidity value by dividing it with the hygroscopic growth factor that corresponds to the ambient relative humidity. Note that this methodology is different from the one used in Choudhury and Tesche (2022a), where the hygroscopicity correction is applied to the particle size distribution before the computation of the ANC. In the present study, the application of the hygroscopicity correction to the extinction coefficient is necessary so that the dry extinction coefficient from the CALIOP measurements can be compared directly with the ATom dataset. The hygroscopicity-corrected extinction coefficient is then used to compute the CALIOP-based ANC using the OMCAM and POLIPHON algorithms. Note that in the case of POLIPHON, we only apply the hygroscopicity correction when RH is greater than 80 % and 60 % for marine and continental aerosols, respectively, and modify the corresponding ambient extinction coefficient to RH values of 80 % and 60 %. This is because the extinction to ANC conversion equations (Eq. 3.1) was formulated assuming such RH values which are representative of typical marine and continental environments.

3.2.4 Data matching and comparison

The ATom data consist of continuous airborne in situ measurements from altitudes of 200 m to 12 km. The measurement tracks for the first ATom campaign are shown in Figure 3.2. For a comparison between the ANC derived from CALIOP observations and airborne in situ measurements conducted during ATom, we need to find those cases for which the two datasets are closest in time and space. In our first attempt at finding intercepts between

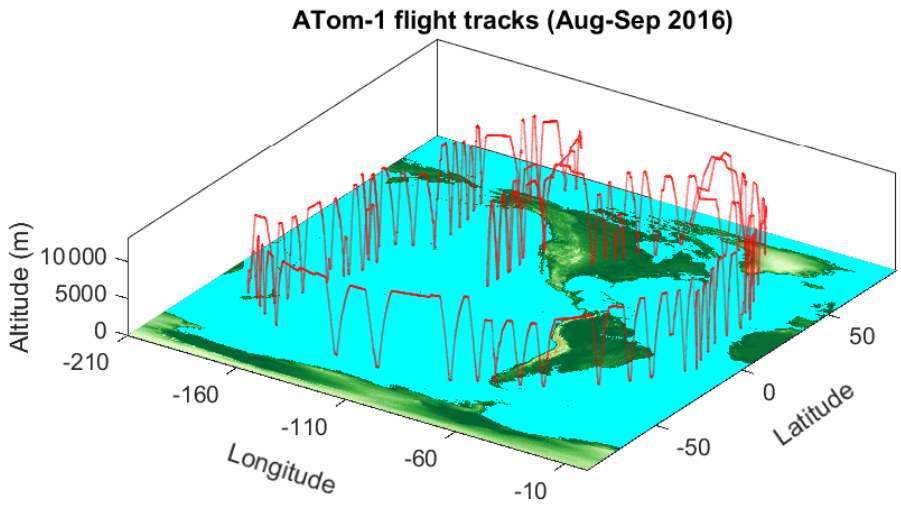

Figure 3.2: Flight tracks during the ATom1 campaign (red lines) carried out from August to September 2016 covering altitudes from 200 m to 12 km over the Pacific and Atlantic oceans.

the tracks from CALIPSO and ATom, we did not consider the aircraft flight level and matched only the 2D latitude and longitude coordinates. As a result, we found that most of the intercepts were found at altitudes above 5 km within the free troposphere. At such altitudes, CALIOP rarely detects aerosol structures except for elevated layers from long-range transport. Hence, we limit the ATom data in the present study to altitudes below 5 km before finding intercepts with the CALIPSO ground track. This slices results in a collection of discontinuous measurements either during ascent or descent or both (v shaped). Such segments have a latitudinal extent of about 1 to 2°, which facilitates the incorporation of the HYSPLIT (Hybrid Single-Particle Lagrangian Integrated Trajectory model) air-parcel trajectory model (Draxler and Rolph, 2010) for finding the intercepts.

Major parts of the ATom measurements were conducted over the Pacific and Atlantic oceans. Compared to the area over land, the aerosol composition over the oceans is rather homogenous, and we can expect a good correlation between ground-based and satellite measurements (Kovacs, 2006; Liu et al., 2008; Tesche et al., 2013). Therefore, we include the CALIPSO tracks that are within 500 km from an ATom measurement in our comparison. Also, for smaller distances, the airborne measurements should be appropriately connected to the nearby CALIPSO overpass. We use HYSPLIT air parcel trajectories to first determine the section of the CALIPSO overpass that is most appropriate for the comparison with the ATom measurements and, second, to estimate the correct temporal difference between the measurements. This approach is also used in Tesche et al. (2013, 2014) for validating CALIPSO measurements against ground-based lidar and in situ measurements. For running HYSPLIT, we use Global Data Assimilation System (GDAS) meteorological files with a spatial and temporal resolution of 1 degree and 3 hours, respectively. The overall track selection methodology is illustrated in Figure 3.3 for an ATom1 flight segment on 8 May 2016. Since the flight measurements are three-dimensional, each of the

HYSPLIT initialization coordinates has a unique combination of latitude, longitude, and altitude. To reduce the complexity of the analysis, we limit the initial trajectory starting points by selecting one out of every 20 points in the segment of the aircraft track. Figure 3.3a shows the forward and backward trajectories starting and ending at different altitudes of the ATom track segment, respectively, and the segment of CALIPSO measurements that is most suitable for the comparison. The vertical displacement of the air parcels along the trajectories is shown in Figure 3.3b. For most of the found intercepts, the vertical displacement of the air parcels along the trajectories is negligible and, hence, not considered in our comparison study. As seen in Figure 3.3a, the trajectories intercept the CALIPSO track at different times. In such situations, we compute the net time difference by averaging the time differences at different height levels. For the example shown in Figure 3.3a, the air parcels take 9 h (between 1 and 3 km) to 13 h (below 1 km) to reach the CALIPSO track, which leads us to apply an average time delay of 11 h. Including the pre-existing time delay of approx. 9 h between the two observations, the average effective time difference for this case is 2 hours. The average distance between the two tracks as calculated using the Haversine formula is found to be 457 km. Following this approach, we identified a total of 53 intercepts for which the measurements of CALIOP and ATom are considered as appropriate for comparison. A detailed overview of these cases is given in Table 3.A1, along with the aerosol-type-specific extinction coefficient contribution and the average distance and time delay between the observations. The average distance between the tracks is less than 500 km for all the intercepts. The time delay between the measurements varies from 0 to 20 h, with 11 cases exceeding 10 h. Marine aerosols are found to be the dominant aerosol type in 44 cases (83 %), followed by polluted continental (four cases), elevated smoke (three cases), and dust (two cases). Such conditions are not unexpected, as most of the observations are over oceans. Note that there were many further intercepts, where factors like signal attenuation due to the presence of clouds, low signal-to-noise ratio due to low aerosol concentrations, or an absence of aerosols lead to CALIOP data that were not suitable for comparison with the ATom measurements. Most of these intercepts were found close to the poles and the Equator.

The atmospheric parameters included in the ATom data are at standard temperature (273.15 k) and pressure (1013.25 hPa) and need to be converted to ambient conditions. The temporal resolution of ATom data used in this work is 10 s, and the corresponding altitudinal resolution varies between 0 and 110 m, depending on the speed of the aircraft. However, the vertical resolution of CALIOP data is 60 m in the troposphere. Also, there can be more than one measurement for a certain altitude range in an ATom segment as it can include both ascending and descending measurements. To compare the two datasets, we thus regrid them to a uniform vertical resolution of 240 m (four CALIOP height bins) between 0 and 5 km altitude by averaging both datasets within these height bins. This approach also compensates for the potential vertical displacement of air parcels along the trajectory between the locations of the measurements of CALIOP and the ATom aircraft. However, a limitation to this methodology is the velocity shear at different height levels. It is worthwhile to note that the main motive of this study is to validate the ANC as retrieved

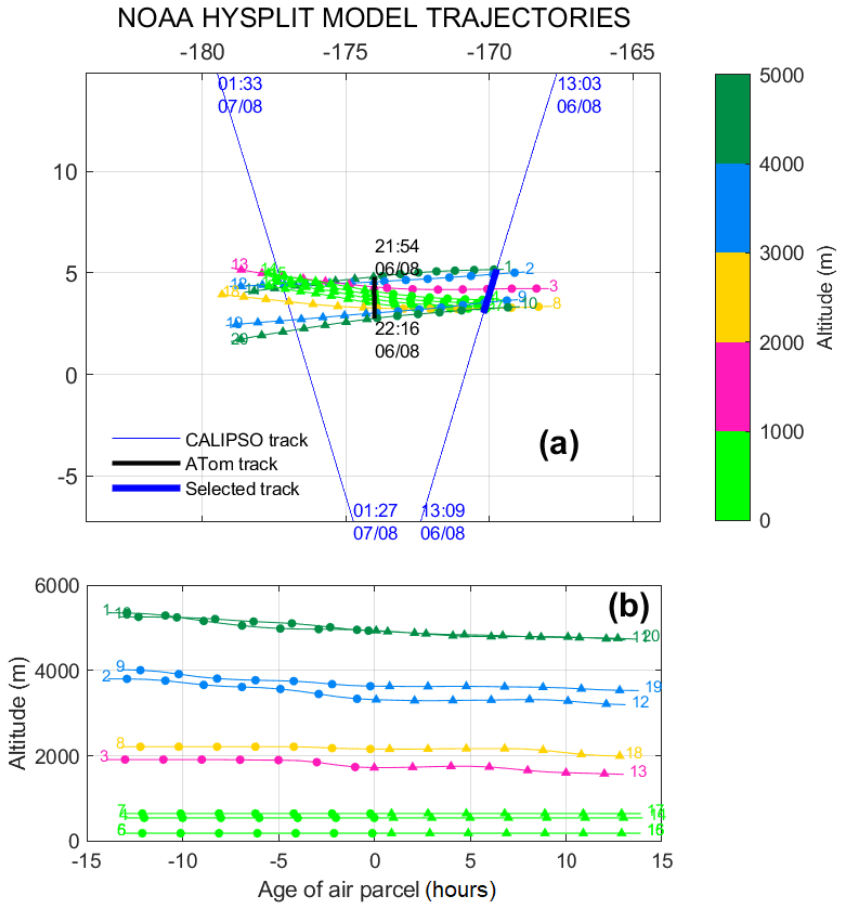

Figure 3.3: (a) CALIPSO overpasses (dark blue lines) close to the ATom measurements on 6 August 2016 with HYSPLIT backward (lines with filled circles) and forward (lines with filled triangles) trajectories starting and ending at different points along the ATom track. The colour bar represents the altitude of the ATom coordinates used to compute the HYSPLIT trajectories. The CALIPSO track selected for comparison is highlighted as a bold blue line in the CALIPSO overpass at 13:04 UTC on 6 August 2016. (b) Vertical displacement of the air parcels along the individual HYSPLIT trajectories. Each track is associated with a number to identify its vertical displacement and time difference.

from CALIOP data rather than the extinction coefficient. Even after considering all the complex screening constraints aimed at identifying the best match between CALIOP and ATom measurements by compensating the temporal and spatial differences between them, disagreement may still arise because of different (i) measuring instruments with dissimilar sensitivities used in ATom and CALIPSO, (ii) measurement techniques, and (iii) spatial and temporal resolutions of the datasets (Tesche et al., 2014). The extinction coefficient from ATom is obtained by applying the Mie theory to the dry aerosol size distributions for radius $<2.4\,\mu m$. This may be inaccurate for coarse-mode non-spherical aerosol particles. The CALIPSO retrievals, on the other hand, have to go through a complex feature detection algorithm to identify aerosol layers and may fail to detect optically thin layers with an inadequate signal to noise ratio. While the airborne in situ data from ATom are point

measurements, the along-swath width of the CALIPSO level 2 data bin is 5 km. Moreover, the HYSPLIT trajectories used to find the intercepts use model outputs and may have associated errors. Even so, it is necessary to perform a closure study utilizing these concurrent measurements for validating the recently developed lidar-based ANC retrieval algorithms. In order to somewhat compensate for such unquantifiable effects in the comparison of ANC, we only use those data bins for which the difference between the dry extinction coefficient from CALIOP is within $\pm 50\,\%$ of that in the ATom data. This additional filter further increases the probability that we are comparing the ANC within the same air parcel.

3.3 Results

3.3.1 Example cases

We start the presentation of results in Figure 3.4 with four comparison examples that present the profiles of the extinction coefficient and ANC as derived from ATom and CALIOP measurements. The first three cases represent different prevailing aerosol types, while the fourth shows a combination of all four types. The majority of the cases includes airborne measurements during both ascent and descent, and hence, there can be two ATom measurements at one level. All CALIPSO overpasses except for the marine-dominated case shown in the examples occurred during nighttime.

The first example case for the CALIPSO and ATom measurement on 15 Feb 2017 is shown in Figures 3.4a & 3.4e. The case is dominated by the presence of marine aerosols with 85 % of the CALIPSO bins below 1 km having RH>80 %. Close to the surface (below 300 m), the RH exceeded 99 %, due to which a finite dry extinction coefficient could not be retrieved. However, for altitudes higher than 300 m, we found a reasonable agreement between the humidity-corrected extinction coefficient from CALIOP and the ATom measurements (Figure 3.4a). This illustrates the ability of the kappa parametrization to account for aerosol hygroscopicity for highly humid marine environments. The $n_{50,\mathrm{dry}}$ profiles derived from CALIOP data using the POLIPHON technique is on par with that measured during ATom. However, the OMCAM estimates are relatively noisy, perhaps because of highly variable RH, and are lower than the ATom measurements for most altitudes. This is also evident in other marine-dominated cases, for example, the near-surface measurements in Figure 4h. However, in the case of $n_{250,\mathrm{dry}}$, both the OMCAM and POLIPHON estimates for marine-dominated CALIPSO retrievals are in much better agreement with the ATom data.

The second example of the intercept on 17 August 2016 is dominated by a mixture of marine and smoke aerosols at altitudes below 1.5 km and only smoke at higher altitudes. Figure 3.4b shows that the extinction coefficients from CALIOP and ATom are on par below 2 km altitude. At higher altitudes, where elevated smoke is the dominant aerosol type, CALIOP gives much higher extinction coefficients than those found from the ATom

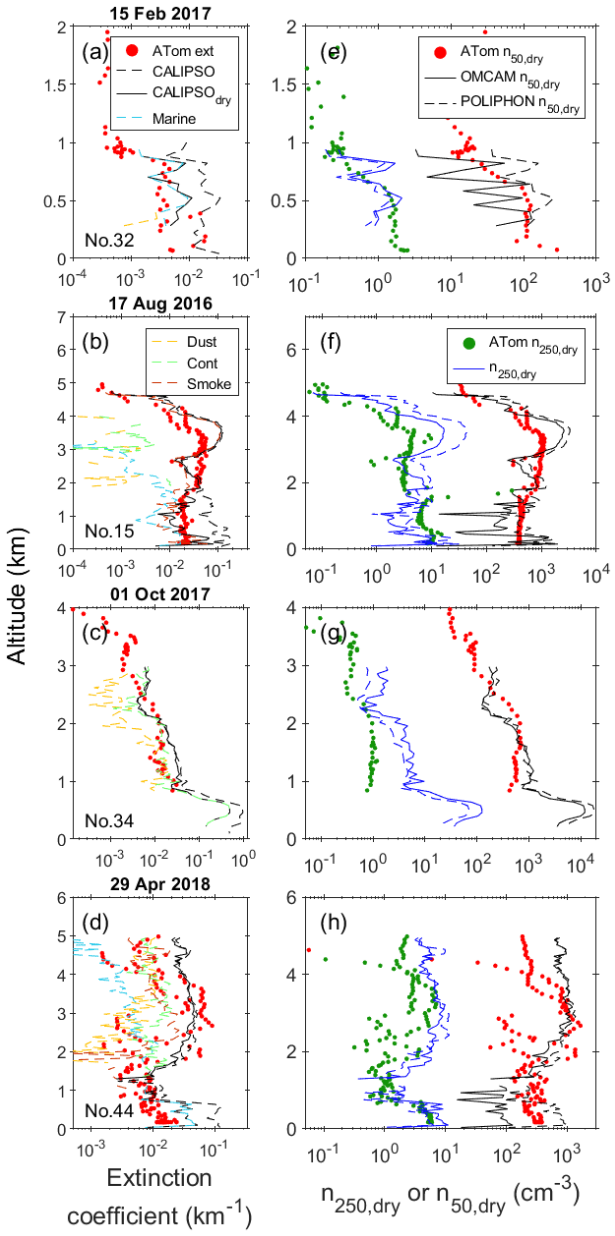

Figure 3.4: Profiles of the aerosol extinction coefficient at 532 nm (a–d), the aerosol number concentration (ANC) with a dry radius > 50 nm (right-hand side of panels e–h) and a with dry radius > 250 nm (left-hand side of panels e–h) retrieved from ATom and CALIPSO measurements for four selected cases (each in one row). The dashed and solid black lines in panels a-d denote the CALIPSO-derived ambient and RH-corrected extinction coefficients, respectively. The dashed coloured lines in (a)–(d) refers to RH corrected extinction coefficients of individual aerosol types. The solid and dashed lines in panels (e)–(h) refer to the ANC derived using OMCAM and POLIPHON techniques, respectively. The serial number of the cases in Table 3.A1 is also given in the lower left corner of the plots.

measurements. A plausible reason behind the larger values is perhaps the temporal (11

h) and spatial (205 km) difference between the observations. The properties of an elevated smoke layer may change drastically with the travelled distance and age of the air parcel. Though the CALIOP-derived $n_{50,\mathrm{dry}}$ and $n_{250,\mathrm{dry}}$ profiles using POLIPHON and OMCAM accurately capture the altitudinal variation revealed in the ATom measurements, they are far more variable with altitude and differ from the in situ measurements at altitudes between 2 km and 4 km.

In the third example of 1 October 2017, the aerosol types detected by the CALIPSO retrieval are polluted continental and mineral dust, with the former dominating. The CALIOP extinction coefficient and $n_{50,\mathrm{dry}}$ are in good agreement with the ATom measurements. However, the $n_{250,\mathrm{dry}}$ (Figure 3.4g) as estimated from CALIOP using both the OMCAM and POLIPHON algorithms, is 2 to 5 times larger than in the ATom measurements. On analysing the geographical locations of the measurements, we found that both of them are over land regions (southern California) and encompass a mixture of urban, rural, and forest continental environments. The aerosol properties can be highly variable over different land regions, which perhaps is the reason behind the disagreement of the $n_{250,\mathrm{dry}}$ values.

The fourth example for the intercept on 29 April 2018 is comprised of a mixture of all four aerosol types with marine aerosols dominating from the surface to 1 km, followed by continental and smoke aerosols until 3 km, and further accompanied by mineral dust over 3 km (Figure 3.4d). The ATom-derived extinction coefficient (for ascending and descending flight-track segments) varies by as much as 1.5 orders of magnitude at heights above 2 km. This highlights the impact of the spatial heterogeneity that may occur over short distances or time periods. The CALIOP-derived humidity-corrected extinction coefficient resembles the in situ measurements during ascent (with larger values than during descent) between 1 and 4 km altitude. Above and below that layer, the CALIOP extinction coefficient exceeds that derived from the in situ measurements. Regarding $n_{50,\mathrm{dry}}$, the POLIPHON estimate overlaps with the ATom measurements up to an altitude of 4 km, above which it fails to replicate the increase in aerosol concentration. The OMCAM-derived profile in Figure 3.4h shows a similar agreement but underestimates $n_{50,\mathrm{dry}}$ at altitudes below 1 km where marine aerosols are dominant. The $n_{250,\mathrm{dry}}$, as estimated from POLIPHON and OMCAM, are both in reasonable agreement with the ATom measurements.

Overall, the example cases in Figure 3.4 present a remarkable resemblance to the aerosol properties derived from CALIOP observations with the ATom measurements at most height levels. The examples that feature the dominance of marine aerosols in the lowermost 2 km illustrate the importance of applying a hygroscopicity correction and indicate that this can be realized to a reasonable degree with the kappa parametrization, even when using static kappa values. In the next section, we present a statistical comparison of the extinction coefficient and ANC for all the identified intercepts.

3.3.2 General findings

Figure 3.5 presents a comparison of the aerosol extinction coefficient as derived from ATom and CALIOP measurements for all the identified intercepts and with the data regridded to a unified altitude profile with 240 m bin width. The correlation of the datasets gives a Spearman's correlation coefficient (R) value of 0.715, a root mean square error (RMSE) of 0.017 km^{-1}, and a bias of -0.007 km^{-1} (Figure 3.5a). For the aerosol-type-specific comparison, individual height bins were separated based on the dominant aerosol type, i.e. the one which shows the largest extinction coefficient. In terms of correlation coefficient, best agreement is found for polluted continental aerosols (R = 0.805), followed by marine (R = 0.744), mineral dust (R = 0.583), and smoke (R = 0.4). A similar level of agreement is also seen in terms of the RMSE and bias values given in Figure 3.5b-e. Moreover, both datasets are in better agreement at altitudes below 2 km irrespective of the dominant aerosol type. Such a result is expected as elevated aerosols above the boundary layer can be easily transported to larger distances compared to those located near the surface which counteracts the comparison approach followed in this study.

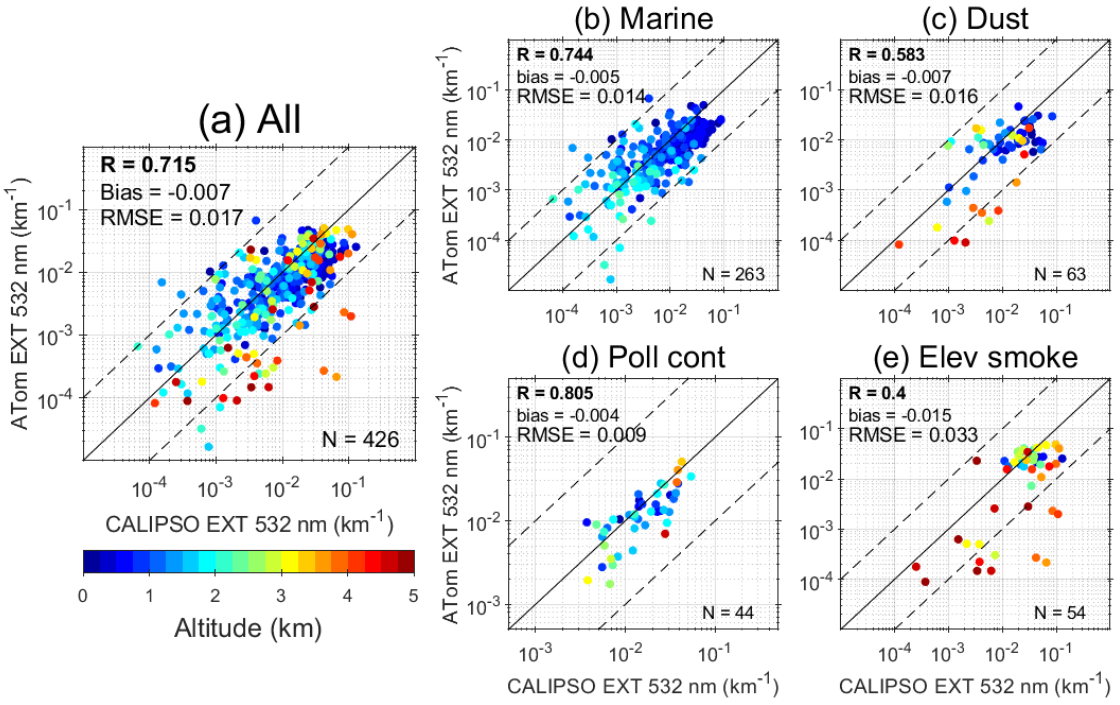

Figure 3.5: Comparison of the dry aerosol extinction coefficient from CALIOP observations and ATom measurements between the surface and 5 km altitude, with the data regridded to a profile with 240 m bin width and colours referring to the altitude of the measurement (a). The bins where marine (b), mineral dust (c), polluted continental (d), and elevated smoke (e) aerosols are dominant are shown separately. Spearman's correlation coefficient (R), bias, the root mean squared error (RMSE), and the sample space (N) are given in the legend. The solid lines represent the identity line and the dotted lines on either side of it represent 1 order of magnitude from the identity line.

As seen from the general comparison and case studies, the aerosol extinction coefficient inferred from ATom measurement is in very good agreement with the CALIPSO retrieval with the exception of a few cases where they can be significantly different. Scenarios that may lead to large differences in the datasets are already discussed in Section 3.3.2 and include the differences in the instrument sensitivities, measurement techniques, spatial and temporal resolutions, and assumptions underlying the intercept identification. In such situations, comparing the corresponding ANC may lead to misleading conclusions. Thus, while comparing the ANC, we only use those altitude bins for which the CALIOP-derived dry extinction coefficient is within $\pm 50\,\%$ of that estimated from ATom measurement. Note that the present study is not focused on the evaluation of CALIPSO products, for which several studies have already been performed (Mamouri et al., 2009; Pappalardo et al., 2010; Omar et al., 2013; Tesche et al., 2013, 2014; Kacenelenbogen et al., 2014; Rogers et al., 2014; Papagiannopoulos et al., 2016). By introducing the additional constraint of a set difference in the extinction coefficient, we aim to further increase the likelihood of comparing the same air parcels.

The comparison of $n_{50,\mathrm{dry}}$, as measured during ATom and estimated from CALIOP measurements using OMCAM and POLIPHON for the altitude bins that pass the extinction coefficient filter, is shown in Figure 3.6. It is found that the POLIPHON estimates of $n_{50,\mathrm{dry}}$ are in better agreement with the ATom measurements with a correlation coefficient of 0.829, RMSE value of $234\,\mathrm{cm}^{-3}$, and bias value of $-96.627\,\mathrm{cm}^{-3}$. In terms of absolute magnitude, OMCAM-estimated $n_{50,\mathrm{dry}}$ are up to an order of magnitude less than that of ATom, especially for aerosol concentrations below $100\,\mathrm{cm}^{-3}$. A closer look at the aerosol-type-specific comparison shows that the lower values seen in OMCAM are primarily from the marine-dominated cases for which POLIPHON estimates of $n_{50,\mathrm{dry}}$ are generally in better agreement with the in situ measurements. For dust-dominated cases, both the algorithms perform similarly, with POLIPHON being slightly better in terms of R, bias, and RMSE values. However, the POLIPHON-derived values for dust aerosols are $n_{100,\mathrm{dry}}$ instead of $n_{50,\mathrm{dry}}$ and thus should, in principle, underestimate the $n_{50,\mathrm{dry}}$. POLIPHON underestimates the $n_{50,\mathrm{dry}}$ for approx. $37\,\%$ retrievals. Given the limited sample space (19 bins) at the current stage, it is hard to comment on the performance of POLIPHON for dust-dominated cases. For the cases where polluted continental aerosols are dominant, the $n_{50,\mathrm{dry}}$, as estimated from both algorithms, are in good agreement with the ATom in situ measurements. Statistically speaking, OMCAM ($\mathrm{R} = 0.609$, $\mathrm{RMSE} = 275.93$, and $\mathrm{bias} = 26.548$) has better agreement with the ATom data than POLIPHON ($\mathrm{R} = 0.457$, $\mathrm{RMSE} = 335.81$, and $\mathrm{bias} = -125.757$). A similar result is also found for cases dominated by elevated smoke for which both the POLIPHON ($\mathrm{R} = 0.658$, $\mathrm{bias} = -171.491$, and $\mathrm{RMSE} = 308.46$) and OMCAM ($\mathrm{R} = 0.791$, $\mathrm{bias} = 105.47$, and $\mathrm{RMSE} = 213.33$) estimates of $n_{50,\mathrm{dry}}$ are in very good agreement with the ATom measurements. Interestingly, after applying the extinction coefficient constraint for comparing both the datasets, the CALIOP-estimated $n_{50,\mathrm{dry}}$ values are in good agreement with the ATom measurements, even at higher altitudes.

Figure 3.7 depicts the comparison of $n_{250,\mathrm{dry}}$, as derived from ATom and CALIOP

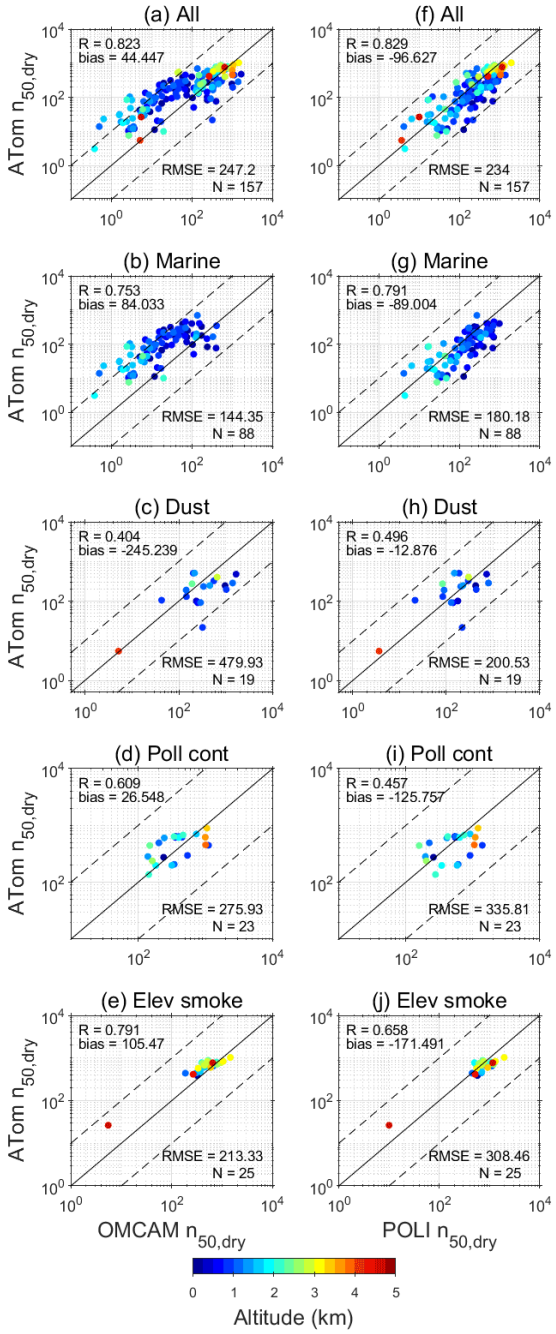

Figure 3.6: Comparison of $n_{50,\mathrm{dry}}$ (in cm^{-3}) retrieved from ATom and CALIPSO measurements using OMCAM (a-e) and POLIPHON (f-j) for 240 m altitude bins between 0 and 5 km for all the identified intersections. The bins where marine (b & g), dust (c & h), polluted continental (d & i), and elevated smoke (e & j) aerosols are dominant are separately shown. The Spearman's correlation coefficient (R), bias, root mean squared error (RMSE), and the sample space (N) are given in the legend.

measurements for the altitude bins that pass the extinction coefficient constraint. From

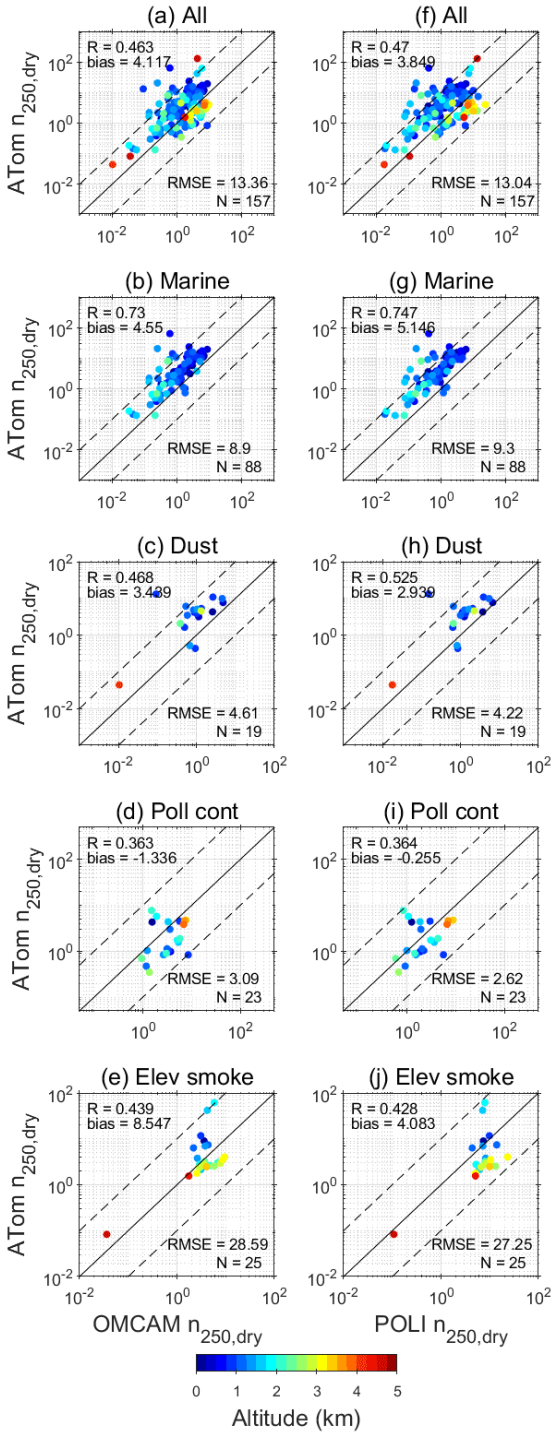

Figure 3.7: Same as Figure 3.6 but for $n_{250,\mathrm{dry}}$.

the figure, we find that both the OMCAM- and POLIPHON-derived $n_{250,\mathrm{dry}}$ are in good agreement with the in situ measurements in terms of the correlation coefficient, RMSE, and bias magnitude. Furthermore, the type-specific comparison shows that, for marine-

dominated cases, both the algorithms yield similar results and show a similar level of agreement with the ATom estimates. For dust-dominated cases, POLIPHON-estimated (R = 0.525, bias = 2.939, and RMSE = 4.22) $n_{250,\mathrm{dry}}$ values are in marginally better agreement with the ATom data than OMCAM (R = 0.468, bias = 3.439, and RMSE = 4.61). For polluted continental and elevated smoke dominant cases, the $n_{250,\mathrm{dry}}$ estimated from the OMCAM and POLIPHON algorithms show similar agreement with the corresponding ATom measurements.

Revised OMCAM algorithm

Figures 3.6b revealed that CALIOP-derived $n_{50,\mathrm{dry}}$ from the OMCAM algorithm for marine-dominated cases resulted in smaller values compared to that from POLIPHON and in situ measurements. In this section, we estimate ANC from CALIOP using a revised OMCAM algorithm in which a marine model derived from 11 AERONET island stations (Sayer et al., 2012) is used to characterize the marine aerosols. This new marine model is used to correct the CALIOP measurements for hygroscopicity by estimating the growth factors at different RH values (Figure 3.1). Also, the conversion factors for $n_{50,\mathrm{dry}}$ and $n_{250,\mathrm{dry}}$ are recalculated (Table 3.4) using the updated marine model following the methodology discussed in Section 3.2.3. It is interesting to note that the conversion factor estimated from the new marine model for $n_{250,\mathrm{dry}}$ only increased by 5 %, compared to 520 % for $n_{50,\mathrm{dry}}$. For comparing the CALIOP and ATom measurements for all of the identified intersections, we only use those 240 m data bins that pass the extinction coefficient constraint (CALIOP RH-corrected extinction coefficient within ± 50 % of the ATom measurement). Figure 3.8 depicts the comparison of $n_{50,\mathrm{dry}}$ and $n_{250,\mathrm{dry}}$, as derived from ATom and inferred from CALIOP data, using the revised OMCAM algorithm. The figure shows that both the OMCAM estimates of $n_{50,\mathrm{dry}}$ and $n_{250,\mathrm{dry}}$ are in very good agreement with the in situ measurements when resorting to the marine model of Sayer et al. (2012) with the $n_{50,\mathrm{dry}}$ comparison giving a correlation coefficient of 0.791, RMSE of 135.42 cm^{-3}, and bias of $-21.68\,\mathrm{cm}^{-3}$. The estimates of ANC from the updated OMCAM algorithm for the marine aerosol type is now on par with that from POLIPHON.

3.4 Discussion

In general, when the RH-corrected extinction coefficient from CALIOP is used, both the OMCAM and POLIPHON algorithms yield values of $n_{50,\mathrm{dry}}$ and $n_{250,\mathrm{dry}}$ that are comparable to in situ measurements for all aerosol types, except for marine-dominated cases. For marine-dominated retrievals, even though the $n_{250,\mathrm{dry}}$ estimated from OMCAM and POLIPHON algorithms were in good agreement with the in situ measurements, OMCAM estimates of $n_{50,\mathrm{dry}}$ were up to an order of magnitude smaller. This is perhaps the result of the limited in situ sea salt size distribution measurements that form the marine aerosol

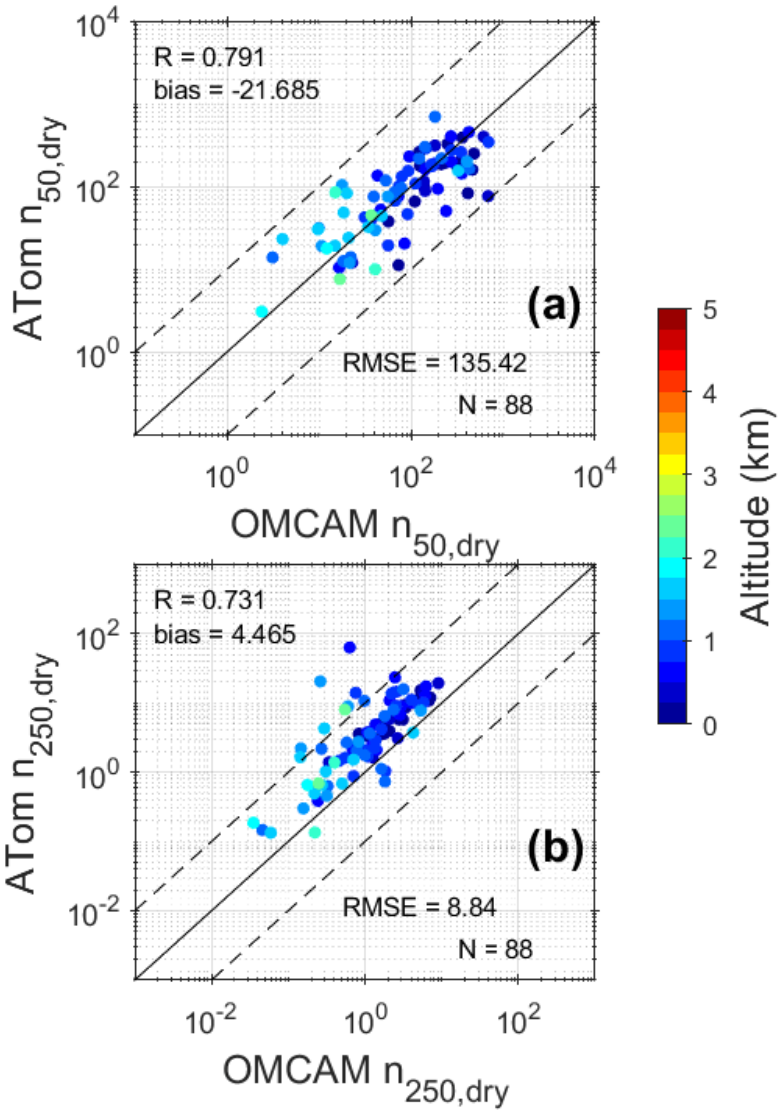

Figure 3.8: The $n_{50,\mathrm{dry}}$ (a) and $n_{250,\mathrm{dry}}$ (b) derived from ATom and CALIOP using the updated OMCAM algorithm for marine-dominated altitude bins.

model used in the OMCAM algorithm (Omar et al., 2009; Choudhury et al., 2022). Nevertheless, using the AERONET-based marine model of Sayer et al. (2012) in OMCAM results in an overall better agreement for both the $n_{50,\mathrm{dry}}$ and $n_{250,\mathrm{dry}}$ values with the independent airborne in situ measurements during ATom.

For dust-dominated retrievals, we find a moderate correlation between CALIOP-derived results and the in situ measurements. For both the $n_{50,\mathrm{dry}}$ and $n_{250,\mathrm{dry}}$, POLIPHON gives a marginally better agreement with the in situ data. Still, the POLIPHON conversion factors for mineral dust relate to $n_{100,\mathrm{dry}}$ and not to $n_{50,\mathrm{dry}}$. For some cases, the ANC estimated from both the algorithms are significantly different from the in situ measurements. Also, both the algorithms result in lower $n_{250,\mathrm{dry}}$ values compared to the in situ

data for most cases, which is contrary to the results from Haarig et al. (2019), who report an excellent agreement between ground-based lidar and airborne in situ measurements taken during the Saharan Aerosol Long-Range Transport and Aerosol–Cloud-Interaction Experiment (SALTRACE) campaign at Barbados. On further investigating the locations of dust-dominated intersections, we found that the underestimation is independent of the geographic location and is evident for retrievals over both the Atlantic and Pacific oceans. The aerosol type identified by CALIPSO for dust-dominated cases is mostly dusty marine (dust + marine) and not pure dust. Under such situations where the dust particles are far away from their source regions, their microphysical properties may change because of either ageing or chemical or cloud processing (Kim and Park, 2012; Ansmann et al., 2019; Goel et al., 2020). Also, three-quarters of the CALIPSO retrieval for dust-dominated cases are daytime retrievals. This might add to the differences observed between the observations.

For retrievals dominated by polluted continental and smoke, we find a medium–high correlation between ATom measurements and CALIOP-inferred estimates of $n_{50,\mathrm{dry}}$ using both algorithms with OMCAM performing slightly better than POLIPHON. For some height bins, the CALIOP estimates vary by more than a factor of 2 (especially for $n_{250,\mathrm{dry}}$) from the in situ measurements. Such a variation may either occur because of the spatial and temporal heterogeneity of aerosols or due to a change in the microphysical properties of the aerosols as a result of chemical or cloud processing. Also, similar to dust aerosols, the conversion factors for smoke and continental aerosols may change with age and geographical location (Ansmann et al., 2021b).

Overall, the $n_{50,\mathrm{dry}}$ and $n_{250,\mathrm{dry}}$ values estimated from the OMCAM algorithm with the updated marine model and the POLIPHON algorithm are overall in good agreement with the ATom in situ measurements. Such concurrence between the satellite estimates of height-resolved ANC (that are most relevant for cloud processes) and the coincident in situ measurements for various aerosol environments has not been achieved yet. This study along with previous concurrent results (Haarig et al., 2019; Marinou et al., 2019; Georgoulias et al., 2020; Choudhury et al., 2022), complements the use of ground-based and spaceborne lidar remote sensing techniques for retrieving height-resolved cloud-relevant aerosol microphysical properties.

3.5 Summary

We present a validation study of the spaceborne lidar-derived aerosol number concentration using the OMCAM and POLIPHON algorithms with the airborne in situ measurements conducted during the ATom campaigns over the Atlantic and Pacific oceans. To identify the comparison cases, we located intercepts between the CALIPSO flight tracks and the ATom aircraft tracks with the help of HYSPLIT trajectories. Out of all intercepts, 53 were found to be suitable for comparison. On comparing the dry extinction coefficients, we found an overall good agreement between the CALIOP data and the in situ measurements

with a correlation coefficient of 0.715. Disagreement was found mostly for retrievals above 3 km altitude. Such differences are most likely due to the spatial heterogeneity of aerosol properties rather than a retrieval error. Therefore, to compare the ANC, we filtered the datasets to select only those retrievals for which the CALIOP extinction coefficient is within $\pm 50\,\%$ of the one obtained from the in situ measurements. This constraint further increases the likelihood of comparing the same air parcel, which is crucial for parameters such as ANC that can easily vary by many orders of magnitude in space and time.

We found that the POLIPHON and OMCAM estimates of $n_{50,\mathrm{dry}}$ are in overall good agreement with the in situ measurements, with an overall correlation coefficient of 0.829 and 0.823, respectively. The agreement is seen for all the dominating aerosol type with the exception of marine aerosols, for which the POLIPHON estimates give a better agreement than the OMCAM. Revising OMCAM with the marine model of Sayer et al. (2012) led to results similar to the ones from POLIPHON and an overall better agreement with the in situ measurements. In the case of $n_{250,\mathrm{dry}}$, it is found that both the OMCAM ($\mathrm{R} = 0.463$) and POLIPHON ($\mathrm{R} = 0.47$) are in reasonable agreement with the in situ measurements. The updated OMCAM algorithm for marine aerosols resulted in no significant change in the $n_{250,\mathrm{dry}}$ concentrations.

Given the importance of knowledge regarding the global 3D distribution of the concentration of cloud-relevant aerosol particles, both the POLIPHON and the OMCAM (with the revised treatment of marine aerosols) algorithms emerge as an effective way of estimating the aerosol number concentrations over different size ranges from spaceborne lidar measurements. Future work includes a direct comparison of the type-specific extinction-to-number-concentration conversion factors from in situ measurements, for instance from Brock et al. (2021), with POLIPHON. The aerosol size distributions used in OMCAM can also be compared with in situ measurements (e.g. Clarke and Kapustin, 2002, 2010; Quinn et al., 2017; Brock et al., 2021) so as to better quantify the uncertainty associated with the output aerosol number concentrations for different aerosol subtypes. Furthermore, we also plan to test the potential of CALIOP measurements in deriving global CCN concentrations by validating them with long-term surface in situ measurements, for example from Schmale et al. (2017). The best-performing algorithm will be used to derive global CCN climatology from CALIPSO. This dataset will be beneficial for evaluating models and other satellite products, region-, and regime-wise detailed ACI studies and better constraining aerosol radiative forcing estimates in climate models.

3.6 Appendix

Table 3.A1: Details of ATom and CALIPSO data for the identified intersections. Δt is the effective time difference between the tracks after incorporating HYSPLIT trajectories. The difference in distance (Δs) and Δt between the measurements are averaged values. Note: D–dust; M–marine; C–polluted continental; S–elevated smoke.

S. No.	ATom			CALIPSO			Extinction coefficient contribution (%)				Δs (km)	Δt (h)
	Date	Time	Latitude	Date	Time	Latitude	D	M	C	S		
1	29/07/16	1655-1719	17.27, 19.43	29/07/16	2126 (D)	17.05, 20.99	39	44	17	0	257	16.5
2	01/08/16	2322-2347	64.35, 65.89	01/08/16	2210 (D)	63.22, 64.96	0	0	100	0	237	3.5
3	04/08/16	0025-0043	30.01, 31.39	03/08/16	1227 (N)	29.52, 31.48	0	100	0	0	126	7
4	06/08/16	1757-1808	18.96, 19.72	06/08/16	2355 (D)	18.54, 20.37	76	24	0	0	83	7
5	06/08/16	1902-1915	17, 17.48	06/08/16	1302 (N)	16.01, 17.98	1	96	3	0	359	14
6	06/08/16	1955-2018	14.03, 15	06/08/16	1303 (N)	13.54, 15.46	0	100	0	0	241	2
7	06/08/16	2154-2216	2.76, 4.80	06/08/16	1306 (N)	3.02, 5.17	0	100	0	0	457	2
8	06/08/16	2302-2314	-0.01, 0.004	06/08/16	1307 (N)	-0.17, 0.13	0	100	0	0	31	10
9	06/08/16	2337-0001	-0.09, 0.001	06/08/16	1307 (N)	-0.26, 0.49	10	90	0	0	446	20
10	08/08/16	1934-1943	-15.02, -14.31	08/08/16	1259 (N)	-15.17, -14.02	0	100	0	0	44	7
11	08/08/16	2019-2055	-22.47, -19.34	08/08/16	1300 (N)	-22.97, -18.81	0	100	0	0	143	7.5
12	13/08/16	0431-0456	-65.24, -64.98	13/08/16	0834 (N)	-64.19, -61.04	14	86	0	0	331	2
13	15/08/16	1114-1140	-50.79, -49.54	15/08/16	1833 (D)	-51.76, -49.23	7	93	0	0	113	9
14	15/08/16	1210-1238	-47.46, -45.96	15/08/16	0459 (N)	-48.76, -46.52	13	87	0	0	336	0.5
15	17/08/16	0855-0919	-3.03, -0.95	17/08/16	0255 (N)	-4.86, -0.02	1	14	3	81	205	11
16	17/08/16	0956-1017	3.48, 5.22	17/08/16	0255 (N)	-0.28, 2.36	2	3	0	95	408	7
17	22/08/16	1748-1819	45.54, 46.13	22/08/16	1906 (D)	45.23, 47.57	18	0	61	0	125	1
18	22/08/16	1831-1851	44.88, 45.07	22/08/16	1906 (D)	44.61, 46.99	10	0	78	0	330	6
19	26/01/17	2148-2212	0.91, 2.01	26/01/17	2140 (D)	0.04, 1.96	19	47	34	0	147	5
20	26/01/17	2249-2311	6, 8	26/01/17	2142 (D)	6.02, 7.98	34	66	0	0	77	0
21	26/01/17	2356-0019	13.51, 15.48	27/01/17	0958 (N)	13.04, 14.96	0	100	0	0	144	5
22	01/02/17	2113-2142	55.03, 56.08	01/02/17	1322 (N)	55.11, 56.97	0	74	26	0	84	9
23	03/02/17	1953-2003	16, 16.5	04/02/17	0013 (D)	16.45, 17.16	14	86	0	0	197	10
24	03/02/17	2220-2245	4.31, 5.75	03/02/17	1324 (N)	3.81, 6.18	0	100	0	0	157	4
25	06/02/17	0241-0305	-56.05, -54.60	06/02/17	1412 (N)	-56.06, -53.63	0	100	0	0	327	18
26	10/02/17	1854-1901	-43.77, -43.50	10/02/17	1344 (N)	-44.99, -44.03	0	75	0	25	113	1
27	10/02/17	2323-2349	-64.71, -64.13	11/02/17	0937 (N)	-65.26, -64.21	0	18	0	82	103	5
28	11/02/17	0312-0331	-59.74, -58.72	11/02/17	0617 (N)	60.18, -58.38	2	98	0	0	75	0
29	13/02/17	1238-1301	-46.76, -45.43	13/02/17	1756 (D)	-50.99, -47.04	44	56	0	0	346	10.5
30	13/02/17	1733-1753	-20.3, -18.87	14/02/17	0319 (N)	-20.95, -19.04	5	93	0	2	443	2.5
31	13/02/17	1930-2001	-9.11, -7.75	13/02/17	1450 (D)	-9.47, -6.52	39	54	6	0	122	10
32	15/02/17	1713-1729	38.76, 39.2	15/02/17	1451 (D)	40.01, 44.98	6	94	0	0	462	10
33	19/02/17	1848-1914	74.2, 76.09	19/02/17	1934 (D)	75.54, 77.59	7	93	0	0	178	5.5
34	01/10/17	1606-1617	34.59, 35.23	01/10/17	0958 (N)	33.81, 35.18	14	0	86	0	74	7
35	06/10/17	2002-2014	16.35, 16.69	07/10/17	0031 (D)	16.22, 16.65	24	61	15	0	60	3
36	06/10/17	2157-2218	10.7, 12.28	06/10/17	1341 (N)	10.12, 12.36	0	100	0	0	141	11
37	07/10/17	0121-0132	-4.44, -3.48	06/10/17	1345 (N)	-3.46, -2.52	0	100	0	0	230	1
38	14/10/17	1246-1311	-60.1, -58.69	14/10/17	1824 (D)	-58.97, -57.04	14	86	0	0	302	2.5
39	17/10/17	1547-1607	-25.72, -24.23	17/10/17	1546 (D)	-26.95, -24.01	22	78	0	0	112	0
40	20/10/17	1428-1448	28.04, 29.79	20/10/17	0355 (N)	26.51, 28.96	0	100	0	0	210	16
41	20/10/17	1527-1546	34.3, 36	20/10/17	0353 (N)	33.84, 36.77	0	100	0	0	140	14.5
42	23/10/17	1847-1859	44.8, 45.32	24/10/17	0642 (N)	44.03, 48.97	5	58	36	0	290	5
43	24/04/18	1905-1929	3.53, 4.97	24/04/18	2200 (D)	2.04, 5.98	15	75	10	0	425	9
44	29/04/18	2124-2152	42.48, 44.8	29/04/18	1302 (N)	41.01, 44.95	13	32	27	28	231	16.5
45	01/05/18	2119-2138	10.71, 12.14	01/05/18	1258 (N)	10.01, 12.96	0	85	0	15	188	0.5
46	01/05/18	2221-2245	4.39, 6.19	01/05/18	1300 (N)	3.04, 6.98	0	88	0	12	385	6
47	01/05/18	2328-0011	-2.02,-0.19	02/05/18	0123 (D)	-1.96, -0.22	0	100	0	0	71	2
48	06/05/18	2021-2033	-43.59, -43.42	06/05/18	1332 (N)	-45.96, -43.01	12	88	0	0	202	9
49	07/05/18	0254-0318	-64.72, -64.27	07/05/18	0746 (N)	-65.18, -63.02	0	100	0	0	99	2
50	12/05/18	1536-1603	-37.22, -35.4	12/05/18	1640 (D)	-37.97, -35.41	29	71	0	0	177	0
51	12/05/18	1932-1956	-16.84, -15	13/05/18	0337 (N)	-16.98, -14.52	28	72	0	0	107	11
52	14/05/18	1649-1712	20.87, 22.63	14/05/18	1505 (D)	22.02, 23.99	5	95	0	0	325	10
53	14/05/18	1932-1952	38.06, 38.95	14/05/18	1510 (D)	38.52, 39.49	52	26	22	0	95	14.5

Chapter 4

Assessment of CALIOP-derived CCN concentrations by in situ surface measurements*

Short summary

The aerosol and CCN number concentrations derived from spaceborne lidar are compared with long-term in-situ measurements collected at seven surface stations covering a variety of aerosol environments. Because the in-situ data includes simultaneous retrievals of aerosol and CCN number concentrations, the CCN parametrizations that convert the former to the latter are also assessed. The result shows the reliability of the CCN parametrizations as well as the ability of the OMCAM algorithm to estimate both aerosol and CCN number concentrations from space. Based on the findings, necessary measures that should be considered for retrieving height- and type-resolved global CCN concentrations are discussed.

*Published as: Choudhury, G. and Tesche, M.: Assessment of CALIOP-Derived CCN Concentrations by In Situ Surface Measurements, Remote Sens., 14, 3342, https://doi.org/10.3390/rs14143342, 2022.

4.1 Introduction

Aerosol particles form an important component of Earth's radiative budget by either interacting directly with short- and longwave radiation, or indirectly by acting as cloud condensation nuclei (CCN), which affect cloud properties. Under most atmospheric conditions, aerosols are required for water vapor to condense into cloud droplets. Thus, changes in aerosol concentration may alter the number of cloud droplets formed within a cloud (Twomey, 1974) and adjust the cloud's extent and lifetime (Albrecht, 1989). These aerosol-cloud interactions (ACIs) are the major contributor to the total aerosol effective radiative forcing and still remain the most uncertain component of anthropogenic radiative forcing (Forster et al., 2021).

The impact of changes in aerosol concentration on cloud droplets is non-linear. It depends not only on the aerosol's physical (size and shape) and chemical properties (hygroscopicity) but also on ambient meteorological parameters such as water vapor content and atmospheric stability (Fan et al., 2016; Seinfeld et al., 2016; Choudhury et al., 2019). The aerosol concentration may vary regionally by several orders of magnitude (10 to $10^5\,\mathrm{cm}^{-3}$) depending on the type, strength, and proximity of sources and sinks. Today, in situ aerosol observatories provide continuous and temporally highly resolved long-term measurements of cloud-relevant aerosol properties such as aerosol-sized distribution and chemical composition and CCN concentrations at different supersaturations (ss). However, they are limited to selected geographical locations. In contrast, satellite instruments can provide global observations of aerosols and clouds and, thus, are used extensively for studying ACIs with constrained meteorology and selected cloud regimes (Oreopoulos et al., 2017; Douglas and L'Ecuyer, 2019; Bellouin et al., 2020).

The fundamental aerosol information needed to study ACIs for liquid clouds is the number of available CCN close to the cloud base as only those will interact with the cloud droplets. Satellite retrievals, however, give aerosol optical properties, which are used either directly as proxies for the number concentration of CCN (n_{CCN}) or to derive information on the cloud-relevant aerosol fraction. Most satellite-based ACI studies use aerosol optical depth (AOD; Feingold et al., 2001; Quaas et al., 2008, 2009) or an aerosol index (AI; Nakajima et al., 2001; Bréon et al., 2002; Lohmann and Lesins, 2002; Gryspeerdt et al., 2017) as CCN proxies. The AOD may not be an accurate proxy for CCN as it does not include any information about the size of the observed aerosol particles. For instance, a large number of small particles can result in the same AOD as a small number of large particles. Furthermore, hydrophobic particles that are less efficient CCN compared to hygroscopic particles may contribute significantly to the AOD. Conversely, the AI, as the product of the AOD, and the Ångström exponent form a slightly better qualitative CCN proxy than the AOD as it is weighted more towards fine aerosols (Stier, 2016; Quaas et al., 2020). To better quantify the radiative forcing associated with ACI, Hasekamp et al. (2019) used polarimetric observations over oceans to infer column-integrated, aerosol-sized distributions. They further used the aerosol number concentration with a wet radius > 150

nm as the CCN proxy and found the forcing estimates to be almost 50 % higher than those where the AOD or AI were used. One of the intrinsic limitations of using any of the three CCN proxies is that they are all column-integrated parameters, i.e., they may not necessarily represent aerosols close to the cloud base, which are the ones relevant for ACI (Costantino and Bréon, 2010, 2013). Moreover, the AI and polarimetric retrievals are not reliable over land (Sayer et al., 2013; Quaas et al., 2020), where most of the anthropogenic aerosols are generated and the concentrations are the highest. A way to overcome the shortcomings associated with CCN products inferred from observations with passive sensors is to shift towards height-resolved aerosol and cloud observations using spaceborne lidar, which is available over both land and ocean (Quaas et al., 2020).

Shinozuka et al. (2015) used in situ measurements to report a linear relation between n_{CCN} and the aerosol extinction coefficient on a log–log scale. Following their work, Mamouri and Ansmann (2016) present the first CCN retrieval algorithm for ground-based lidar, where specific aerosol-type extinction-to-number-concentration conversion factors are used to infer the number concentration of particles larger than a set radius. This particle concentration is subsequently used in CCN parametrizations to estimate n_{CCN} at multiple supersaturations. The application to spaceborne Cloud-Aerosol Lidar with Orthogonal Polarization (CALIOP) observations was found to give aerosol number concentrations that were in reasonable agreement with in situ measurements (Marinou et al., 2019; Georgoulias et al., 2020; Choudhury et al., 2022). In a recent study, Choudhury and Tesche (2022a) presented a CCN retrieval algorithm that had been developed specifically for CALIOP application. The algorithm used normalized size distributions in the CALIOP aerosol model (Omar et al., 2009) and scaled them to reproduce the CALIOP-derived extinction coefficient. These inferred aerosol-type specific-size distributions were integrated to obtain aerosol number concentrations that were found to be in reasonable agreement with airborne in situ measurements (Choudhury et al., 2022). However, a direct comparison of CALIOP-derived CCN concentrations with in situ CCN measurements is still missing in the validation of both algorithms.

Schmale et al. (2017) presented multi-year continuous co-located in situ measurements of n_{CCN} and aerosol size distributions at 11 ground stations that covered a variety of environments with varying aerosol signatures. Here, we compare the n_{CCN} estimated from spaceborne CALIOP data using the aforementioned methodologies with the ground-based in situ measurements of Schmale et al. (2017). The concurrent in situ measurements of n_{CCN} and aerosol-sized distribution were furthermore used to assess the applicability of CCN parameterizations related to different aerosol types and size ranges. Based on our results, we also suggest necessary measures for compiling a global CCN climatology. The article is structured as follows. We describe the datasets, retrieval algorithms, and comparison methodology in Section 4.2. The comparison between the in situ and satellite derived n_{CCN} is given in Section 4.3. The findings and possible steps forward are summarized in the final section.

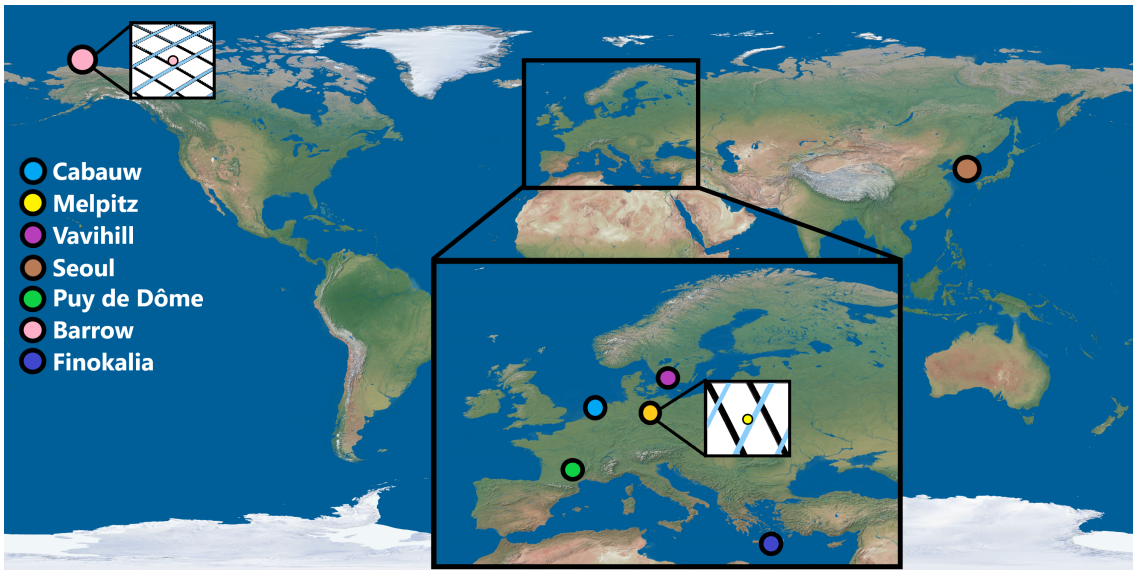

Figure 4.1: Location of the in situ sites used in this study. The large inset gives a closer look of Europe. The small insets present daytime (blue) and nighttime (black) ground tracks of CALIOP that fall within a 3° × 3° latitude–longitude grid box centered at Melpitz and Barrow, respectively, for a randomly selected month. The world map in the background is taken from `http://www.shadedrelief.com/natural3/pages/textures.html` (accessed on 7 July 2022).

4.2 Data and methods

4.2.1 In situ observations

The in situ observations used in this study were obtained from Schmale et al. (2017). The dataset consists of simultaneous measurements of aerosol-sized distributions and n_{CCN} at multiple supersaturations for 11 ground-based stations. The data have a temporal resolution of one hour and include a total of 98,677 h and 157,880 h of n_{CCN} and size distribution measurements, respectively. Of the 11 stations, we used measurements from 7 stations: Barrow, Cabauw, Finokalia, Melpitz, Vavihill, Puy de Dôme, and Seoul. Station selection was based on the availability, location, and proximity of the CALIOP overpasses relative to the station location. Other factors, such as very low aerosol concentrations (Mace Head) and presence of clouds (Jungfraujoch) close to the surface, hindered CALIOP retrievals; thus, such stations were not considered in our comparison. Among the selected stations, Puy de Dôme is a high-altitude station that represents the continental background and free-tropospheric air masses. Barrow and Finokalia are coastal stations covering Arctic and Mediterranean conditions. Cabauw, Melpitz, and Vavihill represent continental background conditions, while Seoul characterizes the polluted urban environment. The geographical location of these stations is shown in Figure 4.1. Details about the altitude, environment, and temporal coverage of each site are listed in Table 4.1. A comprehensive description of the instruments, inlet system, sampling procedure, and quality control measures used in

the data collection at each station is given in Schmale et al. (2017).

Table 4.1: Details of the in situ stations considered in this study.

Station	Environment	Location	Elevation	Temporal Coverage
Cabauw, The Netherlands	near coast, continental background	51°58'N, 4°56'E	−1	1 January 2012–31 December 2014
Melpitz, Germany	continental background	51°32'N, 12°56'E	86 m	1 January 2012–31 December 2014
Vavihill, Sweden	rural background	56°01'N, 13°09'E	172 m	20 December 2012–11 November 2014
Seoul, South Korea	urban, monsoon-influenced	37°34'N 126°58'E	38 m	1 January 2006–31 December 2010
Puy de Dôme, France	mountain, continental background	45°46'N, 02°57'E	1465 m	1 January 2014–1 January 2015
Barrow, USA	Arctic maritime	71°19'N, 156°37'W	11 m	20 July 2007–25 June 2008
Finokalia, Greece	coastal background, Mediterranean	35°20'N, 25°40'E	250 m	1 January 2014–31 December 2015

4.2.2 CALIOP

CALIOP is a two-wavelength polarization-sensitive lidar on the Cloud-Aerosol Lidar and Infrared Pathfinder Satellite Observations (CALIPSO) satellite, which has been observing the vertical distribution and occurrence of aerosols and clouds since June 2006 (Winker et al., 2009). CALIPSO aerosol products include vertical profiles of the aerosol extinction coefficient, aerosol backscatter coefficient, particle–linear depolarization ratio, and aerosol subtype. CALIPSO aerosol subtypes defined in the most recent version 4 data products include marine, dust, dusty marine, polluted dust, clean continental, polluted continental/smoke, and elevated smoke (Kim et al., 2018). In the present work, we used the CALIPSO level 2 version 4.20 aerosol profile product (NASA/LARC/SD/ASDC, 2018), which included aerosol optical properties and subtype information at a uniform horizontal resolution of 5 km and a vertical resolution of 60 m within the troposphere. We also used the relative humidity profiles included in the CALIPSO product obtained from the Global Modelling and Assimilation Office Data Assimilation System (Molod et al., 2015).

CCN Concentrations from CALIOP

The Optical Modelling of CALIPSO Aerosol Microphysics (OMCAM; Choudhury and Tesche, 2022a) and the Polarization Lidar Photometer Networking (POLIPHON; Mamouri and Ansmann, 2015, 2016) are the two techniques for estimating CCN concentrations from CALIOP measurements. Prior to the application of the CALIPSO aerosol parameters, we applied all the quality control measures suggested by Tackett et al. (2018) and only selected high-quality cloud-free retrievals. We also separated the dust mixtures into dust and non-dust contributions following Tesche et al. (2009). In both methods, we first needed to convert the CALIOP extinction coefficient to dry number concentrations of aerosols within a size range where they were likely to act as CCN. The number concentration was then used in aerosol-type specific CCN parametrizations to compute n_{CCN} at defined supersaturations. POLIPHON uses a set of equations to convert the CALIOP extinction coefficient

(α) to a dry aerosol number concentration with radius greater than j nm ($n_{j,\mathrm{dry}}$) as

$$n_{j,\mathrm{dry}} = C \cdot \alpha^{x}, \tag{4.1}$$

where j is 50 nm for continental and marine aerosols and 100 nm for dust aerosols; C is the conversion factor; and x is the extinction exponent obtained from the regression analysis of long-term AERONET measurements of AOD and size distributions (Mamouri and Ansmann, 2016; Ansmann et al., 2019, 2021b). The values of C and x used in this work are listed in Table 4.2. Similar to Choudhury et al. (2022), we used regression constants for continental (clean continental and polluted continental) and marine aerosols from Mamouri and Ansmann (2016), desert dust from Ansmann et al. (2019), and smoke aerosols from Ansmann et al. (2021b).

Table 4.2: Conversion factor (C in Mm cm^{-3}) and extinction exponent (x) values for POLIPHON and OMCAM algorithms used to estimate $n_{j,\mathrm{dry}}$ from Equation (4.1). Note that $x = 1$ for OMCAM.

Type	POLIPHON (Ambient)		OMCAM (Dry)
	C	x	C
Dust	8.855	0.7525	11.085
Clean continental	25.3	0.94	3.6
Marine	7.2	0.85	2.4
Elevated smoke	17	0.79	22
Polluted continental	25.3	0.94	24.93

In contrast to POLIPHON, OMCAM uses the aerosol microphysical properties (normalized size distributions and refractive indices) in the CALIPSO aerosol model (Omar et al., 2009) and scales the size distribution to reproduce the CALIOP extinction coefficient (Choudhury and Tesche, 2022a) using the MOPSMAP modelling package (Gasteiger and Wiegner, 2018). The scaled size distribution is then used to compute the required aerosol number concentration to be used in the corresponding CCN parametrization. While evaluating the OMCAM estimated aerosol number concentrations with airborne in situ measurements, Choudhury et al. (2022) found that the marine model from Omar et al. (2009) resulted in an underestimation of $n_{50,\mathrm{dry}}$ and suggested using the AERONET-based marine model from Sayer et al. (2012). We thus used the OMCAM algorithm with an updated marine model in our validation study. To correct the ambient CALIOP extinction coefficient for the hygroscopicity of hydrophilic aerosols, we used the kappa parametrization (Petters and Kreidenweis, 2007) included in the MOPSMAP package with globally averaged kappa values of 0.3 for continental aerosols (clean continental, polluted continental, elevated smoke), and 0.7 for marine aerosols (Andreae and Rosenfeld, 2008). Schmale et al. (2018) also found similar kappa values using the in situ data considered in this study. Dust is treated as hydrophobic, so no hygroscopicity correction was applied for dust retrievals.

To apply the hygroscopicity correction, following Choudhury et al. (2022), we first estimated the growth factors at different relative humidity (RH) values for different aerosol subtypes using the microphysical properties from the CALIPSO aerosol model and Sayer et al. (2012) (for marine subtype). We then correct the CALIOP extinction coefficient by using these growth factors. Previous studies found this method to yield reasonable results even under highly humid conditions such as within the marine boundary layer (Choudhury and Tesche, 2022a; Choudhury et al., 2022). Choudhury et al. (2022) parametrized the dry aerosol number concentrations linearly ($x = 1$ in Equation (4.1)) for the dry aerosol extinction coefficient. The corresponding values are given in Table 4.2. It is worth noting that the linear relationship in OMCAM held only for the dry extinction coefficient. In contrast, the POLIPHON technique was originally formulated for ambient conditions assuming a constant RH of 80 and 60 % for marine and continental aerosols, respectively (Mamouri and Ansmann, 2016). Thus, for POLIPHON, we only applied the hygroscopicity correction when the ambient RH exceeded these values for the corresponding aerosol types.

The fraction of aerosols that can act as CCN depends not only on the particle's physical and chemical properties but also on the atmospheric water vapor supersaturation, depends on meteorological parameters such as temperature, pressure, water content, vertical wind velocity and the resulting cooling rate. Given the complexities in measuring atmospheric n_{CCN}, Mamouri and Ansmann (2016) defined $n_{j,\mathrm{dry}}$ in Equation (4.1) as representing the n_{CCN} at ss = 0.15–0.20 %. The n_{CCN} at higher supersaturations are expressed as a multiple of $n_{j,\mathrm{dry}}$. In the present work, we considered CALIOP-derived n_{CCN} at ss = 0.2 % (i.e., $n_{j,\mathrm{dry}}$) in the comparison study because this parameter was provided by all of the in situ stations. The in situ data included simultaneous measurements of hourly n_{CCN} and aerosol-sized distributions (Schmale et al., 2017). To assess the CCN parameterizations used in our retrievals, we compared the $n_{j,\mathrm{dry}}$ as estimated from the size distributions with measurements of the n_{CCN} at 0.2 % supersaturation. Figure 4.2 shows a comparison of the in situ n_{CCN} from direct measurements and $n_{j,\mathrm{dry}}$ inferred from the concurrent in situ size-distribution measurements for the sites listed in Table 4.1. We considered $n_{50,\mathrm{dry}}$ for all stations except Finokalia, for which we compared $n_{100,\mathrm{dry}}$ as this particular site is frequently influenced by dust aerosols (Schmale et al., 2017, 2018). This approach was also supported by the CALIOP profiles within a 3° by 3° grid box surrounding the station in which 70–90 % of the monthly extinction coefficients were classified as related to dust, polluted dust, and dusty marine aerosol subtypes (not shown). Figure 4.2 shows very good agreement between in situ $n_{j,\mathrm{dry}}$ and n_{CCN} with a Spearman correlation coefficient (R) of 0.9, a normalized mean bias (NMB) of 20 %, and normalized mean error (NME) of 34 %. We therefore concluded that the use of aerosol-size-based CCN parametrizations as suggested by Mamouri and Ansmann (2016) provided reasonable estimates of n_{CCN}.

4.2.3 Comparison Methodology

Compared to passive sensors and the resulting column-integrated parameters, CALIOP measures height-resolved aerosol properties that can be aggregated to obtain their spatial

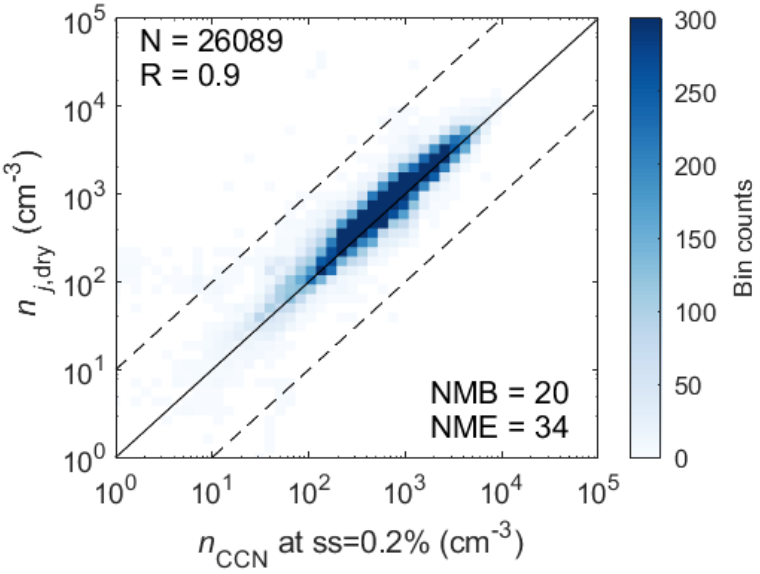

Figure 4.2: Comparison of concurrent in situ measurements of hourly n_{CCN} at 0.2 % supersaturation and $n_{j,\mathrm{dry}}$ ($j = 100$ nm for dust influenced Finokalia station and $j = 50$ nm for other sites). The values of correlation coefficient (R), total number of bins (N), normalized mean bias (NMB) and normalized mean error (NME) are given in the legend.

and vertical distribution. However, CALIOP has a very small footprint on the order of tens of meters compared to the hundreds of kilometers of passive sensors. Hence, monthly CALIPSO level 3 data products are reported at a coarse $2° \times 5°$ latitude-longitude grid (Winker et al., 2013; Tackett et al., 2018). To compare CALIOP observations with those at the in situ stations considered in this study, we defined a $3° \times 3°$ latitude–longitude grid box centered at the geographical location of a station and then considered all the CALIPSO level 2 profiles within that domain. Thus, the selected profiles were used to compute the n_{CCN} as discussed in Section 2.2. These individual profiles were then averaged to obtain monthly mean profiles of n_{CCN} for each grid box that was compared to the in situ data. Monthly averaging was used to compensate for (i) the relatively large area in the satellite-to-surface comparison that might include scenarios in which CALIOP and an in situ site observed different air masses and (ii) the local extremes in the in situ time series that were unlikely to be covered in the satellite observations. Note that our grid was finer than the $5° \times 5°$ in Fanourgakis et al. (2019) for comparing multi-model simulations of n_{CCN} with surface in situ measurements. For comparison to the in situ data at ground, CALIOP-derived profiles of CCN concentration were averaged from the surface to 1 km in height (to capture boundary-layer aerosols) except for the alpine site (Puy de Dôme), for which the averaging was extended to a height of 2 km. The comparison method used to determine the absolute error between the satellite and in situ measurement was the NME and to assess the relative bias of the satellite retrieval it was the NMB. The Spearman correlation coefficient (R) was used to assess the ability of satellite retrievals to represent the variability in the in situ

measurements. As the CALIOP-derived n_{CCN} represented $n_{j,\mathrm{dry}}$ ($j = 50\,\mathrm{nm}$ for continental and marine, and 100 nm for dust aerosols) at 0.2 % supersaturation, we also compared them with the in situ measurements of $n_{j,\mathrm{dry}}$ ($j = 100\,\mathrm{nm}$ for dust influenced Finokalia station and 50 nm for other stations). This approach enabled us to consider in situ measurements also for months that were lacking CCN measurements and to increases the number of data points to be considered in the statistical analysis.

4.3 Comparison of CCN Concentrations

The comparison of the monthly mean n_{CCN} (at $\mathrm{ss} = 0.2\,\%$) at the in situ stations and inferred from CALIOP measurements is presented in Figure 4.3 and Table 4.3. At all sites, monthly in situ $n_{j,\mathrm{dry}}$ are either comparable or larger than the directly measured in situ n_{CCN} with average NMB and NME values of 20.7 and 39.8 %, respectively and nearly identical monthly variations. Overall, the CALIOP estimates of monthly n_{CCN} using OMCAM algorithm were larger than the in situ observations with a mean NMB and NME of 49 % (31 %) and 76 % (93 %) for nighttime (daytime) retrievals, respectively. The POLIPHON algorithm resulted in even larger CCN values with NMB and NME values of 129 % (89 %) and 138.5 % (133.2 %) for nighttime (daytime) retrievals, respectively. A fraction of this overestimation comes from the consideration of pure size-based CCN parameterization (Equation (4.1)), which considers all aerosols within the selected size limit to be CCN active. This is also seen in Figure 4.2 and Figure 4.3, where $n_{j,\mathrm{dry}}$ overestimated n_{CCN} with a positive bias of about 20 %. The statistics improve somewhat for the comparison of $n_{j,\mathrm{dry}}$ (Table 4.3). The best n_{CCN} absolute error agreement was found at Puy de Dôme with nighttime OMCAM estimates resulting in an absolute error of about 43 %. Overall, worst agreement between CALIOP and in situ measurements was found at dust-influenced Finokalia with NME values as high as a factor of 1 for OMCAM and 1.5 for POLIPHON retrievals. Such disagreement was also reported in Choudhury et al. (2022) for dust and marine aerosol mixtures and may be because of changes in the microphysical properties of the aerosol types caused by either chemical or cloud processing. Assuming dust aerosols to be hydrophobic may also have contributed to the disagreement. Overall, about 88 % (91 %) and 77 % (88 %) of either of the daytime or nighttime monthly CALIOP n_{CCN} estimates from OMCAM and POLIPHON algorithms, respectively, stayed within a factor of 1.5 of the monthly in situ n_{CCN} ($n_{j,\mathrm{dry}}$) measurements. In some cases, the findings from CALIOP daytime and nighttime retrievals differed by several orders of magnitude. On closer inspection, we found that the daytime and nighttime tracks covered different geographical locations within a grid box. Furthermore, in any given month, the number of days with a daytime CALIPSO track within the considered domain was not always the same as that for nighttime overpasses. Also, the sensitivity of CALIOP to aerosols was different during day and night. These factors were likely to have caused the differences observed between the daytime and nighttime n_{CCN} retrievals.

It is known that CALIOP may fail to detect aerosol layers with a lower aerosol load (Ma

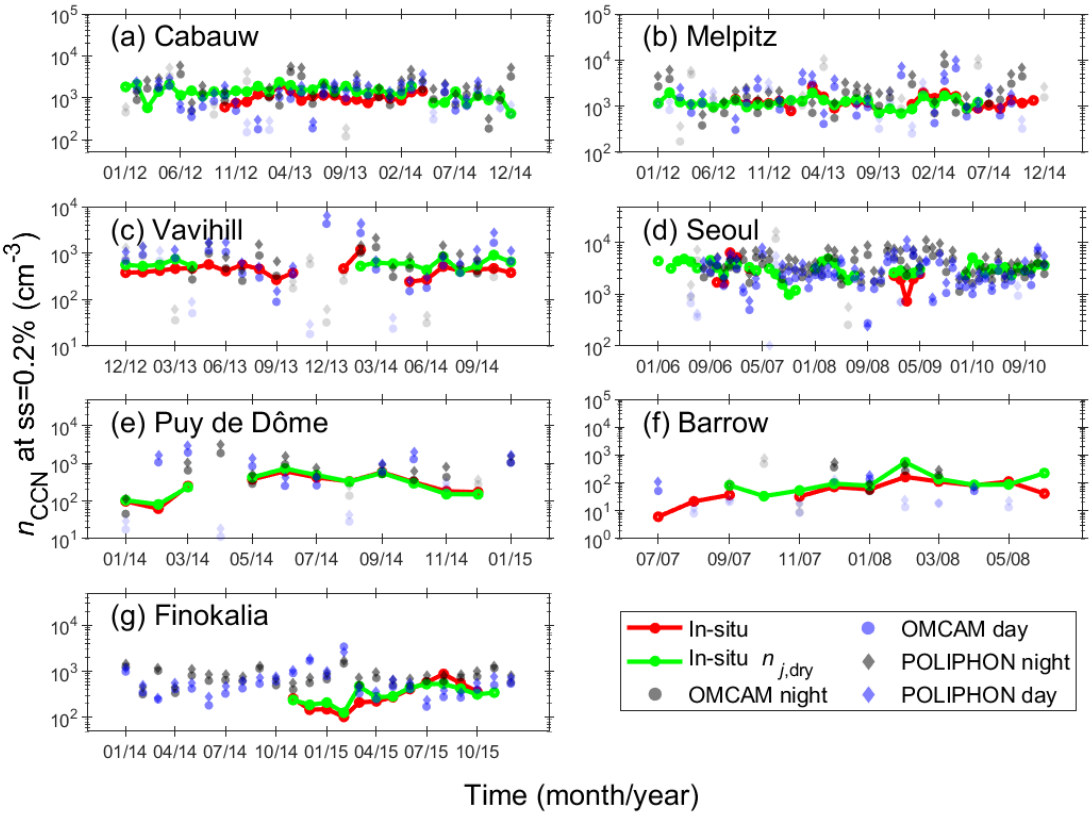

Figure 4.3: Monthly time series of $n_{j,\mathrm{dry}}$ (green) and n_{CCN} (red) as derived from ground-based in situ measurements and n_{CCN} inferred from CALIOP observations using the OMCAM (gray dots for nighttime data and blue for daytime data) and POLIPHON (gray diamonds for nighttime and blue for daytime data) algorithms at Cawbauw (a), Melpitz (b), Vavihill (c), Seoul (d), Puy de Dôme (e), Barrow (f), and Finokalia (g) stations. The semi-transparent data points are for the cases where the number of CALIOP data bins with finite aerosol retrievals used to produce the monthly average are less than 100.

et al., 2018; Watson-Parris et al., 2018; Quaas et al., 2020). On analyzing the number of CALIOP data bins with valid aerosol retrieval ($\mathrm{N_{bins}}$) used to compute the monthly n_{CCN} time series in Figure 4.3, we identified several cases where $\mathrm{N_{bins}} < 100$ (25^{th} percentile) coincided with outliers (semi-transparent points in Figure 4.3). Figure 4.4 shows how the comparison of CALIOP-derived CCN concentrations with the in situ measurements improved when only months with $\mathrm{N_{bins}} > 100$ are considered in the analysis. In that case, the CALIOP estimates of n_{CCN} using POLIPHON are in reasonable agreement with the in situ $n_{j,\mathrm{dry}}$ and n_{CCN} with NME values of 83 and 123 %, NMB values of 62 and 108 %, and R values of 0.61 and 0.7, respectively. The OMCAM estimates were in even better agreement with the in situ $n_{j,\mathrm{dry}}$ and n_{CCN} with NME values of 54 and 71 %, NMB values of 9 and 39 %, and R values of 0.63 and 0.68, respectively.

Along with the aerosol load, the number of days in a month observed (DMO) by CALIOP within a grid box may also have a significant impact on the n_{CCN} retrieval.

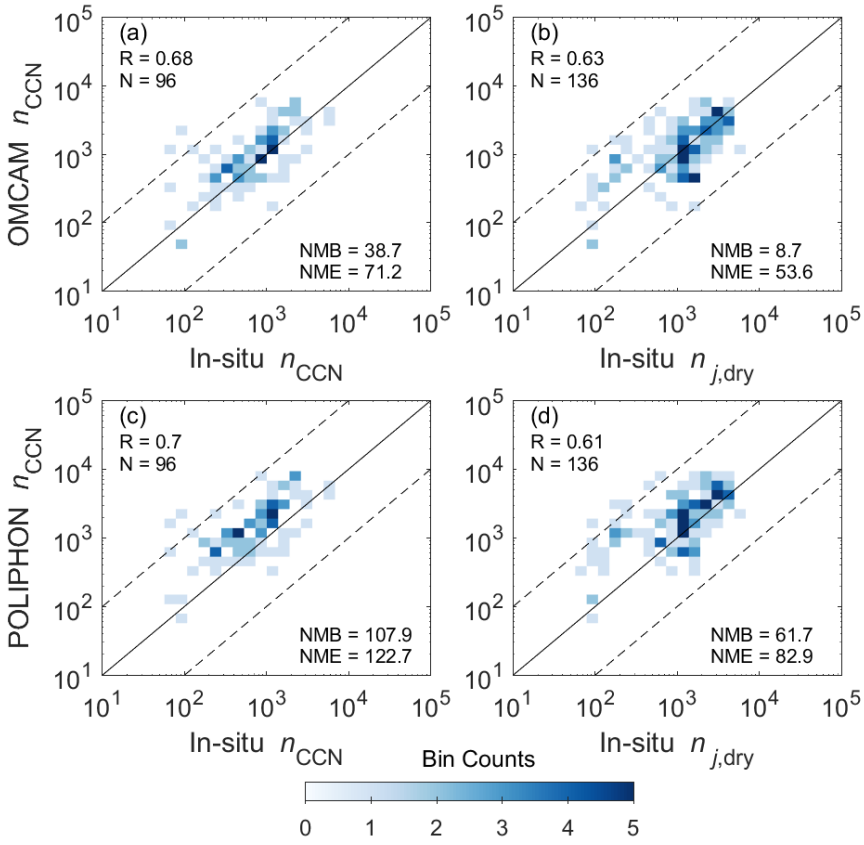

Figure 4.4: Comparison of n_{CCN} (a,c) and $n_{j,dry}$ (b,d) from in situ and CALIOP (day and night combined) measurements using OMCAM (a,b) and POLIPHON (c,d) for $N_{bins} > 100$ at all sites given in Table 4.1

.

In general, CALIOP-derived monthly values are expected to be more representative of a region within higher DMO. The DMO value depends on the geographical location (about 19 days at high latitude Barrow and 7 days at Melpitz station) and the size of the grid box, especially along the longitude. As the former cannot be modulated, increasing the grid box for CALIOP sampling is the only possible way to get higher DMO values. We therefore suggest using a relatively coarse $2° \times 5°$ latitude–longitude grid (also used in CALIPSO level 3 data (Tackett et al., 2018)) to estimate a global height-resolved n_{CCN} to obtain a regionally representative result. Even so, CALIOP has the potential to provide height- and type-resolved n_{CCN} over both land and oceans. With regards to the ACI study, the height-resolved measurements can be used to estimate the n_{CCN} close to cloud base and the type-resolved measurements to quantify the anthropogenic component. The availability of more than a decade of CALIOP measurements provides a unique opportunity to study the global and seasonal distribution of CCN concentrations for different aerosol types. How-

Table 4.3: Comparison statistics of monthly n_{CCN} at ss = 0.2 % (in cm^{-3}) and $n_{j,\mathrm{dry}}$ (in cm^{-3}) derived from in situ and CALIOP measurements. The values enclosed within brackets are for daytime CALIOP retrievals and the unbracketed values represent nighttime retrievals. The normalized mean bias (NMB) and normalized mean error (NME) are given along with their averages weighted by the number of observation months for each station.

Stations	NMB (%)				NME (%)			
	OMCAM		POLIPHON		OMCAM		POLIPHON	
	n_{CCN}	$n_{j,\mathrm{dry}}$	n_{CCN}	$n_{j,\mathrm{dry}}$	n_{CCN}	$n_{j,\mathrm{dry}}$	n_{CCN}	$n_{j,\mathrm{dry}}$
Cabauw	44 (−9.9)	14.2 (−30.3)	123.3 (36.7)	79.8 (6.13)	72 (53.2)	66.6 (40.6)	134.8.1 (84.6)	102.6 (47.7)
Melpitz	47 (7.8)	43 (53.1)	134.9 (62.5)	128.5 (135)	82.7 (70)	78 (97.8)	151.6 (104.6)	140.3 (154.1)
Vavihill	17 (54.3)	12.1 (33.7)	99.6 (147.6)	83.6 (115)	44.2 (82.2)	47.8 (66.5)	105.4 (159.2)	92.1 (129)
Seoul	31.5 (19.6)	2.7 (−10.6)	88.3 (62.9)	48.9 (23.5)	75.3 (80)	39.7 (49)	106.5 (97.9)	63.5 (59)
Puy de Dôme	29.5 (100.8)	23.5 (122.2)	125.7 (219.2)	115.2 (254.6)	43 (157.3)	41.4 (172.3)	125.7 (254.1)	115.2 (281.1)
Barrow	113.6 (−41.7)	1 (−15)	241.7 (−15.7)	61.6 (56.7)	117.5 (84.9)	72.5 (55.8)	241.7 (94.2)	80.7 (70.9)
Finokalia	93.9 (127.3)	109.8 (126.3)	151.9 (146.1)	167.8 (150)	106.8 (189.3)	109.8 (170.4)	154.7 (196)	167.8 (174.1)
Average	48.8 (31.1)	26.7 (25.3)	128.6 (89)	91.2 (78.4)	75.9 (93.3)	62.6 (79.4)	138.5 (133.2)	104.3 (107.9)

ever, such a study is not within the scope of the present work and will be presented in future studies.

4.4 Conclusions

We presented a comparison of monthly in situ CCN concentrations (n_{CCN}) and dry aerosol number concentrations ($n_{j,\mathrm{dry}}$) with the spaceborne lidar CALIOP retrievals. POLIPHON and OMCAM algorithms were used to estimate $n_{j,\mathrm{dry}}$ and n_{CCN} from CALIOP measurements. Both techniques rely on size-based CCN parametrizations. A comparison of the concurrent in situ measurements of n_{CCN} and $n_{j,\mathrm{dry}}$ at all stations supported the applicability of the size-based CCN parametrizations. We found that the CALIOP estimates of monthly n_{CCN} at 0.2 % supersaturation were generally in good agreement with the in situ measurements: about 88 % (91 %) and 77 % (88 %) of n_{CCN} ($n_{j,\mathrm{dry}}$) estimates from OMCAM and POLIPHON algorithms remaining within a factor of 1.5 of the in situ measurements, respectively. Disagreement was primarily found for the monthly retrievals where the number of aerosol samples detected by CALIOP was less than 100 (25th percentile). Excluding such retrievals, we found the OMCAM n_{CCN} estimates to have better agreement with the in situ measurements with a normalized mean error of 71 %, normalized mean bias of 39 %, and correlation coefficient of 0.68. The in situ stations considered in this validation study cover different continental environments. Future studies involving a direct comparison of CALIOP retrievals with measurements over oceans, (e.g., from Hudson et al. (2010)) will provide better insight into the ability of CALIOP to estimate marine n_{CCN}. Having said that, our findings along with previous comparison studies (Marinou et al., 2019; Georgoulias et al., 2020; Choudhury and Tesche, 2022a; Choudhury et al., 2022) support the feasibility of constructing a global height-resolved n_{CCN} climatology from CALIOP measurements. Such a dataset would be invaluable not only for studying aerosol-cloud

interactions (Bellouin et al., 2020; Quaas et al., 2020) but also serve as a benchmark for regional and global climate models.

Summary and conclusions

This dissertation presents a novel CCN retrieval algorithm based on optical modelling of CALIPSO aerosol microphysics (OMCAM) and is designed specifically for application to CALIPSO lidar measurements. OMCAM uses the CALIPSO level 2 aerosol profile product together with the CALIPSO aerosol model that includes a set of normalized size distributions and refractive indices of specific aerosol subtypes called *clean marine, dust, polluted continental, clean continental, elevated smoke, polluted dust*, and *dusty marine*. OMCAM requires four aerosol input parameters from CALIPSO data: extinction coefficient, backscatter coefficient, depolarization ratio, and subtype mask. The depolarization ratio is first used to separate the extinction coefficient of aerosol mixtures (*polluted dust* and *dusty marine*) according to the contributions of spherical and non-spherical particles. The resulting type-specific aerosol extinction coefficients are then used to estimate the aerosol size distribution. This is done by linearly scaling the total aerosol number concentrations of the normalized dry size distribution of the CALIPSO aerosol model in light scattering calculations with the MOPSMAP optical modelling package (Gasteiger and Wiegner, 2018) to match the CALIPSO-inferred extinction coefficient. The final adjusted size distributions are then used to infer concentration of particles with a dry radius larger than a certain threshold which forms the input needed in the CCN parametrizations (Mamouri and Ansmann, 2016) that enables an estimation of CCN concentrations (n_{CCN}) at multiple supersaturations independent of geographical location and underlying surface type. The algorithm also accounts for the hygroscopic growth of hydrophilic aerosols by using the kappa parametrization (Petters and Kreidenweis, 2007) within the MOPSMAP package. The globally averaged kappa values of 0.3 for continental aerosols (*polluted continental, clean continental,* and *elevated smoke*) and 0.7 for marine aerosols are considered (Andreae and Rosenfeld, 2008). The RH correction can either be applied to the initial dry normalized size distribution or the ambient CALIPSO measurement.

The OMCAM algorithm is build around the initial normalized size distributions given in the CALIPSO aerosol model that are assumed to retain their shape for different aerosol concentrations, i.e., the volume fraction, standard deviation, and mean radius of the size distributions are assumed to be intensive and independent of the aerosol volume. While this approximation holds good in most scenarios (Omar et al., 2005), it may result in errors in situations with complicated aerosol mixtures, and may not account for natural variability as a result of chemical processing and ageing. Thus, a sensitivity study was performed in which the initial size distribution parameters were varied to quantify the uncertainty

associated with the algorithm. Furthermore, the algorithm outputs were validated thoroughly using temporally and spatially co-located in-situ measurements. For the validation, airborne observations conducted over the Pacific and Atlantic oceans during the ATom campaign (Wofsy et al., 2018) were used along with the long-term surface in-situ measurements collected at seven selected ground stations (Schmale et al., 2017). The airborne profile measurements are crucial to assess the ability of OMCAM to estimate height-resolved n_{CCN}. While the surface stations may not provide height-resolved information, they offer long-term measurements at a very high temporal resolution. Such data are necessary to evaluate the ability of OMCAM in capturing the temporal variations of n_{CCN}. The main findings and the derived conclusions are summarized in the following sections.

Sensitivity analysis

To estimate the uncertainty associated with the OMCAM algorithm, sensitivity studies were performed by modifying the input parameters. OMCAM relies primarily on the fixed volume-normalized aerosol size distributions derived from CALIPSO aerosol model. While such approximation may simplify the algorithm, it does not account for natural processes like aerosol ageing and chemical processing that may change the size distributions and hygroscopicity of aerosols. To account for such errors that may arise because of the assumptions, the standard deviation, mean radius, and volume fraction of the initial normalized size distributions and the RH values were varied and the output CCN concentrations were found to remain within a factor of 1.5 and 2. Incorporating further uncertainties from the CCN parametrizations and the CALIPSO retrievals, the overall uncertainty associated with the OMCAM-derived CCN concentrations was estimated to be within a factor of 2 and 3. This level of uncertainty is usually expected for remote sensing of cloud-relevant aerosol number concentrations (Shinozuka et al., 2015; Mamouri and Ansmann, 2016).

Validation

The primary output of the OMCAM algorithm is the aerosol number concentration, which is further used in the predefined CCN parametrizations suggested by Mamouri and Ansmann (2016) to infer CCN concentrations at multiple supersaturations. Thus, to evaluate the results of the algorithm, the aerosol and CCN number concentrations have to be compared to the results of in-situ observations.

In the first step of the validation, the OMCAM-estimated aerosol number concentrations are evaluated with the airborne measurements performed during the ATom campaigns. The comparison shows an acceptable agreement between the OMCAM-estimated and in-situ measured $n_{50,\mathrm{dry}}$ with a correlation coefficient of 0.82, a mean of $283.4\,\mathrm{cm}^{-3}$, a root mean square error (RMSE) of $247.2\,\mathrm{cm}^{-3}$, and a bias of $44.45\,\mathrm{cm}^{-3}$. A closer look at the comparison for different aerosol subtypes reveals a reasonable agreement for all subtypes except

marine aerosols (mean =134.6 cm^{-3}, RMSE = 144.3 cm^{-3}, and bias = 84 cm^{-3}), for which the OMCAM estimates are about an order smaller than ATom measurements. A possible reason for the underestimation of magnitude was attributed to the marine aerosol model used in CALIPSO as it was built from a small number of in-situ measurements of sea salt size distributions. Thus, the algorithm was revised by replacing the existing marine model with an updated AERONET-based marine model (Sayer et al., 2012). The revised algorithm results in improved $n_{50,\mathrm{dry}}$ estimates for marine-dominated cases with mean = 176.3 cm^{-3}, RMSE = 135.42 cm^{-3}, and bias = $-21.7\,\mathrm{cm}^{-3}$. This level of agreement between spaceborne and in-situ derived aerosol number concentrations across different height levels and aerosol types has not been achieved before.

In the second step of the validation uses the in-situ data from Schmale et al. (2017), which include simultaneous measurements of aerosol number and CCN concentrations at seven surface in-situ stations covering different aerosol environments. The simultaneous in-situ measurements of $n_{j,\mathrm{dry}}$ and n_{CCN} are used also to evaluate the CCN parametrizations given in Mamouri and Ansmann (2016). The in-situ $n_{j,\mathrm{dry}}$ agree with the in-situ n_{CCN} with a 20 % normalized mean bias (NMB) and 34 % normalized mean error (NME). This demonstrates the potential of simple aerosol-size-based CCN parametrizations. Further, the CALIPSO-estimated monthly time-series n_{CCN} are found to agree with the in-situ measurements with a 39 % NMB and 71 % NME. CALIPSO-estimated $n_{j,\mathrm{dry}}$ agree somewhat better with in-situ measurements with 8.7 % NMB and 53.6 % NME. To summarize the validation effort, it is found that OMCAM shows great promise in capturing the temporal evolution of $n_{j,\mathrm{dry}}$ and n_{CCN} when applied to spaceborne CALIPSO lidar.

The spaceborne CALIPSO lidar has now collected a unique data set of more than 15 years of global height- and type-resolved aerosol optical properties. The OMCAM algorithm presented in this dissertation enables the conversion of the aerosol optical properties into cloud-relevant microphysical properties such as aerosol and CCN number concentration. The OMCAM retrieval is found to be reasonably consistent with co-located independent in-situ measurements at different altitude ranges over both land and ocean. Such an agreement has not yet been achieved for spaceborne estimates of CCN concentrations. The findings presented in this thesis therefore demonstrates the potential of OMCAM to derive 3D global climatological data related to aerosol and CCN number concentration that would be extremely helpful for studying aerosol-cloud interactions and evaluating and constraining global model simulations.

Outlook

Global 3D CCN climatology

The OMCAM validation results in Chapters 3 and 4 together with the length of the CALIPSO time series of more than 15 years pave the way towards inferring a global height-resolved climatology of CCN concentrations. To construct regional representative gridded data from CALIPSO lidar measurements, a minimum temporal resolution of one month and a latitude–longitude grid resolution of $2° \times 5°$ is recommended (Choudhury and Tesche, 2022b). The monthly time resolution accounts for the rather long 16 days orbital cycle of CALIPSO. The coarser grid resolution ensures a sufficient sampling frequency within each grid box during one month. The annual average column-integrated n_{CCN} at 0.2 % supersaturation estimated from applying OMCAM to CALIPSO measurements during the year 2007 with the suggested spatial and temporal resolution is shown in Figure 6.1b. In comparison to POLDER retrievals of n_{CCN} (Figure 6.1a and Hasekamp et al., 2019) over oceans for the year 2006, the OMCAM-retrieved values are smaller by about 1 to 2 orders of magnitude. The distribution of CCN is, however, similar in both the retrievals with hotspots close to the continents and decreasing magnitude further away from the continents. Also, there are noticeable differences in the regional aerosol distributions, for instance over Indonesia and the eastern Pacific ocean. Such regional differences may may be related to the fact that different years were considered for estimating the annual averages. Other factors like the difference in sampling frequency and spatial–temporal resolution may also contribute to the differences.

The OMCAM-derived n_{CCN} can be further separated into contributions from different aerosol types. Figure 6.2 depicts the global distribution of column-integrated n_{CCN} averaged over the year 2007 as derived for the four aerosol types: dust, polluted continental, marine, and elevated smoke. Dust and polluted continental aerosols are the dominant contributors to global n_{CCN} with the former found also far from its continental sources. As expected, emerging economies in Asia are the hotspots for CCN related to polluted continental aerosols. Dry and arid regions of the Middle East and Northern Africa are dominated by dust. Smoke aerosols are mostly confined to regions that are affected by forest fires. Marine aerosols are limited to oceans and are the most spatially homogenous and least abundant type of CCN. The application of OMCAM will be further expanded to the complete CALIPSO data set to construct a global 3D n_{CCN} climatology. The thus obtained data set will be crucial for studying the latitudinal, longitudinal, and altitudi-

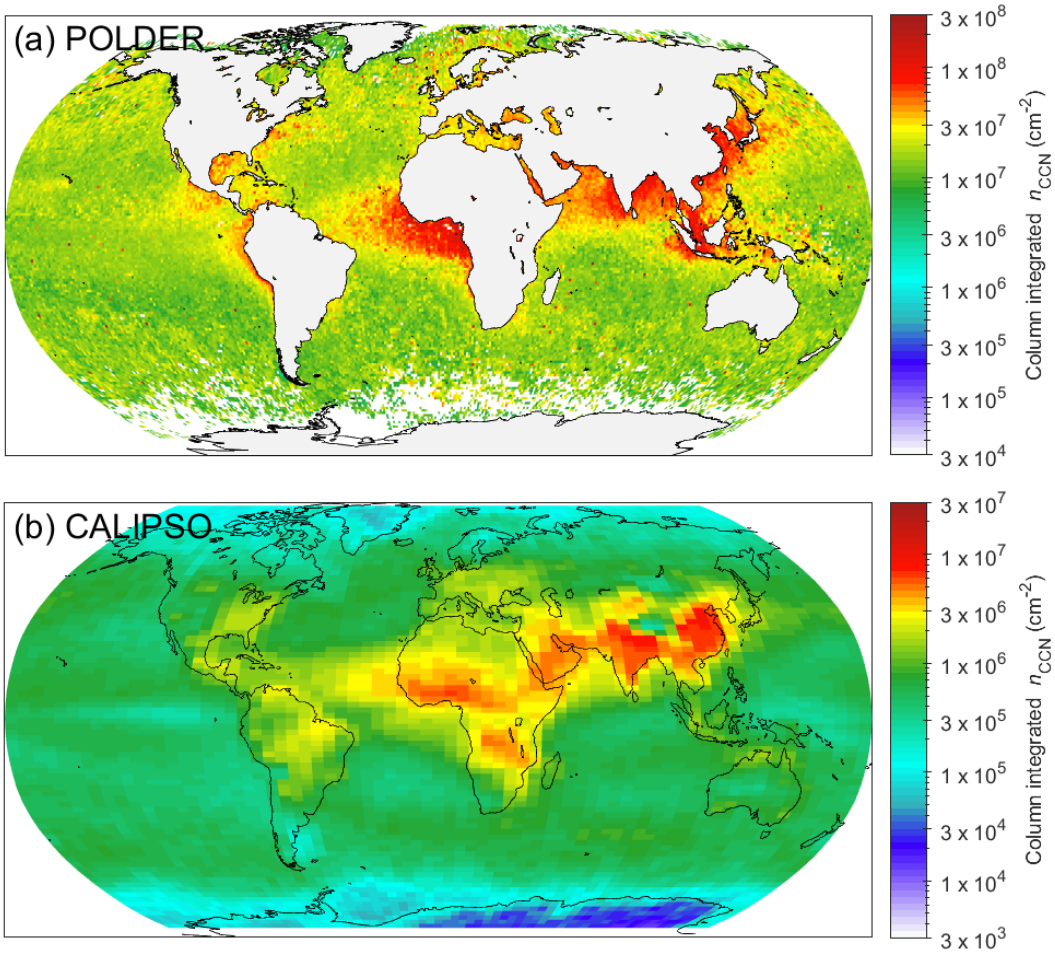

Figure 6.1: Annual average column integrated n_{CCN} from POLDER for the year 2006 (a) and CALIPSO for the year 2007 (b). CALIPSO measurements started in June 2006 and, therefore, the year 2007 is selected to obtain the annual mean concentrations for comparison.

nal distributions of n_{CCN} for different aerosol types as well as their seasonal and annual variations and trends.

Extending OMCAM to retrieve INP concentrations

Following the basic idea of Mamouri and Ansmann (2016), OMCAM can also be used to infer the number concentration of aerosols with a dry radius $> 250\,\mathrm{nm}$ ($n_{250,\mathrm{dry}}$) from spaceborne CALIPSO lidar measurements. This parameter then forms the input to INP parameterizations (DeMott et al., 2010, 2015; Ullrich et al., 2017) for estimating the concentrations of activated INPs (n_{INP}) at different temperatures via multiple nucleation pathways. As presented in Chapter 3 (Choudhury et al., 2022), the OMCAM-derived $n_{250,\mathrm{dry}}$ are in reasonable agreement with in-situ measurements. However, a direct comparison with in-situ

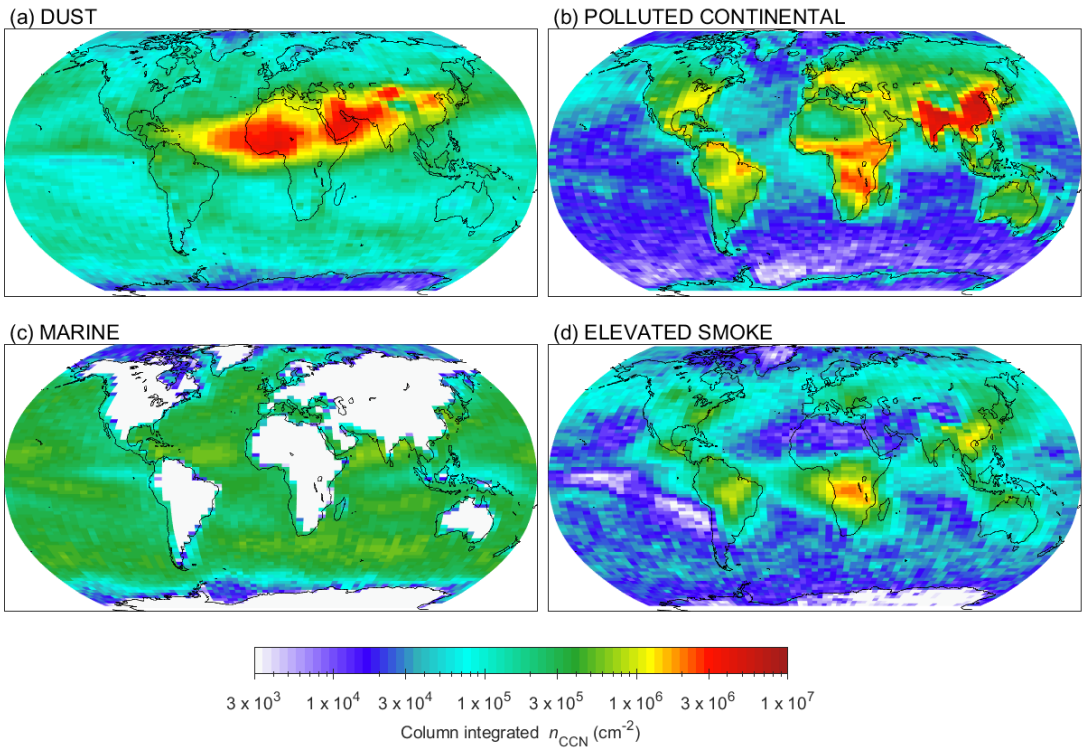

Figure 6.2: Annual average column-integrated n_{CCN} from CALIPSO for dust (a), polluted continental (b), marine (c), and elevated smoke (d) aerosols for the year 2007.

INP measurements would be required to further evaluate the reliability of an OMCAM-derived INP product. Extending OMCAM towards also retrieving INP concentrations is a logical next step that would enable the compilation of a global 3D INP climatology. As there is currently no global INP information, neither from atmospheric models nor from observations, such a data set would make a step change in studying ACI in ice-containing clouds on a global scale.

Radiative forcing due to ACI

The OMCAM-derived information on n_{CCN} and n_{INP} can be combined with cloud parameters from passive sensors to quantify the radiative forcing associated with ACI (Bellouin et al., 2020). Figure 6.1 shows the annual average n_{CCN} derived from POLDER and CALIPSO lidar measurements. Compared to the polarimetric retrievals of n_{CCN} (Figure 6.1a) that were recently used by Hasekamp et al. (2019) to study ACI, CALIPSO lidar has no limitations for retrievals over land. Furthermore, the OMCAM-derived n_{CCN} is height-resolved and, thus, provides the possibility to consider only those aerosols that lie close to cloud base and are actually in a position to interact with clouds in ACI studies. As shown in Figure 6.2, the OMCAM-derived n_{CCN} can be further separated into contributions from

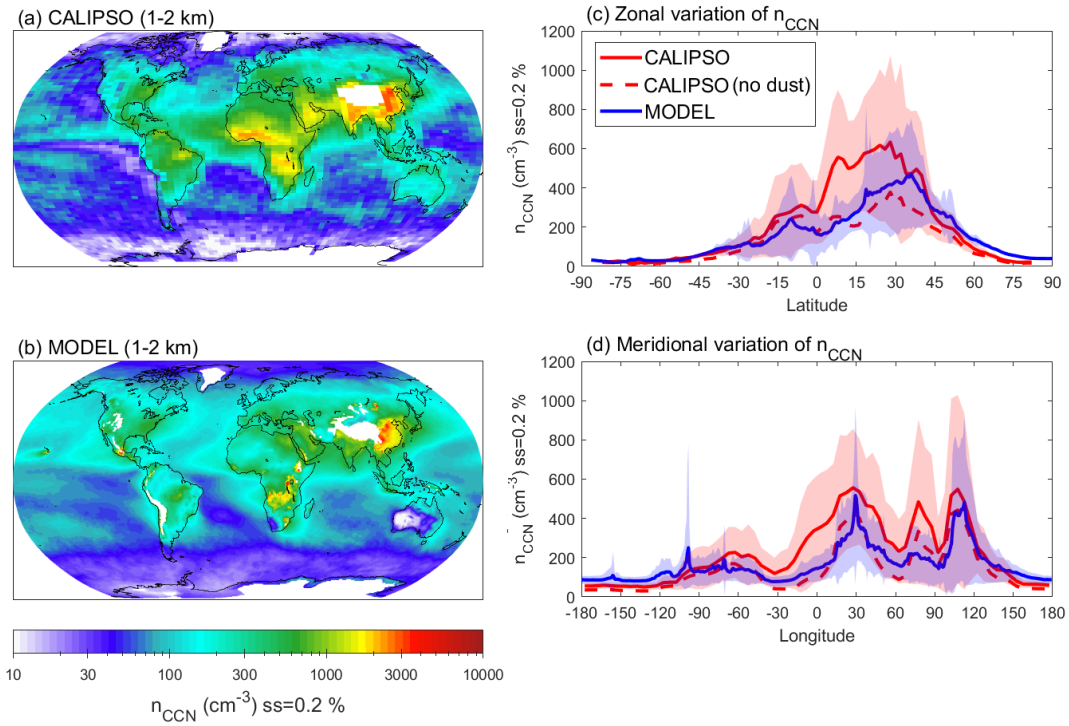

Figure 6.3: Annual n_{CCN} within 1–2 km height above mean sea level from CALIPSO (a) and box model (b) along with their zonal (c) and meridional (d) variations averaged over the year 2007.

different aerosol types. This is crucial for quantifying the anthropogenic or human-induced radiative forcing. Global n_{INP} can be used in estimating the forcing associated with ice-containing clouds, which is still not considered even in the recent IPCC report (Forster et al., 2021). The retrieved n_{CCN} and n_{INP} products can be used to obtain a more reliable radiative forcing estimates and, therefore, improve the physical basis of future climate projections.

Model evaluation

The OMCAM-derived global height-resolved n_{CCN} data are also invaluable for evaluating the representation of such particles in global model. Figure 6.3 compares the OMCAM-derived annual average n_{CCN} and the outputs from an aerosol box model (Haghighatnasab et al., 2022) at a supersaturation of 0.2 % within an altitude range from 1 to 2 km above mean sea level during the year 2007. The model estimates n_{CCN} by coupling the aerosol mass mixing ratio as derived from Copernicus Atmospheric Monitoring Service (CAMS) reanalysis data (Inness et al., 2019) with the CCN parameterization from Abdul-Razzak and Ghan (2000). The preliminary comparison shows that the modelled n_{CCN} values are comparable with OMCAM retrievals over oceans. However, the OMCAM estimates are noticeably larger in magnitude than the model over land. Interestingly, this difference is more

evident in dust-influenced regions (Figure 6.2a). When dust aerosols are not considered, the OMCAM-derived n_{CCN} values are in very good agreement with the model (Figures 6.3c and 6.3d). Furthermore, the modelled values over Australia are almost an order of magnitude smaller than that derived with OMCAM. A possible reason for the lower model-derived values can be attributed to missing aerosol sources over land regions in CAMS data (Errera et al., 2021). However, a more detailed comparison involving multi-year data is necessary before reaching more robust conclusions. The long-term OMCAM n_{CCN} data will be a benchmark for validating the ability of models to capture the spatial, temporal, and altitudinal distribution of CCN in the atmosphere.

References

Abdul-Razzak, H. and Ghan, S. J.: A parameterization of aerosol activation: 2. Multiple aerosol types, Journal of Geophysical Research: Atmospheres, 105, 6837–6844, doi: https://doi.org/10.1029/1999JD901161, 2000.

Aitken, J.: Collected Scientific Papers, edited by G. G. Knott, Cambridge University Press, London, 591 pp, 1923.

Albrecht, B. A.: Aerosols, Cloud Microphysics, and Fractional Cloudiness, Science, 245, 1227–1230, doi:10.1126/science.245.4923.1227, 1989.

Altaratz, O., Bar-Or, R. Z., Wollner, U., and Koren, I.: Relative humidity and its effect on aerosol optical depth in the vicinity of convective clouds, Environmental Research Letters, 8, 034 025, doi:10.1088/1748-9326/8/3/034025, 2013.

Anderson, T. L., Masonis, S. J., Covert, D. S., Charlson, R. J., and Rood, M. J.: In situ measurement of the aerosol extinction-to-backscatter ratio at a polluted continental site, Journal of Geophysical Research: Atmospheres, 105, 26 907–26 915, doi: 10.1029/2000JD900400, 2000.

Andreae, M. O. and Rosenfeld, D.: Aerosol–cloud–precipitation interactions. Part 1. The nature and sources of cloud-active aerosols, Earth-Science Reviews, 89, 13–41, doi: 10.1016/j.earscirev.2008.03.001, 2008.

Andreae, M. O., Rosenfeld, D., Artaxo, P., Costa, A. A., Frank, G. P., Longo, K. M., and Silva-Dias, M. a. F.: Smoking rain clouds over the Amazon, Science (New York, N.Y.), 303, 1337–1342, doi:10.1126/science.1092779, 2004.

Ansmann, A., Mamouri, R.-E., Hofer, J., Baars, H., Althausen, D., and Abdullaev, S. F.: Dust mass, cloud condensation nuclei, and ice-nucleating particle profiling with polarization lidar: updated POLIPHON conversion factors from global AERONET analysis, Atmospheric Measurement Techniques, 12, 4849–4865, doi:10.5194/amt-12-4849-2019, 2019.

Ansmann, A., Ohneiser, K., Chudnovsky, A., Baars, H., and Engelmann, R.: CALIPSO Aerosol-Typing Scheme Misclassified Stratospheric Fire Smoke: Case Study From the 2019 Siberian Wildfire Season, Frontiers in Environmental Science, 9, doi: 10.3389/fenvs.2021.769852, 2021a.

Ansmann, A., Ohneiser, K., Mamouri, R.-E., Knopf, D. A., Veselovskii, I., Baars, H., Engelmann, R., Foth, A., Jimenez, C., Seifert, P., and Barja, B.: Tropospheric and stratospheric wildfire smoke profiling with lidar: mass, surface area, CCN, and INP retrieval, Atmospheric Chemistry and Physics, 21, 9779–9807, doi:10.5194/acp-21-9779-2021, 2021b.

Bellouin, N., Quaas, J., Morcrette, J.-J., and Boucher, O.: Estimates of aerosol radiative forcing from the MACC re-analysis, Atmospheric Chemistry and Physics, 13, 2045–2062, doi:10.5194/acp-13-2045-2013, 2013.

Bellouin, N., Quaas, J., Gryspeerdt, E., Kinne, S., Stier, P., Watson-Parris, D., Boucher, O., Carslaw, K. S., Christensen, M., Daniau, A.-L., Dufresne, J.-L., Feingold, G., Fiedler, S., Forster, P., Gettelman, A., Haywood, J. M., Lohmann, U., Malavelle, F., Mauritsen, T., McCoy, D. T., Myhre, G., Mülmenstädt, J., Neubauer, D., Possner, A., Rugenstein, M., Sato, Y., Schulz, M., Schwartz, S. E., Sourdeval, O., Storelvmo, T., Toll, V., Winker, D., and Stevens, B.: Bounding Global Aerosol Radiative Forcing of Climate Change, Reviews of Geophysics, 58, e2019RG000 660, doi:10.1029/2019RG000660, 2020.

Bohren, C. F. and Huffman, D. R.: Absorption and scattering of light by small particles, John Wiley & Sons, doi:10.1002/9783527618156, 2008.

Boucher, O., Randall, D., Artaxo, P., Bretherton, C., Feingold, G., Forster, P., Kerminen, V. M., Kondo, Y., Liao, H., and Lohmann, U.: Climate change 2013: the physical science basis. Contribution of Working Group I to the Fifth Assessment Report of the Intergovernmental Panel on Climate Change, K., Tignor, M., Allen, SK, Boschung, J., Nauels, A., Xia, Y., Bex, V., and Midgley, PM, Cambridge University Press, Cambridge, UK, 2013.

Brock, C. A., Williamson, C., Kupc, A., Froyd, K. D., Erdesz, F., Wagner, N., Richardson, M., Schwarz, J. P., Gao, R.-S., Katich, J. M., Campuzano-Jost, P., Nault, B. A., Schroder, J. C., Jimenez, J. L., Weinzierl, B., Dollner, M., Bui, T., and Murphy, D. M.: Aerosol size distributions during the Atmospheric Tomography Mission (ATom): methods, uncertainties, and data products, Atmospheric Measurement Techniques, 12, 3081–3099, doi:10.5194/amt-12-3081-2019, 2019.

Brock, C. A., Froyd, K. D., Dollner, M., Williamson, C. J., Schill, G., Murphy, D. M., Wagner, N. J., Kupc, A., Jimenez, J. L., Campuzano-Jost, P., Nault, B. A., Schroder, J. C., Day, D. A., Price, D. J., Weinzierl, B., Schwarz, J. P., Katich, J. M., Wang, S., Zeng, L., Weber, R., Dibb, J., Scheuer, E., Diskin, G. S., DiGangi, J. P., Bui, T., Dean-Day, J. M., Thompson, C. R., Peischl, J., Ryerson, T. B., Bourgeois, I., Daube, B. C., Commane, R., and Wofsy, S. C.: Ambient aerosol properties in the remote atmosphere from global-scale in situ measurements, Atmospheric Chemistry and Physics, 21, 15 023–15 063, doi:10.5194/acp-21-15023-2021, 2021.

Bréon, F.-M., Tanré, D., and Generoso, S.: Aerosol Effect on Cloud Droplet Size Monitored from Satellite, Science, 295, 834–838, doi:10.1126/science.1066434, 2002.

Chauvigné, A., Sellegri, K., Hervo, M., Montoux, N., Freville, P., and Goloub, P.: Comparison of the aerosol optical properties and size distribution retrieved by sun photometer with in situ measurements at midlatitude, Atmospheric Measurement Techniques, 9, 4569–4585, doi:10.5194/amt-9-4569-2016, 2016.

Chen, Y.-C., Christensen, M. W., Xue, L., Sorooshian, A., Stephens, G. L., Rasmussen, R. M., and Seinfeld, J. H.: Occurrence of lower cloud albedo in ship tracks, Atmospheric Chemistry and Physics, 12, 8223–8235, doi:10.5194/acp-12-8223-2012, 2012.

Chen, Y.-C., Christensen, M. W., Stephens, G. L., and Seinfeld, J. H.: Satellite-based estimate of global aerosol–cloud radiative forcing by marine warm clouds, Nature Geoscience, 7, 643–646, doi:10.1038/ngeo2214, 2014.

Chen-Chen, H., Pérez-Hoyos, S., and Sánchez-Lavega, A.: Dust particle size, shape and optical depth during the 2018/MY34 martian global dust storm retrieved by MSL Curiosity rover Navigation Cameras, Icarus, 354, 114 021, doi:10.1016/j.icarus.2020.114021, 2021.

Cheung, H. C., Chou, C. C.-K., Lee, C. S. L., Kuo, W.-C., and Chang, S.-C.: Hygroscopic properties and cloud condensation nuclei activity of atmospheric aerosols under the influences of Asian continental outflow and new particle formation at a coastal site in eastern Asia, Atmospheric Chemistry and Physics, 20, 5911–5922, doi:10.5194/acp-20-5911-2020, 2020.

Choudhury, G. and Tesche, M.: Estimating cloud condensation nuclei concentrations from CALIPSO lidar measurements, Atmospheric Measurement Techniques, 15, 639–654, doi:10.5194/amt-15-639-2022, 2022a.

Choudhury, G. and Tesche, M.: Assessment of CALIOP-Derived CCN Concentrations by In Situ Surface Measurements, Remote Sensing, 14, doi:10.3390/rs14143342, 2022b.

Choudhury, G., Tyagi, B., Vissa, N. K., Singh, J., Sarangi, C., and Tripathi, S. N.: Aerosol-orography-precipitation – A critical assessment, Atmospheric Environment, 214, 116 831, doi:10.1016/j.atmosenv.2019.116831, 2019.

Choudhury, G., Tyagi, B., Vissa, N. K., Singh, J., Sarangi, C., Tripathi, S. N., and Tesche, M.: Aerosol-enhanced high precipitation events near the Himalayan foothills, Atmospheric Chemistry and Physics, 20, 15 389–15 399, doi:10.5194/acp-20-15389-2020, 2020.

Choudhury, G., Ansmann, A., and Tesche, M.: Evaluation of aerosol number concentrations from CALIPSO with ATom airborne in situ measurements, Atmospheric Chemistry and Physics, 22, 7143–7161, doi:10.5194/acp-22-7143-2022, 2022.

Christensen, M. W. and Stephens, G. L.: Microphysical and macrophysical responses of marine stratocumulus polluted by underlying ships: Evidence of cloud deepening, Journal of Geophysical Research: Atmospheres, 116, doi:https://doi.org/10.1029/2010JD014638, 2011.

Christensen, M. W., Chen, Y.-C., and Stephens, G. L.: Aerosol indirect effect dictated by liquid clouds, Journal of Geophysical Research: Atmospheres, 121, 14,636–14,650, doi:10.1002/2016JD025245, 2016.

Christensen, M. W., Neubauer, D., Poulsen, C. A., Thomas, G. E., McGarragh, G. R., Povey, A. C., Proud, S. R., and Grainger, R. G.: Unveiling aerosol–cloud interactions – Part 1: Cloud contamination in satellite products enhances the aerosol indirect forcing estimate, Atmospheric Chemistry and Physics, 17, 13 151–13 164, doi:10.5194/acp-17-13151-2017, 2017.

Christensen, M. W., Gettelman, A., Cermak, J., Dagan, G., Diamond, M., Douglas, A., Feingold, G., Glassmeier, F., Goren, T., Grosvenor, D. P., Gryspeerdt, E., Kahn, R., Li, Z., Ma, P.-L., Malavelle, F., McCoy, I. L., McCoy, D. T., McFarquhar, G., Mülmenstädt, J., Pal, S., Possner, A., Povey, A., Quaas, J., Rosenfeld, D., Schmidt, A., Schrödner, R., Sorooshian, A., Stier, P., Toll, V., Watson-Parris, D., Wood, R., Yang, M., and Yuan, T.: Opportunistic experiments to constrain aerosol effective radiative forcing, Atmospheric Chemistry and Physics, 22, 641–674, doi:10.5194/acp-22-641-2022, 2022.

Clarke, A. and Kapustin, V.: Hemispheric Aerosol Vertical Profiles: Anthropogenic Impacts on Optical Depth and Cloud Nuclei, Science, 329, 1488–1492, doi:10.1126/science.1188838, 2010.

Clarke, A., Kapustin, V., Howell, S., Moore, K., Lienert, B., Masonis, S., Anderson, T., and Covert, D.: Sea-Salt Size Distributions from Breaking Waves: Implications for Marine Aerosol Production and Optical Extinction Measurements during SEAS, Journal of Atmospheric and Oceanic Technology, 20, 1362–1374, doi:10.1175/1520-0426(2003)020¡1362:SSDFBW¿2.0.CO;2, 2003.

Clarke, A. D. and Kapustin, V. N.: A Pacific Aerosol Survey. Part I: A Decade of Data on Particle Production, Transport, Evolution, and Mixing in the Troposphere, Journal of the Atmospheric Sciences, 59, 363 – 382, doi:10.1175/1520-0469(2002)059¡0363:APASPI¿2.0.CO;2, 2002.

Coakley, J. A. and Walsh, C. D.: Limits to the Aerosol Indirect Radiative Effect Derived from Observations of Ship Tracks, Journal of the Atmospheric Sciences, 59, 668–680, doi:10.1175/1520-0469(2002)059¡0668:LTTAIR¿2.0.CO;2, 2002.

Coakley, J. A., Bernstein, R. L., and Durkee, P. A.: Effect of Ship-Stack Effluents on Cloud Reflectivity, Science, 237, 1020–1022, doi:10.1126/science.237.4818.1020, 1987.

Costantino, L. and Bréon, F.-M.: Analysis of aerosol-cloud interaction from multi-sensor satellite observations, Geophysical Research Letters, 37, doi:10.1029/2009GL041828, 2010.

Costantino, L. and Bréon, F.-M.: Aerosol indirect effect on warm clouds over South-East Atlantic, from co-located MODIS and CALIPSO observations, Atmospheric Chemistry and Physics, 13, 69–88, doi:10.5194/acp-13-69-2013, 2013.

Coulier, P. J.: Note sur une nouvelle propriete de l'air, Jour. pharm. chim., 8, 165–172, 1875.

DeMott, P. J., Prenni, A. J., Liu, X., Kreidenweis, S. M., Petters, M. D., Twohy, C. H., Richardson, M. S., Eidhammer, T., and Rogers, D. C.: Predicting global atmospheric ice nuclei distributions and their impacts on climate, Proceedings of the National Academy of Sciences, 107, 11 217–11 222, doi:10.1073/pnas.0910818107, 2010.

DeMott, P. J., Prenni, A. J., McMeeking, G. R., Sullivan, R. C., Petters, M. D., Tobo, Y., Niemand, M., Möhler, O., Snider, J. R., Wang, Z., and Kreidenweis, S. M.: Integrating laboratory and field data to quantify the immersion freezing ice nucleation activity of mineral dust particles, Atmospheric Chemistry and Physics, 15, 393–409, doi:10.5194/acp-15-393-2015, 2015.

Deng, Z. Z., Zhao, C. S., Ma, N., Liu, P. F., Ran, L., Xu, W. Y., Chen, J., Liang, Z., Liang, S., Huang, M. Y., Ma, X. C., Zhang, Q., Quan, J. N., Yan, P., Henning, S., Mildenberger, K., Sommerhage, E., Schäfer, M., Stratmann, F., and Wiedensohler, A.: Size-resolved and bulk activation properties of aerosols in the North China Plain, Atmospheric Chemistry and Physics, 11, 3835–3846, doi:10.5194/acp-11-3835-2011, https://acp.copernicus.org/articles/11/3835/2011/, 2011.

Douglas, A. and L'Ecuyer, T.: Quantifying variations in shortwave aerosol–cloud–radiation interactions using local meteorology and cloud state constraints, Atmospheric Chemistry and Physics, 19, 6251–6268, doi:10.5194/acp-19-6251-2019, 2019.

Draxler, R. and Rolph, G.: HYSPLIT (HYbrid Single-Particle Lagrangian Integrated Trajectory) model access via NOAA ARL READY website (http://ready.arl.noaa.gov/HYSPLIT.php), NOAA Air Resources Laboratory, Silver Spring, MD, 25, 2010.

Dubovik, O., Smirnov, A., Holben, B. N., King, M. D., Kaufman, Y. J., Eck, T. F., and Slutsker, I.: Accuracy assessments of aerosol optical properties retrieved from Aerosol Robotic Network (AERONET) Sun and sky radiance measurements, Journal of Geophysical Research: Atmospheres, 105, 9791–9806, doi:10.1029/2000JD900040, 2000.

Dubovik, O., Sinyuk, A., Lapyonok, T., Holben, B. N., Mishchenko, M., Yang, P., Eck, T. F., Volten, H., Muñoz, O., Veihelmann, B., van der Zande, W. J., Leon, J.-F., Sorokin, M., and Slutsker, I.: Application of spheroid models to account for aerosol particle nonsphericity in remote sensing of desert dust, Journal of Geophysical Research: Atmospheres, 111, doi:10.1029/2005JD006619, 2006.

Durkee, P. A., Noone, K. J., and Bluth, R. T.: The Monterey Area Ship Track Experiment, Journal of the Atmospheric Sciences, 57, 2523–2541, doi:10.1175/1520-0469(2000)057¡2523:TMASTE¿2.0.CO;2, 2000.

Dusek, U., Frank, G. P., Hildebrandt, L., Curtius, J., Schneider, J., Walter, S., Chand, D., Drewnick, F., Hings, S., Jung, D., Borrmann, S., and Andreae, M. O.: Size Matters More Than Chemistry for Cloud-Nucleating Ability of Aerosol Particles, Science, 312, 1375–1378, doi:10.1126/science.1125261, 2006.

Eagan, R. C., Hobbs, P. V., and Radke, L. F.: Measurements of Cloud Condensation Nuclei and Cloud Droplet Size Distributions in the Vicinity of Forest Fires, Journal of Applied Meteorology (1962-1982), 13, 553–557, 1974.

Ebmeier, S. K., Sayer, A. M., Grainger, R. G., Mather, T. A., and Carboni, E.: Systematic satellite observations of the impact of aerosols from passive volcanic degassing on local cloud properties, Atmospheric Chemistry and Physics, 14, 10 601–10 618, doi: 10.5194/acp-14-10601-2014, 2014.

Efraim, A., Rosenfeld, D., Schmale, J., and Zhu, Y.: Satellite Retrieval of Cloud Condensation Nuclei Concentrations in Marine Stratocumulus by Using Clouds as CCN Chambers, Journal of Geophysical Research: Atmospheres, 125, doi:10.1029/2020JD032409, 2020.

Errera, Q., Bennouna, Y., Schulz, M., Eskes, H., Basart, S., Benedictow, A., Blechschmidt, A.-M., Chabrillat, S., Clark, H., Cuevas, E., et al.: Validation report of the CAMS global Reanalysis of aerosols and reactive gases, years 2003-2020, Copernicus Atmosphere Monitoring Service (CAMS) report, doi:10.24380/8gf9-k005, 2021.

Fan, J., Wang, Y., Rosenfeld, D., and Liu, X.: Review of Aerosol–Cloud Interactions: Mechanisms, Significance, and Challenges, Journal of the Atmospheric Sciences, 73, 4221–4252, doi:10.1175/JAS-D-16-0037.1, 2016.

Fanourgakis, G. S., Kanakidou, M., Nenes, A., Bauer, S. E., Bergman, T., Carslaw, K. S., Grini, A., Hamilton, D. S., Johnson, J. S., Karydis, V. A., Kirkevåg, A., Kodros, J. K., Lohmann, U., Luo, G., Makkonen, R., Matsui, H., Neubauer, D., Pierce, J. R., Schmale, J., Stier, P., Tsigaridis, K., van Noije, T., Wang, H., Watson-Parris, D., Westervelt, D. M., Yang, Y., Yoshioka, M., Daskalakis, N., Decesari, S., Gysel-Beer, M., Kalivitis, N., Liu, X., Mahowald, N. M., Myriokefalitakis, S., Schrödner, R., Sfakianaki, M., Tsimpidi, A. P., Wu, M., and Yu, F.: Evaluation of global simulations of aerosol particle and cloud condensation nuclei number, with implications for cloud droplet formation, Atmospheric Chemistry and Physics, 19, 8591–8617, doi:10.5194/acp-19-8591-2019, 2019.

Feingold, G., Remer, L. A., Ramaprasad, J., and Kaufman, Y. J.: Analysis of smoke impact on clouds in Brazilian biomass burning regions: An extension of Twomey's approach, Journal of Geophysical Research: Atmospheres, 106, 22 907–22 922, doi: 10.1029/2001JD000732, 2001.

Forster, P., Storelvmo, T., Armour, K., Collins, W., Dufresne, J.-L., Frame, D., Lunt, D. J., Mauritsen, T., Palmer, M. D., Watanabe, M., Wild, M., and Zhang, X.: The Earth's energy budget, climate feedbacks, and climate sensitivity, in Climate Change 2021: The

Physical Science Basis. Contribution of Working Group I to the Sixth Assessment Report of the Intergovernmental Panel on Climate Change, edited by V. Masson-Delmotte, P. Zhai, A. Pirani, S. L. Connors, C. Péan, S. Berger, N. Caud, Y. Chen, L. Goldfarb, M. I. Gomis, M. Huang, K. Leitzell, E. Lonnoy, J. B. R. Matthews, T. K. Maycock, T. Waterfield, O. Yelekçi, R. Yu, and B. Zhou, Cambridge University Press, 2021.

Gasteiger, J. and Wiegner, M.: MOPSMAP v1.0: a versatile tool for the modeling of aerosol optical properties, Geoscientific Model Development, 11, 2739–2762, doi:10.5194/gmd-11-2739-2018, 2018.

Genz, C., Schrödner, R., Heinold, B., Henning, S., Baars, H., Spindler, G., and Tegen, I.: Estimation of cloud condensation nuclei number concentrations and comparison to in situ and lidar observations during the HOPE experiments, Atmospheric Chemistry and Physics, 20, 8787–8806, doi:10.5194/acp-20-8787-2020, `https://acp.copernicus.org/articles/20/8787/2020/`, 2020.

Georgoulias, A. K., Marinou, E., Tsekeri, A., Proestakis, E., Akritidis, D., Alexandri, G., Zanis, P., Balis, D., Marenco, F., Tesche, M., and Amiridis, V.: A First Case Study of CCN Concentrations from Spaceborne Lidar Observations, Remote Sensing, 12, 1557, doi:10.3390/rs12101557, 2020.

Goel, V., Mishra, S. K., Pal, P., Ahlawat, A., Vijayan, N., Jain, S., and Sharma, C.: Influence of chemical aging on physico-chemical properties of mineral dust particles: A case study of 2016 dust storms over Delhi, Environmental Pollution, 267, 115 338, doi:10.1016/j.envpol.2020.115338, 2020.

Goren, T. and Rosenfeld, D.: Decomposing aerosol cloud radiative effects into cloud cover, liquid water path and Twomey components in marine stratocumulus, Atmospheric Research, 138, 378–393, doi:https://doi.org/10.1016/j.atmosres.2013.12.008, 2014.

Gryspeerdt, E. and Stier, P.: Regime-based analysis of aerosol-cloud interactions, Geophysical Research Letters, 39, doi:10.1029/2012GL053221, 2012.

Gryspeerdt, E., Quaas, J., and Bellouin, N.: Constraining the aerosol influence on cloud fraction, Journal of Geophysical Research: Atmospheres, 121, 3566–3583, doi:https://doi.org/10.1002/2015JD023744, 2016.

Gryspeerdt, E., Quaas, J., Ferrachat, S., Gettelman, A., Ghan, S., Lohmann, U., Morrison, H., Neubauer, D., Partridge, D. G., Stier, P., Takemura, T., Wang, H., Wang, M., and Zhang, K.: Constraining the instantaneous aerosol influence on cloud albedo, Proceedings of the National Academy of Sciences, 114, 4899–4904, doi:10.1073/pnas.1617765114, 2017.

Gryspeerdt, E., Goren, T., Sourdeval, O., Quaas, J., Mülmenstädt, J., Dipu, S., Unglaub, C., Gettelman, A., and Christensen, M.: Constraining the aerosol influence on cloud liquid water path, Atmospheric Chemistry and Physics, 19, 5331–5347, doi:10.5194/acp-19-5331-2019, 2019.

Haarig, M., Walser, A., Ansmann, A., Dollner, M., Althausen, D., Sauer, D., Farrell, D., and Weinzierl, B.: Profiles of cloud condensation nuclei, dust mass concentration, and ice-nucleating-particle-relevant aerosol properties in the Saharan Air Layer over Barbados from polarization lidar and airborne in situ measurements, Atmospheric Chemistry and Physics, 19, 13 773–13 788, doi:10.5194/acp-19-13773-2019, 2019.

Haghighatnasab, M., Kretzschmar, J., Block, K., and Quaas, J.: Impact of Holuhraun volcano aerosols on clouds in cloud-system-resolving simulations, Atmospheric Chemistry and Physics, 22, 8457–8472, doi:10.5194/acp-22-8457-2022, https://acp.copernicus.org/articles/22/8457/2022/, 2022.

Han, Q., Rossow, W. B., Chou, J., and Welch, R. M.: Global variation of column droplet concentration in low-level clouds, Geophysical Research Letters, 25, 1419–1422, doi:10.1029/98GL01095, 1998a.

Han, Q., Rossow, W. B., Chou, J., and Welch, R. M.: Global Survey of the Relationships of Cloud Albedo and Liquid Water Path with Droplet Size Using ISCCP, Journal of Climate, 11, 1516–1528, doi:10.1175/1520-0442(1998)011¡1516:GSOTRO¿2.0.CO;2, 1998b.

Hasekamp, O. P., Litvinov, P., and Butz, A.: Aerosol properties over the ocean from PARASOL multiangle photopolarimetric measurements, Journal of Geophysical Research: Atmospheres, 116, doi:10.1029/2010JD015469, 2011.

Hasekamp, O. P., Gryspeerdt, E., and Quaas, J.: Analysis of polarimetric satellite measurements suggests stronger cooling due to aerosol-cloud interactions, Nature Communications, 10, 5405, doi:10.1038/s41467-019-13372-2, 2019.

Hegg, D. A., Covert, D. S., Jonsson, H. H., and Woods, R. K.: A simple relationship between cloud drop number concentration and precursor aerosol concentration for the regions of Earth's large marine stratocumulus decks, Atmospheric Chemistry and Physics, 12, 1229–1238, doi:10.5194/acp-12-1229-2012, 2012.

Holben, B., Eck, T., Slutsker, I., Tanré, D., Buis, J., Setzer, A., Vermote, E., Reagan, J., Kaufman, Y., Nakajima, T., Lavenu, F., Jankowiak, I., and Smirnov, A.: AERONET—A Federated Instrument Network and Data Archive for Aerosol Characterization, Remote Sensing of Environment, 66, 1–16, doi:10.1016/S0034-4257(98)00031-5, 1998.

Hudson, J. G., Noble, S., and Jha, V.: Stratus cloud supersaturations, Geophysical Research Letters, 37, doi:https://doi.org/10.1029/2010GL045197, 2010.

Inness, A., Ades, M., Agustí-Panareda, A., Barré, J., Benedictow, A., Blechschmidt, A.-M., Dominguez, J. J., Engelen, R., Eskes, H., Flemming, J., Huijnen, V., Jones, L., Kipling, Z., Massart, S., Parrington, M., Peuch, V.-H., Razinger, M., Remy, S., Schulz, M., and Suttie, M.: The CAMS reanalysis of atmospheric composition, Atmospheric Chemistry and Physics, 19, 3515–3556, doi:10.5194/acp-19-3515-2019, 2019.

Jia, H., Ma, X., Yu, F., and Quaas, J.: Significant underestimation of radiative forcing by aerosol–cloud interactions derived from satellite-based methods, Nature communications, 12, 1–11, doi:10.1038/s41467-021-23888-1, 2021.

Jiang, J. H., Su, H., Huang, L., Wang, Y., Massie, S., Zhao, B., Omar, A., and Wang, Z.: Contrasting effects on deep convective clouds by different types of aerosols, Nature Communications, 9, 3874, doi:10.1038/s41467-018-06280-4, 2018.

Jiang, M., Liu, X., Han, J., Wang, Z., and Xu, M.: Influence of particle properties on measuring a low-particulate-mass concentration by light extinction method, Fuel, 286, 119 460, doi:10.1016/j.fuel.2020.119460, 2021.

Kacenelenbogen, M., Redemann, J., Vaughan, M. A., Omar, A. H., Russell, P. B., Burton, S., Rogers, R. R., Ferrare, R. A., and Hostetler, C. A.: An evaluation of CALIOP/CALIPSO's aerosol-above-cloud detection and retrieval capability over North America, Journal of Geophysical Research: Atmospheres, 119, 230–244, doi:10.1002/2013JD020178, 2014.

Kalashnikova, O. V. and Sokolik, I. N.: Importance of shapes and compositions of wind-blown dust particles for remote sensing at solar wavelengths, Geophysical Research Letters, 29, 38–1–38–4, doi:10.1029/2002GL014947, 2002.

Kant, S., Panda, J., Pani, S. K., and Wang, P. K.: Long-term study of aerosol–cloud–precipitation interaction over the eastern part of India using satellite observations during pre-monsoon season, Theoretical and Applied Climatology, 136, 605–626, doi:10.1007/s00704-018-2509-2, 2019.

Kaufman, Y. J. and Koren, I.: Smoke and Pollution Aerosol Effect on Cloud Cover, Science, 313, 655–658, doi:10.1126/science.1126232, 2006.

Kim, J.-S. and Park, K.: Atmospheric Aging of Asian Dust Particles During Long Range Transport, Aerosol Science and Technology, 46, 913–924, doi:10.1080/02786826.2012.680984, 2012.

Kim, M.-H., Omar, A. H., Tackett, J. L., Vaughan, M. A., Winker, D. M., Trepte, C. R., Hu, Y., Liu, Z., Poole, L. R., Pitts, M. C., Kar, J., and Magill, B. E.: The CALIPSO version 4 automated aerosol classification and lidar ratio selection algorithm, Atmospheric Measurement Techniques, 11, 6107–6135, doi:10.5194/amt-11-6107-2018, 2018.

Koehler, K. A., Kreidenweis, S. M., DeMott, P. J., Petters, M. D., Prenni, A. J., and Carrico, C. M.: Hygroscopicity and cloud droplet activation of mineral dust aerosol, Geophysical Research Letters, 36, doi:https://doi.org/10.1029/2009GL037348, https://agupubs.onlinelibrary.wiley.com/doi/abs/10.1029/2009GL037348, 2009.

Kovacs, T.: Comparing MODIS and AERONET aerosol optical depth at varying separation distances to assess ground-based validation strategies for spaceborne lidar, Journal of Geophysical Research: Atmospheres, 111, doi:10.1029/2006JD007349, 2006.

Kumar, P., Sokolik, I. N., and Nenes, A.: Cloud condensation nuclei activity and droplet activation kinetics of wet processed regional dust samples and minerals, Atmospheric Chemistry and Physics, 11, 8661–8676, doi:10.5194/acp-11-8661-2011, https://acp.copernicus.org/articles/11/8661/2011/, 2011.

Lacagnina, C., Hasekamp, O. P., and Torres, O.: Direct radiative effect of aerosols based on PARASOL and OMI satellite observations, Journal of Geophysical Research: Atmospheres, 122, 2366–2388, doi:https://doi.org/10.1002/2016JD025706, 2017.

Lebsock, M. D., Stephens, G. L., and Kummerow, C.: Multisensor satellite observations of aerosol effects on warm clouds, Journal of Geophysical Research: Atmospheres, 113, doi:https://doi.org/10.1029/2008JD009876, 2008.

Liu, T., Liu, Q., Chen, Y., Wang, W., Zhang, H., Li, D., and Sheng, J.: Effect of aerosols on the macro- and micro-physical properties of warm clouds in the Beijing-Tianjin-Hebei region, Science of The Total Environment, 720, 137 618, doi:10.1016/j.scitotenv.2020.137618, 2020.

Liu, Z., Omar, A., Vaughan, M., Hair, J., Kittaka, C., Hu, Y., Powell, K., Trepte, C., Winker, D., Hostetler, C., Ferrare, R., and Pierce, R.: CALIPSO lidar observations of the optical properties of Saharan dust: A case study of long-range transport, Journal of Geophysical Research: Atmospheres, 113, doi:10.1029/2007JD008878, 2008.

Lohmann, U. and Lesins, G.: Stronger Constraints on the Anthropogenic Indirect Aerosol Effect, Science, 298, 1012–1015, doi:10.1126/science.1075405, 2002.

Lu, M.-L., Conant, W. C., Jonsson, H. H., Varutbangkul, V., Flagan, R. C., and Seinfeld, J. H.: The Marine Stratus/Stratocumulus Experiment (MASE): Aerosol-cloud relationships in marine stratocumulus, Journal of Geophysical Research: Atmospheres, 112, doi:10.1029/2006JD007985, 2007.

Lu, M.-L., Feingold, G., Jonsson, H. H., Chuang, P. Y., Gates, H., Flagan, R. C., and Seinfeld, J. H.: Aerosol-cloud relationships in continental shallow cumulus, Journal of Geophysical Research: Atmospheres, 113, doi:10.1029/2007JD009354, 2008.

Ma, P.-L., Rasch, P. J., Chepfer, H., Winker, D. M., and Ghan, S. J.: Observational constraint on cloud susceptibility weakened by aerosol retrieval limitations, Nature Communications, 9, 2640, doi:10.1038/s41467-018-05028-4, 2018.

Mamali, D., Marinou, E., Sciare, J., Pikridas, M., Kokkalis, P., Kottas, M., Binietoglou, I., Tsekeri, A., Keleshis, C., Engelmann, R., Baars, H., Ansmann, A., Amiridis, V., Russchenberg, H., and Biskos, G.: Vertical profiles of aerosol mass concentration derived by unmanned airborne in situ and remote sensing instruments during dust events, Atmospheric Measurement Techniques, 11, 2897–2910, doi:10.5194/amt-11-2897-2018, 2018.

Mamouri, R. E. and Ansmann, A.: Estimated desert-dust ice nuclei profiles from polarization lidar: methodology and case studies, Atmospheric Chemistry and Physics, 15, 3463–3477, doi:10.5194/acp-15-3463-2015, 2015.

Mamouri, R.-E. and Ansmann, A.: Potential of polarization lidar to provide profiles of CCN- and INP-relevant aerosol parameters, Atmospheric Chemistry and Physics, 16, 5905–5931, doi:10.5194/acp-16-5905-2016, 2016.

Mamouri, R. E., Amiridis, V., Papayannis, A., Giannakaki, E., Tsaknakis, G., and Balis, D. S.: Validation of CALIPSO space-borne-derived attenuated backscatter coefficient profiles using a ground-based lidar in Athens, Greece, Atmospheric Measurement Techniques, 2, 513–522, doi:10.5194/amt-2-513-2009, 2009.

Mann, G. W., Carslaw, K. S., Spracklen, D. V., Ridley, D. A., Manktelow, P. T., Chipperfield, M. P., Pickering, S. J., and Johnson, C. E.: Description and evaluation of GLOMAP-mode: a modal global aerosol microphysics model for the UKCA composition-climate model, Geoscientific Model Development, 3, 519–551, doi:10.5194/gmd-3-519-2010, 2010.

Marinou, E., Tesche, M., Nenes, A., Ansmann, A., Schrod, J., Mamali, D., Tsekeri, A., Pikridas, M., Baars, H., Engelmann, R., Voudouri, K.-A., Solomos, S., Sciare, J., Groß, S., Ewald, F., and Amiridis, V.: Retrieval of ice-nucleating particle concentrations from lidar observations and comparison with UAV in situ measurements, Atmospheric Chemistry and Physics, 19, 11 315–11 342, doi:10.5194/acp-19-11315-2019, 2019.

Masonis, S. J., Anderson, T. L., Covert, D. S., Kapustin, V., Clarke, A. D., Howell, S., and Moore, K.: A Study of the Extinction-to-Backscatter Ratio of Marine Aerosol during the Shoreline Environment Aerosol Study, Journal of Atmospheric and Oceanic Technology, 20, 1388–1402, doi:10.1175/1520-0426(2003)020¡1388:ASOTER¿2.0.CO;2, 2003.

McCoy, D. T., Bender, F. A.-M., Mohrmann, J. K. C., Hartmann, D. L., Wood, R., and Grosvenor, D. P.: The global aerosol-cloud first indirect effect estimated using MODIS, MERRA, and AeroCom, Journal of Geophysical Research: Atmospheres, 122, 1779–1796, doi:10.1002/2016JD026141, 2017.

McCoy, I. L., McCoy, D. T., Wood, R., Regayre, L., Watson-Parris, D., Grosvenor, D. P., Mulcahy, J. P., Hu, Y., Bender, F. A.-M., Field, P. R., Carslaw, K. S., and Gordon, H.: The hemispheric contrast in cloud microphysical properties constrains aerosol forcing, Proceedings of the National Academy of Sciences, 117, 18 998–19 006, doi:10.1073/pnas.1922502117, 2020.

Molod, A., Takacs, L., Suarez, M., and Bacmeister, J.: Development of the GEOS-5 atmospheric general circulation model: evolution from MERRA to MERRA2, Geoscientific Model Development, 8, 1339–1356, doi:10.5194/gmd-8-1339-2015, 2015.

Nakajima, T., Higurashi, A., Kawamoto, K., and Penner, J. E.: A possible correlation between satellite-derived cloud and aerosol microphysical parameters, Geophysical Research Letters, 28, 1171–1174, doi:10.1029/2000GL012186, 2001.

NASA/LARC/SD/ASDC: CALIPSO Lidar Level 2 Aerosol Profile, V4-20, doi: 10.5067/CALIOP/CALIPSO/LID_L2_05KMAPRO-STANDARD-V4-20, 2018.

Nenes, A., Murray, B., and Bougiatioti, A.: Mineral Dust and its Microphysical Interactions with Clouds, pp. 287–325, Springer Netherlands, Dordrecht, doi:10.1007/978-94-017-8978-3_12, 2014.

Omar, A. H., Won, J.-G., Winker, D. M., Yoon, S.-C., Dubovik, O., and McCormick, M. P.: Development of global aerosol models using cluster analysis of Aerosol Robotic Network (AERONET) measurements, Journal of Geophysical Research: Atmospheres, 110, doi:10.1029/2004JD004874, 2005.

Omar, A. H., Winker, D. M., Vaughan, M. A., Hu, Y., Trepte, C. R., Ferrare, R. A., Lee, K.-P., Hostetler, C. A., Kittaka, C., Rogers, R. R., Kuehn, R. E., and Liu, Z.: The CALIPSO Automated Aerosol Classification and Lidar Ratio Selection Algorithm, Journal of Atmospheric and Oceanic Technology, 26, 1994–2014, doi:10.1175/2009JTECHA1231.1, 2009.

Omar, A. H., Winker, D. M., Tackett, J. L., Giles, D. M., Kar, J., Liu, Z., Vaughan, M. A., Powell, K. A., and Trepte, C. R.: CALIOP and AERONET aerosol optical depth comparisons: One size fits none, Journal of Geophysical Research: Atmospheres, 118, 4748–4766, doi:10.1002/jgrd.50330, 2013.

Oreopoulos, L., Cho, N., and Lee, D.: Using MODIS cloud regimes to sort diagnostic signals of aerosol-cloud-precipitation interactions, Journal of Geophysical Research: Atmospheres, 122, 5416–5440, doi:10.1002/2016JD026120, 2017.

Papagiannopoulos, N., Mona, L., Alados-Arboledas, L., Amiridis, V., Baars, H., Binietoglou, I., Bortoli, D., D'Amico, G., Giunta, A., Guerrero-Rascado, J. L., Schwarz, A., Pereira, S., Spinelli, N., Wandinger, U., Wang, X., and Pappalardo, G.: CALIPSO climatological products: evaluation and suggestions from EARLINET, Atmospheric Chemistry and Physics, 16, 2341–2357, doi:10.5194/acp-16-2341-2016, 2016.

Pappalardo, G., Wandinger, U., Mona, L., Hiebsch, A., Mattis, I., Amodeo, A., Ansmann, A., Seifert, P., Linné, H., Apituley, A., Alados Arboledas, L., Balis, D., Chaikovsky, A., D'Amico, G., De Tomasi, F., Freudenthaler, V., Giannakaki, E., Giunta, A., Grigorov, I., Iarlori, M., Madonna, F., Mamouri, R.-E., Nasti, L., Papayannis, A., Pietruczuk, A., Pujadas, M., Rizi, V., Rocadenbosch, F., Russo, F., Schnell, F., Spinelli, N., Wang, X., and Wiegner, M.: EARLINET correlative measurements for CALIPSO: First intercomparison results, Journal of Geophysical Research: Atmospheres, 115, doi:10.1029/2009JD012147, 2010.

Penner, J. E., Xu, L., and Wang, M.: Satellite methods underestimate indirect climate forcing by aerosols, Proceedings of the National Academy of Sciences, 108, 13 404–13 408, doi:10.1073/pnas.1018526108, 2011.

Petters, M. D. and Kreidenweis, S. M.: A single parameter representation of hygroscopic growth and cloud condensation nucleus activity, Atmospheric Chemistry and Physics, 7, 1961–1971, doi:10.5194/acp-7-1961-2007, 2007.

Pringle, K. J., Tost, H., Pozzer, A., Pöschl, U., and Lelieveld, J.: Global distribution of the effective aerosol hygroscopicity parameter for CCN activation, Atmospheric Chemistry and Physics, 10, 5241–5255, doi:10.5194/acp-10-5241-2010, 2010.

Quaas, J., Boucher, O., and Bréon, F.-M.: Aerosol indirect effects in POLDER satellite data and the Laboratoire de Météorologie Dynamique–Zoom (LMDZ) general circulation model, Journal of Geophysical Research: Atmospheres, 109, doi:10.1029/2003JD004317, 2004.

Quaas, J., Boucher, O., and Lohmann, U.: Constraining the total aerosol indirect effect in the LMDZ and ECHAM4 GCMs using MODIS satellite data, Atmospheric Chemistry and Physics, 6, 947–955, doi:10.5194/acp-6-947-2006, 2006.

Quaas, J., Boucher, O., Bellouin, N., and Kinne, S.: Satellite-based estimate of the direct and indirect aerosol climate forcing, Journal of Geophysical Research: Atmospheres, 113, doi:10.1029/2007JD008962, 2008.

Quaas, J., Ming, Y., Menon, S., Takemura, T., Wang, M., Penner, J. E., Gettelman, A., Lohmann, U., Bellouin, N., Boucher, O., Sayer, A. M., Thomas, G. E., McComiskey, A., Feingold, G., Hoose, C., Kristjánsson, J. E., Liu, X., Balkanski, Y., Donner, L. J., Ginoux, P. A., Stier, P., Grandey, B., Feichter, J., Sednev, I., Bauer, S. E., Koch, D., Grainger, R. G., Kirkev&aring, G, A., Iversen, T., Seland, O., Easter, R., Ghan, S. J., Rasch, P. J., Morrison, H., Lamarque, J.-F., Iacono, M. J., Kinne, S., and Schulz, M.: Aerosol indirect effects – general circulation model intercomparison and evaluation with satellite data, Atmospheric Chemistry and Physics, 9, 8697–8717, doi:10.5194/acp-9-8697-2009, 2009.

Quaas, J., Arola, A., Cairns, B., Christensen, M., Deneke, H., Ekman, A. M. L., Feingold, G., Fridlind, A., Gryspeerdt, E., Hasekamp, O., Li, Z., Lipponen, A., Ma, P.-L., Mülmenstädt, J., Nenes, A., Penner, J. E., Rosenfeld, D., Schrödner, R., Sinclair, K., Sourdeval, O., Stier, P., Tesche, M., van Diedenhoven, B., and Wendisch, M.: Constraining the Twomey effect from satellite observations: issues and perspectives, Atmospheric Chemistry and Physics, 20, 15 079–15 099, doi:10.5194/acp-20-15079-2020, 2020.

Quinn, P., Coffman, D., Johnson, J., Upchurch, L., and Bates, T.: Small fraction of marine cloud condensation nuclei made up of sea spray aerosol, Nature Geoscience, 10, 674–679, doi:10.1038/ngeo3003, 2017.

Quinn, P. K., Bates, T. S., Coffman, D. J., and Covert, D. S.: Influence of particle size and chemistry on the cloud nucleating properties of aerosols, Atmospheric Chemistry and Physics, 8, 1029–1042, doi:10.5194/acp-8-1029-2008, https://acp.copernicus.org/articles/8/1029/2008/, 2008.

Remer, L. A., Kaufman, Y. J., Tanré, D., Mattoo, S., Chu, D. A., Martins, J. V., Li, R.-R., Ichoku, C., Levy, R. C., Kleidman, R. G., Eck, T. F., Vermote, E., and Holben, B. N.: The MODIS Aerosol Algorithm, Products, and Validation, Journal of the Atmospheric Sciences, 62, 947–973, doi:10.1175/JAS3385.1, 2005.

Rogers, R. R., Vaughan, M. A., Hostetler, C. A., Burton, S. P., Ferrare, R. A., Young, S. A., Hair, J. W., Obland, M. D., Harper, D. B., Cook, A. L., and Winker, D. M.: Looking through the haze: evaluating the CALIPSO level 2 aerosol optical depth using airborne high spectral resolution lidar data, Atmospheric Measurement Techniques, 7, 4317–4340, doi:10.5194/amt-7-4317-2014, 2014.

Rose, D., Nowak, A., Achtert, P., Wiedensohler, A., Hu, M., Shao, M., Zhang, Y., Andreae, M. O., and Pöschl, U.: Cloud condensation nuclei in polluted air and biomass burning smoke near the mega-city Guangzhou, China – Part 1: Size-resolved measurements and implications for the modeling of aerosol particle hygroscopicity and CCN activity, Atmospheric Chemistry and Physics, 10, 3365–3383, doi:10.5194/acp-10-3365-2010, https://acp.copernicus.org/articles/10/3365/2010/, 2010.

Rosenfeld, D., Andreae, M. O., Asmi, A., Chin, M., de Leeuw, G., Donovan, D. P., Kahn, R., Kinne, S., Kivekäs, N., Kulmala, M., Lau, W., Schmidt, K. S., Suni, T., Wagner, T., Wild, M., and Quaas, J.: Global observations of aerosol-cloud-precipitation-climate interactions, Reviews of Geophysics, 52, 750–808, doi:10.1002/2013RG000441, 2014.

Rosenfeld, D., Zheng, Y., Hashimshoni, E., Pöhlker, M. L., Jefferson, A., Pöhlker, C., Yu, X., Zhu, Y., Liu, G., Yue, Z., Fischman, B., Li, Z., Giguzin, D., Goren, T., Artaxo, P., Barbosa, H. M. J., Pöschl, U., and Andreae, M. O.: Satellite retrieval of cloud condensation nuclei concentrations by using clouds as CCN chambers, Proceedings of the National Academy of Sciences, 113, 5828–5834, doi:10.1073/pnas.1514044113, 2016.

Sayer, A. M., Smirnov, A., Hsu, N. C., and Holben, B. N.: A pure marine aerosol model, for use in remote sensing applications, Journal of Geophysical Research: Atmospheres, 117, doi:10.1029/2011JD016689, 2012.

Sayer, A. M., Hsu, N. C., Bettenhausen, C., and Jeong, M.-J.: Validation and uncertainty estimates for MODIS Collection 6 "Deep Blue" aerosol data, Journal of Geophysical Research: Atmospheres, 118, 7864–7872, doi:10.1002/jgrd.50600, 2013.

Schafer, J. S., Eck, T. F., Holben, B. N., Thornhill, K. L., Ziemba, L. D., Sawamura, P., Moore, R. H., Slutsker, I., Anderson, B. E., Sinyuk, A., Giles, D. M., Smirnov, A., Beyersdorf, A. J., and Winstead, E. L.: Intercomparison of aerosol volume size distributions derived from AERONET ground-based remote sensing and LARGE in situ aircraft

profiles during the 2011–2014 DRAGON and DISCOVER-AQ experiments, Atmospheric Measurement Techniques, 12, 5289–5301, doi:10.5194/amt-12-5289-2019, 2019.

Schmale, J., Henning, S., Henzing, B., Keskinen, H., Sellegri, K., Ovadnevaite, J., Bougiatioti, A., Kalivitis, N., Stavroulas, I., Jefferson, A., Park, M., Schlag, P., Kristensson, A., Iwamoto, Y., Pringle, K., Reddington, C., Aalto, P., Äijälä, M., Baltensperger, U., Bialek, J., Birmili, W., Bukowiecki, N., Ehn, M., Fjæraa, A. M., Fiebig, M., Frank, G., Fröhlich, R., Frumau, A., Furuya, M., Hammer, E., Heikkinen, L., Herrmann, E., Holzinger, R., Hyono, H., Kanakidou, M., Kiendler-Scharr, A., Kinouchi, K., Kos, G., Kulmala, M., Mihalopoulos, N., Motos, G., Nenes, A., O'Dowd, C., Paramonov, M., Petäjä, T., Picard, D., Poulain, L., Prévôt, A. S. H., Slowik, J., Sonntag, A., Swietlicki, E., Svenningsson, B., Tsurumaru, H., Wiedensohler, A., Wittbom, C., Ogren, J. A., Matsuki, A., Yum, S. S., Myhre, C. L., Carslaw, K., Stratmann, F., and Gysel, M.: Collocated observations of cloud condensation nuclei, particle size distributions, and chemical composition, Scientific data, 4, 1–27, doi:10.1038/sdata.2017.3, 2017.

Schmale, J., Henning, S., Decesari, S., Henzing, B., Keskinen, H., Sellegri, K., Ovadnevaite, J., Pöhlker, M. L., Brito, J., Bougiatioti, A., Kristensson, A., Kalivitis, N., Stavroulas, I., Carbone, S., Jefferson, A., Park, M., Schlag, P., Iwamoto, Y., Aalto, P., Äijälä, M., Bukowiecki, N., Ehn, M., Frank, G., Fröhlich, R., Frumau, A., Herrmann, E., Herrmann, H., Holzinger, R., Kos, G., Kulmala, M., Mihalopoulos, N., Nenes, A., O'Dowd, C., Petäjä, T., Picard, D., Pöhlker, C., Pöschl, U., Poulain, L., Prévôt, A. S. H., Swietlicki, E., Andreae, M. O., Artaxo, P., Wiedensohler, A., Ogren, J., Matsuki, A., Yum, S. S., Stratmann, F., Baltensperger, U., and Gysel, M.: Long-term cloud condensation nuclei number concentration, particle number size distribution and chemical composition measurements at regionally representative observatories, Atmospheric Chemistry and Physics, 18, 2853–2881, doi:10.5194/acp-18-2853-2018, 2018.

Seinfeld, J. H., Bretherton, C., Carslaw, K. S., Coe, H., DeMott, P. J., Dunlea, E. J., Feingold, G., Ghan, S., Guenther, A. B., Kahn, R., Kraucunas, I., Kreidenweis, S. M., Molina, M. J., Nenes, A., Penner, J. E., Prather, K. A., Ramanathan, V., Ramaswamy, V., Rasch, P. J., Ravishankara, A. R., Rosenfeld, D., Stephens, G., and Wood, R.: Improving our fundamental understanding of the role of aerosol-cloud interactions in the climate system, Proceedings of the National Academy of Sciences, 113, 5781–5790, doi:10.1073/pnas.1514043113, 2016.

Shinozuka, Y., Clarke, A. D., Nenes, A., Jefferson, A., Wood, R., McNaughton, C. S., Ström, J., Tunved, P., Redemann, J., Thornhill, K. L., Moore, R. H., Lathem, T. L., Lin, J. J., and Yoon, Y. J.: The relationship between cloud condensation nuclei (CCN) concentration and light extinction of dried particles: indications of underlying aerosol processes and implications for satellite-based CCN estimates, Atmospheric Chemistry and Physics, 15, 7585–7604, doi:10.5194/acp-15-7585-2015, 2015.

Stap, F. A., Hasekamp, O. P., and Röckmann, T.: Sensitivity of PARASOL multi-angle

photopolarimetric aerosol retrievals to cloud contamination, Atmospheric Measurement Techniques, 8, 1287–1301, doi:10.5194/amt-8-1287-2015, 2015.

Stier, P.: Limitations of passive remote sensing to constrain global cloud condensation nuclei, Atmospheric Chemistry and Physics, 16, 6595–6607, doi:10.5194/acp-16-6595-2016, 2016.

Tackett, J. L., Winker, D. M., Getzewich, B. J., Vaughan, M. A., Young, S. A., and Kar, J.: CALIPSO lidar level 3 aerosol profile product: version 3 algorithm design, Atmospheric Measurement Techniques, 11, 4129–4152, doi:10.5194/amt-11-4129-2018, 2018.

Tesche, M., Ansmann, A., Müller, D., Althausen, D., Engelmann, R., Freudenthaler, V., and Groß, S.: Vertically resolved separation of dust and smoke over Cape Verde using multiwavelength Raman and polarization lidars during Saharan Mineral Dust Experiment 2008, Journal of Geophysical Research: Atmospheres, 114, doi:10.1029/2009JD011862, 2009.

Tesche, M., Wandinger, U., Ansmann, A., Althausen, D., Müller, D., and Omar, A. H.: Ground-based validation of CALIPSO observations of dust and smoke in the Cape Verde region, Journal of Geophysical Research: Atmospheres, 118, 2889–2902, doi:10.1002/jgrd.50248, 2013.

Tesche, M., Zieger, P., Rastak, N., Charlson, R. J., Glantz, P., Tunved, P., and Hansson, H.-C.: Reconciling aerosol light extinction measurements from spaceborne lidar observations and in situ measurements in the Arctic, Atmospheric Chemistry and Physics, 14, 7869–7882, doi:10.5194/acp-14-7869-2014, 2014.

Toll, V., Christensen, M., Gassó, S., and Bellouin, N.: Volcano and Ship Tracks Indicate Excessive Aerosol-Induced Cloud Water Increases in a Climate Model, Geophysical Research Letters, 44, 12,492–12,500, doi:https://doi.org/10.1002/2017GL075280, 2017.

Toll, V., Christensen, M., Quaas, J., and Bellouin, N.: Weak average liquid-cloud-water response to anthropogenic aerosols, Nature, 572, 51–55, doi:10.1038/s41586-019-1423-9, 2019.

Tsekeri, A., Amiridis, V., Marenco, F., Nenes, A., Marinou, E., Solomos, S., Rosenberg, P., Trembath, J., Nott, G. J., Allan, J., Le Breton, M., Bacak, A., Coe, H., Percival, C., and Mihalopoulos, N.: Profiling aerosol optical, microphysical and hygroscopic properties in ambient conditions by combining in situ and remote sensing, Atmospheric Measurement Techniques, 10, 83–107, doi:10.5194/amt-10-83-2017, 2017.

Twohy, C. H., Petters, M. D., Snider, J. R., Stevens, B., Tahnk, W., Wetzel, M., Russell, L., and Burnet, F.: Evaluation of the aerosol indirect effect in marine stratocumulus clouds: Droplet number, size, liquid water path, and radiative impact, Journal of Geophysical Research: Atmospheres, 110, doi:10.1029/2004JD005116, 2005.

Twomey, S.: Pollution and the planetary albedo, Atmospheric Environment (1967), 8, 1251–1256, doi:10.1016/0004-6981(74)90004-3, 1974.

Twomey, S.: The Influence of Pollution on the Shortwave Albedo of Clouds, Journal of the Atmospheric Sciences, 34, 1149–1152, doi:10.1175/1520-0469(1977)034¡1149:TIOPOT¿2.0.CO;2, 1977.

Ullrich, R., Hoose, C., Möhler, O., Niemand, M., Wagner, R., Höhler, K., Hiranuma, N., Saathoff, H., and Leisner, T.: A New Ice Nucleation Active Site Parameterization for Desert Dust and Soot, Journal of the Atmospheric Sciences, 74, 699 – 717, doi:10.1175/JAS-D-16-0074.1, 2017.

Vergara-Temprado, J., Murray, B. J., Wilson, T. W., O'Sullivan, D., Browse, J., Pringle, K. J., Ardon-Dryer, K., Bertram, A. K., Burrows, S. M., Ceburnis, D., DeMott, P. J., Mason, R. H., O'Dowd, C. D., Rinaldi, M., and Carslaw, K. S.: Contribution of feldspar and marine organic aerosols to global ice nucleating particle concentrations, Atmospheric Chemistry and Physics, 17, 3637–3658, doi:10.5194/acp-17-3637-2017, 2017.

Várnai, T. and Marshak, A.: Effect of Cloud Fraction on Near-Cloud Aerosol Behavior in the MODIS Atmospheric Correction Ocean Color Product, Remote Sensing, 7, 5283–5299, doi:10.3390/rs70505283, 2015.

Warner, J. and Twomey, S.: The Production of Cloud Nuclei by Cane Fires and the Effect on Cloud Droplet Concentration, Journal of the Atmospheric Sciences, 24, 704–706, doi:10.1175/1520-0469(1967)024¡0704:TPOCNB¿2.0.CO;2, 1967.

Watson-Parris, D., Schutgens, N., Winker, D., Burton, S. P., Ferrare, R. A., and Stier, P.: On the Limits of CALIOP for Constraining Modeled Free Tropospheric Aerosol, Geophysical Research Letters, 45, 9260–9266, doi:10.1029/2018GL078195, 2018.

Wetzel, M. and Stowe, L. L.: Satellite-observed patterns in stratus microphysics, aerosol optical thickness, and shortwave radiative forcing, Journal of Geophysical Research: Atmospheres, 104, 31 287–31 299, doi:10.1029/1999JD900922, 1999.

Williamson, C., Kupc, A., Bilsback, K., Bui, T., Jost, P., Dollner, M., Froyd, K., Hodshire, A., Jimenez, J., Kodros, J., Luo, G., Murphy, D., Nault, B., Ray, E., Weinzierl, B., Yu, F., Yu, P., Pierce, J., and Brock, C.: ATom: In Situ Tropical Aerosol Properties and Comparable Global Model Outputs, doi:10.3334/ORNLDAAC/1684, 2019.

Winker, D. M., Vaughan, M. A., Omar, A., Hu, Y., Powell, K. A., Liu, Z., Hunt, W. H., and Young, S. A.: Overview of the CALIPSO Mission and CALIOP Data Processing Algorithms, Journal of Atmospheric and Oceanic Technology, 26, 2310–2323, doi:10.1175/2009JTECHA1281.1, 2009.

Winker, D. M., Tackett, J. L., Getzewich, B. J., Liu, Z., Vaughan, M. A., and Rogers, R. R.: The global 3-D distribution of tropospheric aerosols as characterized by CALIOP, Atmospheric Chemistry and Physics, 13, 3345–3361, doi:10.5194/acp-13-3345-2013, 2013.

Wofsy, S., Afshar, S., Allen, H., Apel, E., Asher, E., Barletta, B., Bent, J., Bian, H., Biggs, B., Blake, D., Blake, N., Bourgeois, I., Brock, C., Brune, W., Budney, J., Bui, T., Butler, A., Campuzano-Jost, P., Chang, C., Chin, M., Commane, R., Correa, G., Crounse, J., Cullis, P. D., Daube, B., Day, D., Dean-Day, J., Dibb, J., DiGangi, J., Diskin, G., Dollner, M., Elkins, J., Erdesz, F., Fiore, A., Flynn, C., Froyd, K., Gesler, D., Hall, S., Hanisco, T., Hannun, R., Hills, A., Hintsa, E., Hoffman, A., Hornbrook, R., Huey, L., Hughes, S., Jimenez, J., Johnson, B., Katich, J., Keeling, R., Kim, M., Kupc, A., Lait, L., Lamarque, J.-F., Liu, J., McKain, K., Mclaughlin, R., Meinardi, S., Miller, D., Montzka, S., Moore, F., Morgan, E., Murphy, D., Murray, L., Nault, B., Neuman, J., Newman, P., Nicely, J., Pan, X., Paplawsky, W., Peischl, J., Prather, M., Price, D., Ray, E., Reeves, J., Richardson, M., Rollins, A., Rosenlof, K., Ryerson, T., Scheuer, E., Schill, G., Schroder, J., Schwarz, J., St.Clair, J., Steenrod, S., Stephens, B., Strode, S., Sweeney, C., Tanner, D., Teng, A., Thames, A., Thompson, C., Ullmann, K., Veres, P., Vieznor, N., Wagner, N., Watt, A., Weber, R., Weinzierl, B., Wennberg, P., Williamson, C., Wilson, J., Wolfe, G., Woods, C., and Zeng, L.: ATom: Merged Atmospheric Chemistry, Trace Gases, and Aerosols, doi:10.3334/ORNLDAAC/1581, 2018.

Yuan, T., Remer, L. A., and Yu, H.: Microphysical, macrophysical and radiative signatures of volcanic aerosols in trade wind cumulus observed by the A-Train, Atmospheric Chemistry and Physics, 11, 7119–7132, doi:10.5194/acp-11-7119-2011, 2011.

Zieger, P., Fierz-Schmidhauser, R., Weingartner, E., and Baltensperger, U.: Effects of relative humidity on aerosol light scattering: results from different European sites, Atmospheric Chemistry and Physics, 13, 10 609–10 631, doi:10.5194/acp-13-10609-2013, 2013.

List of Abbreviations

ACI	aerosol-cloud interaction
AE	Angstrom exponent
AERONET	Aerosol Robotic Network
ANC	aerosol number concentration
AOD	aerosol optical depth
ARI	aerosol-radiation interaction
ATom	Atmospheric Tomography Mission
AVHRR	Advanced Very High Resolution Radiometer
CALIOP	Cloud-Aerosol Lidar with Orthogonal Polarization
CALIPSO	Cloud-Aerosol Lidar and Infrared Pathfinder Satellite Observation
CAMel	CALIPSO aerosol model
CCN	cloud condensation nuclei
CDNC	cloud droplet number concentration
CERES	Clouds and the Earth's Radiant Energy System
DMO	days in a month observed
ERF	effective radiative forcing
ERF_{ACI}	effective radiative forcing due to ACI
ERF_{ARI}	effective radiative forcing due to ARI
GLOMAP	Global Model of Aerosol Processes
GMAO	Global Modelling and Assimilation Office
HYSPLIT	Hybrid Single-Particle Lagrangian Integrated Trajectory model
IGOM	improved geometric optics method
INP	ice nucleating particles
IPCC	Intergovernmental Panel on Climate Change
IRF	instantaneous radiative forcing
IRF_{ACI}	instantaneous radiative forcing due to ACI
IRF_{ARI}	instantaneous radiative forcing due to ARI
LAS	Laser Aerosol Spectrometer
LWP	liquid water path
MODIS	Moderate Resolution Imaging Spectroradiometer

MOPSMAP	modelled optical properties of ensembles of aerosol particles
NMASS	Nucleation-mode Aerosol Size Spectrometer
NMB	normalized mean bias
NME	normalized mean error
NOAA	National Oceanic and Atmospheric Administration
AI	aerosol index
NVSD	normalized volume size distribution
OMCAM	Optical Modelling of CALIPSO Aerosol Microphysics
POLDER	Polarization and Directionality of the Earth's Reflectances
POLIPHON	Polarization Lidar Photometer Networking
RH	relative humidity
RMSE	root mean square error
SEAS	Shoreline Environment Aerosol Study
STP	standard temperature and pressure
UHSAS	Ultra-high Sensitivity Aerosol Size Spectrometer

List of Variables

C	Conversion factor
f_{ss}	Enhancement factor
n_{CCN}	Number concentration of CCN
$n_{j,\mathrm{dry}}$	Aerosol number concentration with dry radius $> j$ nm
m	Complex refractive index
m_r	Real part of complex refractive index
m_i	Imaginary part of complex refractive index
N	Sample size
R	Spearman's correlation coefficient
r	Radius
r_{wet}	Wet radius
r_{dry}	Dry radius
K_α	Extinction cross-section
V_t	Total volume of bi-modal lognormal size distribution
$V(r)$	Volume of particle with radius r
v	Volume fraction
v_f	Fine-mode volume fraction
v_c	Coarse mode volume fraction
x	Extinction exponent
α	Extinction coefficient
α_n	Normalized extinction coefficient
β_p	Particle backscatter coefficient
β_d	Dust backscatter coefficient
β_{nd}	Non-dust backscatter coefficient
κ	Aerosol hygroscopicity
σ	Standard deviation
σ_f	Fine-mode standard deviation
σ_c	Coarse-mode standard deviation
μ	Mean radius

μ_f	Fine-mode mean radius
μ_c	Coarse-mode mean radius
δ_p	Particle depolarization ratio
z	Height

List of Figures

1.1 Schematics of aerosol-climate interactions 2
1.2 Uncertainty in aerosol radiative forcing 4
1.3 Arrangements of aerosols and clouds in atmosphere 9

2.1 Flowchart of the OMCAM algorithm 22
2.2 Sensitivity of $n_{j,\mathrm{dry}}$ to size distribution parameters 25
2.3 CALIPSO aerosol model 26
2.4 Collective output of $n_{j,\mathrm{dry}}$ sensitivity studies 29
2.5 Theoretical comparison of OMCAM and POLIPHON algorithms 31
2.6 CALIPSO measurements during ACEMED campaign 33
2.7 Comparison of $n_{50,\mathrm{dry}}$ from CALIPSO and in situ data 34

3.1 Growth factors vs RH for different aerosol subtypes 47
3.2 Flight path during ATom campaign 49
3.3 Intersection identification using HYSPLIT trajectories 51
3.4 Example cases for comparison between CALIPSO and ATom data 53
3.5 Extinction coefficient comparison for all identified intersections 55
3.6 $n_{50,\mathrm{dry}}$ comparison for all identified intersections 57
3.7 $n_{250,\mathrm{dry}}$ comparison for all identified intersections 58
3.8 Comparison for updated OMCAM algorithm 60

4.1 In situ station locations used in the comparison study 68
4.2 In situ $n_{j,\mathrm{dry}}$ vs n_{CCN} at ss = 0.2 % 72
4.3 Monthly n_{CCN} time series from in situ and CALIPSO measurements . . . 74
4.4 Correlation plots for comparison between CALIPSO and in situ retrievals 75

6.1 Annual average column-integrated n_{CCN} from POLDER and CALIPSO . 84
6.2 Annual average aerosol type-specific column-integrated n_{CCN} from CALIPSO 85
6.3 Annual average n_{CCN} between 1 and 2 km height from CALIPSO and box model 86

List of Tables

2.1 POLIPHON regression constants 20
2.2 Microphysical properties from CALIPSO aerosol model 28
2.3 Statistics from sensitivity studies 29
2.4 Comparison of CALIPSO with ACEMED in situ data 35

3.1 Details of ATom in situ data 42
3.2 POLIPHON regression constants for $n_{50,\mathrm{dry}}$ and $n_{250,\mathrm{dry}}$ 43
3.3 Aerosol microphysical properties used in OMCAM 45
3.4 OMCAM conversion factors 46
3.A1 Details of intersections between ATom and CALIPSO tracks 63

4.1 Details of the in situ stations 69
4.2 POLIPHON and OMCAM regression constants 70
4.3 In situ vs CALIPSO comparison statistics 76

List of Publications

1. Choudhury, G. and Tesche, M.: Estimating cloud condensation nuclei concentrations from CALIPSO lidar measurements, Atmos. Meas. Tech., 15, 639–654, https://doi.org/10.5194/amt-15-639-2022, 2022.

   MT conceptualized the study. GC developed the methodology under the guidance of MT. GC performed the data analysis and prepared the plots. GC prepared the initial manuscript. GC and MT contributed to the interpretation of the data and revisions of the manuscript.

2. Choudhury, G., Ansmann, A., and Tesche, M.: Evaluation of aerosol number concentrations from CALIPSO with ATom airborne in situ measurements, Atmos. Chem. Phys., 22, 7143–7161, https://doi.org/10.5194/acp-22-7143-2022, 2022.

   GC conceptualized the study, performed the data analysis, and prepared the plots under the guidance of MT. GC prepared the initial manuscript. GC, MT, and AA contributed to the discussion of the findings and the revisions of the paper.

3. Choudhury, G. and Tesche, M.: Assessment of CALIOP-Derived CCN Concentrations by In Situ Surface Measurements. Remote Sensing, 14(14), p.3342, https://doi.org/10.3390/rs14143342, 2022.

   GC conceptualized the study, performed the data analysis, and prepared the plots under the guidance of MT. GC prepared the initial manuscript. GC and MT contributed to the discussion of the findings and the revisions of the paper.

Acknowledgements

This work has been conducted at the Leipzig Institute for Meteorology (LIM), Leipzig University and is supported by the Franco-German Fellowship Program on Climate, Energy, and Earth System Research (Make Our Planet Great Again-German Research Initiative (MOPGA-GRI), grant number 57429422) of the German Academic Exchange Service (DAAD), funded by the German Ministry of Education and Research.

First and foremost, I would like to express my sincere gratitude to my supervisor, Matthias Tesche, for his heartfelt support, optimistic attitude, and invaluable guidance throughout my PhD. He has given me the freedom to pursue my research, while unobtrusively ensuring that I stay on the right track. I shall eternally be grateful to him for his trust and support. I am thankful to Albert Ansmann (TROPOS) for his additional support and fruitful suggestions that made me even more confident. I am grateful to Josef Gasteiger (University of Vienna) for his technical support in compiling the modelling package and to Otto Hasekamp (SRON, Netherlands) for providing the POLDER data.

I am thankful to my lab mates Torsten Seelig, Peter Bräuer, Peggy Achtert, Fani Alexandri, and Felix Müller for their help and support. Deep thanks to my colleagues cum friends Fani, Alex, Kátia, Elena, Andrea, Carola, Vasilis, Iris, Stamatis, Dimitris, and so forth, for so many memorable moments during the last years. I want to thank my flatmates Pallav, Krupa, Swamini, and Phill for making me feel at home in Leipzig.

I want to dedicate this work to my parents. Without their love, compassion, and consistent support, I would not be where I am today. They have sacrificed a lot so that I can achieve my dreams. Words are not enough to express how thankful I am for all you have done and all the love you have given me.